ABSTRACT

LIM, CHEMIN. Low Cycle Fatigue Life Prediction of Four Bolt Extended Unstiffened End Plate Moment Connections. (Under the direction of Emmett A Sumner.)

The end plate moment connection (EPMC) has been studied for many years to investigate and understood its behavior under monotonic and cyclic loading. After the 1994 Northridge, California earthquake, additional research on EPMCs was performed as a part of the SAC steel project. Results from this research concluded that the EPMC could be designed to resist large cyclic (seismic) forces and provide a large amount of ductility. While the research on the behavior of EPMC under cyclic loading has been conducted, very little information on the LCF behavior is available. To evaluate the accumulation of LCF damage, the LCF life prediction, three phases of experimental tests were conducted. To investigate critical geometric parameters for 4E EPMCs in the LCF behavior, parametric study was conducted using a validated FEM model. In the first phase of the experimental testing four reduced EPMCs (T-stubs) were tested to investigate the general behavior of the connection. In second phase of the experimental testing, three different levels of constant peak displacement loading were applied to three full scale EPMCs for developing a LCF model in second phase of the experimental test. In the last phase, an accumulated damage model was evaluated using one full scale EPMC test subjected to random loading. In all phases three-dimensional finite element numerical analysis and theoretical analysis were adopted to predict the experimental behavior. The results of the experimental tests were used to develop the LCF model for the 4E EPMC and it closely predicted the observed LCF life of connection. The parametric study identified the end plate thickness, the beam flange thickness, and the bolt pitch distance as the three critical geometry parameters.

Low Cycle Fatigue Life Prediction of Four Bolt Extended Unstiffened End Plate Moment Connections

by
Chemin Lim

A dissertation submitted to the Graduate Faculty of
North Carolina State University
in partial fulfillment of the
requirements for the Degree of
Doctor of Philosophy

Civil Engineering

Raleigh, North Carolina

2009

APPROVED BY:

Dr. Emmett Sumner Chair of Advisory Committee Civil Engineering	Dr. Sami Rizkalla Co-Chair of Advisory Committee Civil Engineering
Dr. Tasnim Hassan Advisory Committee Civil Engineering	Dr. Jeffrey Eischen Advisory Committee Mechanical & Aerospace Engineering

BIOGRAPHY

Chemin Lim received his Bachelor of Science degree with Civil Engineering in 1998 from the Kyungwon University. Following the completion of this degree, he then served the Korean Army by the Field Engineer Officer during 28 month. In 2003, he received his Master of Science in Civil Engineering from the Ajou University. Following the completion of this degree, he then moved to North Carolina to pursue his PhD degree in 2004 summer.

ACKNOWLEDGEMENTS

Most of all, I give thanks to my sincere God for his working. Since "***I can do all things through Christ which strengtheneth me.***" (Philippians 4:13)

I would like to express my sincere gratitude to Dr. Emmett Sumner for his guidance and encouragement during the course of research and over the past 5 years. When I became too serious, his humor and friendly sarcasm allowed me to laugh and lightened my perspective. Thanks also to Dr. Sami Rizkalla, Dr. Jeffrey W Eischen, and Dr. Tasnim Hassan for serving on my graduate committee. Dr. Rizkalla was my first advisor and he helped me to start work at the CFL during my first semester in U.S. Despite Dr. Hassan being in his sabbatical year, he always showed interest in my research and advised me. Although Dr. Eischen is not a part of my department, he always showed interest in my research and advised me. I want to acknowledge Dr. Richard Kim for all of his help, support, and mentoring not only in academics but also in life. A great deal of thanks is extended to Jerry Atkinson, Johnathan McEntire, Greg Lucier, and my friend Bill Dunleavy for their help in the laboratory with the many hours of experimental testing.

It has been a long journey and I could not have come this far without the assistance of my family. I want to express my deepest appreciation to them. My parents, Imtaek Lim and Yuja Bae, have always believed in me and helped me reach my goals. Their support forged my desire to achieve all that I could in life. I owe them everything and wish I could show them just how much I love and appreciate them. My wife, Jinyoung Shim, whose love and encouragement allowed me to finish this journey, already has my heart so I will just give her a heartfelt “thanks".

TABLE OF CONTENTS

LIST OF FIGURES

LIST OF TABLES

Chapter 1 Introduction

1.1 Introduction

After the 1950s, vast research was conducted in the field of fully restrained moment resisting frames under seismic loading. In recent years it has become a dominant type of seismic resisting building system. Moment resisting frames have utilized several types of connections including riveted, bolted, and welded connections. The, bolted web welded flange (BWWF) connections and end plate moment connections (EPMC) are two of the most common moment connections in use. The BWWF connections were fabricated with the beam flanges attached directly to the column flanges by full penetration welds and with the beam webs bolted to single plate shear tabs which were welded to the column flange as shown in Figure 1.1 (a). End plate moment connections (EPMC) are composed of a steel plate welded to the end of a beam section with attachment to an adjacent member using fully tensioned high-strength bolts as shown in Figure 1.1 (b).

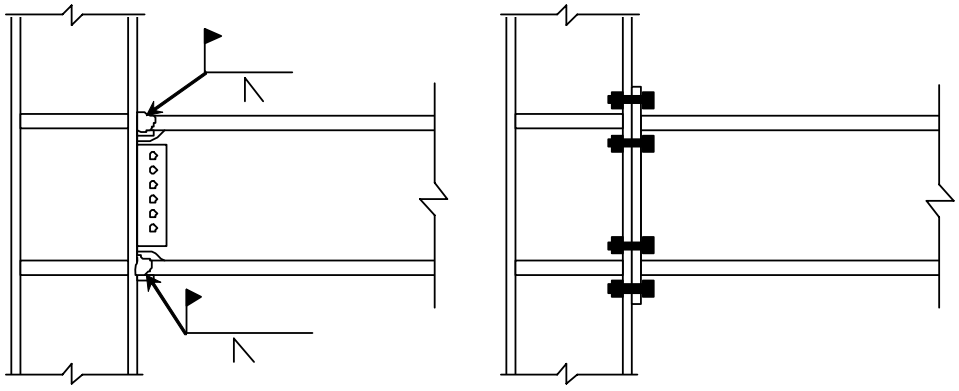

(a) Bolted web welded flange connection (b) End plate moment connection

Figure 1.1 Moment resisting connections

1.2 Statement of Problem

Before the 1994 Northridge earthquake most engineers and researchers believed the BWWF connections provided sufficient ductility to sustain significant seismic loading. However, during the Northridge earthquake almost 150 steel buildings were seriously damaged at the BWWF connections and several exhibited brittle failures. (**FEMA**, 2000a) The SAC Joint Venture which consisted of the Structural Engineers Association of California (**SEAOC**), the Applied Technology Council (**ATC**), and the California Universities for Research in Earthquake Engineering (**CUREE**) conducted extensive analytical and laboratory investigations to verify this unanticipated structure behavior. As a result, failure modes of the connections were classified into four categories based on observed behavior during these investigations. (FEMA, 2000a)

1. Severe stress was occurred at beam flange-column flange weld joint.
2. Inappropriate design, joint material discontinuity.
3. Poor quality field welding, low toughness of weld material.
4. Low cycle fatigue originated from strain concentration.

To address the observed failures, several alternative connection methods were investigated as a part of the SAC steel project. The EPMC received attention because it was shown to provide sufficient energy dissipation capacity, ductility, and several advantages. (AISC, 2004)

The advantages of EPMC are:

1. The connection is suitable for winter erection in that only field bolting is required.
2. All welding is done in the shop, eliminating problems associated with field welding.
3. Without the need for field welding, the erection process is relatively fast and generally inexpensive.
4. If fabrication is accurate, it is easy to maintain plumbness of the frame.
5. Competitive total installed cost, for most cases.

As a result of the SAC steel project, the two configurations of the EPMC (four bolt extended and eight bolt extended stiffened) were prequalified by the American Institute of Steel Construction (AISC) for use as rigid connections in moment resisting frames constructed in high seismic regions. However, a third configuration (four bolts wide extended) that was investigated as a part of the SAC steel project did not exhibit acceptable strength and ductility and was not prequalified by AISC. The four bolts wide extended end plate connection tests resulted low cycle fatigue failure as indicated by the ductile tearing of the end plate in the heat affected zone (HAZ) at the beam flange to end-plate weld (Sumner, 2003). Although this failure mode was identified, no further research has conducted on this connection configuration. Further investigation of this failure mechanism as it relates to EPMC is the focus of

this proposed research.

The low cycle fatigue (LCF) concept is originated from the mechanical research on brittle failure of high temperature and high pressure vessels under cyclic loading (Coffin, 1954). It was developed not only to explain the observed behavior characteristics but also to predict the accumulation of damage. This concept has been applied to the design of moment resisting frames from the 1970s (Butcher, 1970) and several research studies on the LCF behavior of BWWF connections under cyclic loading have been conducted. While the research on the behavior of end plate moment connections (EPMC) under cyclic loading has been conducted very little information on the LCF behavior is available.

1.3 Objective of the Study

The primary objectives of this study are to: (i) investigate critical geometric and material parameters for EPMCs on the LCF life of the connections; (ii) evaluate the accumulation of LCF damage so that the LCF life can be predicted. These objectives will be accomplished through analytical modeling and experimental testing of end plate moment connections and related connection details.

1.4 Scope of Dissertation

The scope of this research includes total 8 experimental tests conducted in three phases. Four reduced end plate moment connections (T-stub connections) were tested to verify the elastic range of the connection system and general behavior of the connection. In the second phase, three different levels of constant peak displacement loadings were applied to three full scale end plate moment connections. The results

from this phase are used to develop a LCF model using Coffin-Manson's equation (Coffin, 1954). In the last phase, an accumulated damage model was evaluated by one full scale end plate moment connection test using random loading. In order to develop the accumulated damage model, Miner's rule (Manson 1958) was adopted. In all phases, three-dimensional finite element numerical analysis and theoretical analysis were used to predict the experimental behavior. Figure 1.2 presents the procedure of study. The experimental tests were designed and tested at the Constructed Facilities Laboratory.

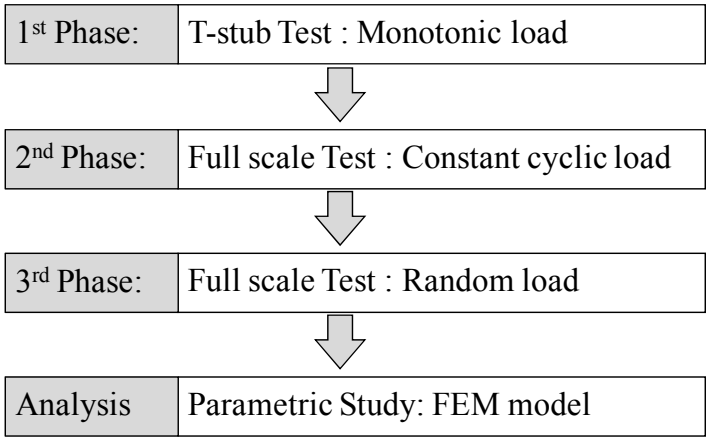

Figure 1.2 Procedure of study

Past research related to the investigation of LCF life has shown that seven to ten specimens are required to determine the low cycle fatigue model for a metallic material (ASTM, 1969). Due to the large number of material and geometric parameters related to EPMCs, testing seven to ten specimens of each configuration is not reasonable. A more cost effective way to simulate the behavior of the end-plate connection is through the testing of bolted T-stub specimens. The T-stub specimens were fabricated with two steel plates, one to simulate the end plate and the other to

simulate the beam flange. This method has been successfully used for many years in the investigation of EPMCs.

Three-dimensional finite element analysis was used to assist in the design of the test specimens. After the FEM model was verified with experimental test result, FEM simulation was utilized to extend the range of geometric parameters investigated. Analytical investigation was conducted through application of existing LCF models and damage accumulation prediction models to evaluate their accuracy. A modification to the LCF and damage accumulation models was developed as appropriate.

1.5 Outline of Dissertation

This dissertation consists of six chapters. It is started with an introduction of study which includes object of study and scope of dissertation. Literature review is described into chapter 2. The body of dissertation is consisted with three journal paper style chapters. Chapter 3 covers reduced end plate moment connection as pre-analysis. Chapter 4 covers low cycle fatigue model development and evaluation of low cycle fatigue damage for full scale four bolts extended unstiffened end plate moment connection (4E EPMC). Chapter 5 covers the parametric study of 4E EPMC with critical parameters. The last chapter is a summary and conclusions the dissertation.

Chapter 2 Background

2.1 Overview

As the welding techniques have improved, structural welding became widely used in construction industry in the late 1950s. Since bolted web welled flange connection was studied by Lehigh University in 1950s and University of California at Berkeley in 1960s, many building industries have adopted this connection method as their primary moment, beam-column, connection. This new skill translated the flange connection method from bolted or riveted to a welded connection. Figure 2.1 shows a typical BWWF connection which was used for beam-column moment connections for seismic design before the Northridge earthquake in 1994.

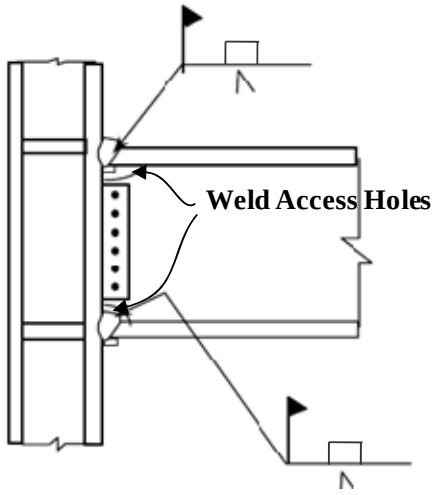

Figure 2.1 Typical welded moment-resisting connection prior to 1994 (FEMA 1997)

On January 17, 1994, an earthquake in Northridge, California caused extensive damage to variety steel structures. The primary damage was to moment resisting frame connections. Almost 150 buildings and a vast range of connections were

damaged. Many of the failures were due to prattle fracture in the connection region. These unanticipated brittle fractures highlighted the need to study for this failure mechanism.

The need, investigation and resolution of the Northridge earthquake damage, convened an international workshop in Los Angeles (SAC, 1994). This investigation was coordinated by the SAC Joint Venture, the American Iron and Steel Institute and National Institute of Standards and Technology.

At the first phase of investigation, "the development of FEMA-267- Interim Guidelines: Evaluation, Repair, Modification, and Design of Welded Steel Moment Frame Structures" was published as the result of investigation. Then the second phase of the SAC steel project started at September 1995, the SAC Joint Venture continued the research which focuses on moment resisting steel frames and various moment connections. As this research result, FEMA-350- *Recommended Seismic Design Criteria for New Steel Moment-Frame Building,* 351- *Recommended Seismic Evaluation and Upgrade Criteria for Existing Welded Steel Moment-Frame Building*, 352- *Recommended Post earthquake Evaluation and Repair Criteria for Welded Steel Moment-Frame Building*, 353- *Recommended Specifications and Quality Assurance Guidelines for Steel Moment-Frame Construction for Seismic Applications*, 355A- *State of the Art Report on Base Metals and Fracture*, 355B- *State of the Art Report on Welding and Inspection*, 355C- *State of the Art Report on Systems Performance of steel Moment Frames Subject to Earthquake Ground shaking*, 355D- *State of the Art Report on connection Performance,* 355E- *State of the Art Report on Past Performance of Steel Moment-Frame Buildings in Earthquakes* and 355F- *State of the Art Report on Performance Prediction and Evaluation of Steel Moment-Frame*

Buildings" were published (FEMA 2000a, 2000b).

As a result of the SAC research, one of the main reasons of ductile failure on moment connection was low-cycle fatigue failure. "Depending on their geometry, severe strain concentrations can occur in the beam flange at the toe of these weld access holes. These strain concentrations can result in low-cycle fatigue and the initiation of ductile tearing of the beam flanges after only a few cycles of moderate plastic deformation". (FEMA-351, 2000) In structures with low-toughness welds, girder flange cracking within the heat-affected zone can occur as an extension of brittle fractures that initiate in the weld root. This is particularly likely to occur at connections in which improper welding procedure were followed, resulting in a brittle heat-affected zone. However, these fractures can also occur in connections with tough welded joints (made following appropriate procedures), as a result of low-cycle fatigue, exacerbated by the high stress concentrations that occur at the toe of the weld access hole, in unreinforced beam-column connections. Like the visually similar type "outside of Heat Affected Zone(HAZ) beam flange damage" which can also result from low-cycle fatigue conditions at the toe of the weld access hole, it results in a complete loss of flange tensile capacity, and consequently significant reduction in the contribution to frame lateral strength and stiffness from the connection" (FEMA 351)

This literature review is presented in four main sections. The first section provides an overview of the study background. The definition and theory of the low cycle fatigue are reviewed. The third section provides the overview study of end plate moment connection. It includes the modeling techniques to predict the behavior of end plate moment connection using analytical and finite element methods. Finally, other moment connection studies of low cycle fatigue are discussed.

2.2 Low Cycle Fatigue Life

2.2.1 Low cycle fatigue

The definition of fatigue life is the number of load cycles it takes to produce a failure (usually a fracture) within the specimen or member. If the fatigue life is relatively short, less than ten thousand cycles, then the failure is considered a low cycle fatigue (LCF) failure. In steel structures, low cycle fatigue failures are typically observed when the applied load cycles produce large plastic strains within the specimen. To produce failure in a few cycles, strain (displacement) rather than stress (load) must be controlled. From 1950s, many researchers were interested in cyclic strain rather than cyclic stress because the need of information on metals when subjected to relatively few cycles of controlled cyclic strain. Coffin and Manson (1950s) first developed for Low Cycle Fatigue problems, gas turbines and nuclear reactors. (Coffin, 1954) They interested in thermal loading caused large plastic strain and very short fatigue lives. And they determined a power relationship existed between plastic strain amplitude and fatigue life. The method refined in 1960s (Morrow, 1965, Neuber, 1961) to deal with wider variety of fatigue situations.

Know as Load-Life power equation (Equation 2-1), this simple equation is common model in fatigue life. Since it is basic mathematic equation, there is no underlying theoretical justification.

$$Load = A(life)^{B} \qquad \textbf{Equation 2-1}$$

Where load can be defined in stress, strain or actual load and life can be defined in cycles, reversals or events. Constant A and B is a certain set of parameters depend on material, structural feature, type of weld joint, etc.

Basquin (1910) developed the load-life power equation for stress range material fatigue life. (Equation 2-2)

$$S_a = A(N_f)^B \qquad \textbf{Equation 2-2}$$

Where, S_a is the stress amplitude, b is the slope, and N_f is number of reversal. When both axes have logarithmic scales, Basquin's equation becomes a straight line is strain amplitude. Basquin was looking for a universal exponent B with a coefficient A related to tensile strength. For a wide variety of metals Basquin showed that the exponent rages from -0.05 to -0.12. However, this equation was primary used for high cycle fatigue.

Coffin and Manson (1950) proposed that the fatigue life could be explicitly related to the plastic strain amplitude. Where the stress is high enough for plastic deformation to occur, the account in terms of stress is less useful and the strain in the material offers a simpler description. Low-cycle fatigue is usually characterized by the *Coffin-Manson relation* (popularized by L. F. Coffin in 1979 based on S. S. Manson's 1960 work). Mathematically, the expression may be written as:

$$\varepsilon_{ap} = \varepsilon'_f (2N_f)^C \qquad \textbf{Equation 2-3}$$

Where, $\varepsilon_{ap} = \Delta\varepsilon_p / 2$, the plastic strain amplitude is half width of the hysteresis loop. ε'_f is an empirical constant known as the *fatigue ductility coefficient*, the failure strain for a single reversal. C is an empirical constant known as the *fatigue ductility exponent*, commonly ranging from -0.5 to -0.7 for metals. It can be calculated from experimental data using the least square fit procedure if the experimental data are plotted in a log ($\Delta\varepsilon_p / 2$) and log ($2N_f$). 2*N* is the number of reversals to failure (*N* cycles).

Strain-life equation (Equation 2-4) was work done by Landgraf, Morrow, and Endo (Landgraf, 1969). It combined and improved the Basquin, elastic range, and Coffin-Manson, plastic range, equation.

$$\frac{\Delta\varepsilon}{2} = \frac{\sigma'_f}{E}(2N_f)^b + \varepsilon'_f(2N_f)^C \qquad \textbf{Equation 2-4}$$

Where $\Delta\varepsilon/2$ is strain amplitude (load parameter). $2N_f$ is fatigue life in reversals. E is modulus of elasticity. σ'_f is fatigue strength coefficient. b is fatigue strength exponent. ε'_f is fatigue ductility coefficient. c is fatigue ductility exponent.

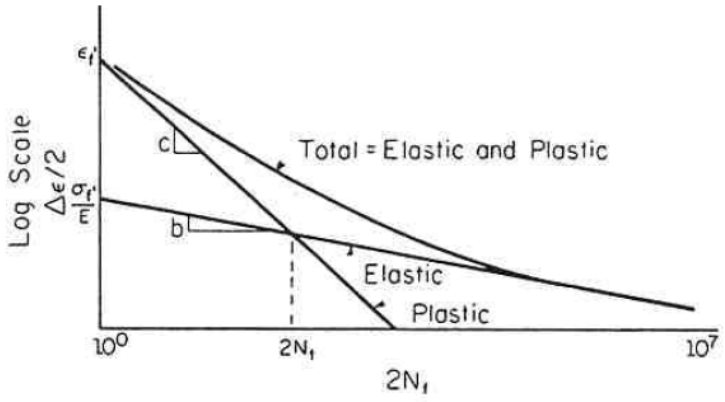

Figure 2.2 Total elastic and plastic strain components stain-life curves (Fuchs 1980)

In the Figure 2.1, it can be observed that for a given life N, the total strain is the sum of the elastic and plastic strains. Both the elastic and plastic curves can be approximated as straight lines. At short fatigue lives, low cycle fatigue, plastic stains dominate and at long fatigue lives, high cycle fatigue, elastic strains dominate the fatigue life. This method allows for the characterization of fatigue properties for a material throughout the entire life range.

2.2.2 Linear damage rule

To verify the damage of the system under variable loading, the Linear Damage Rule was first proposed by Palmgren in 1924 and was further developed by Miner in 1945. Today the method is commonly known as Miner's Rule. The Linear Damage Rule is based on the concept of fatigue damage (Equation 2-5). A damage fraction, D, is defined as the fraction of life used up by an event or a series of events. Failure is predicted to occur when the sum of D_i reaches unity.

$$\sum_{i=1}^{I} D_i = X \qquad \textbf{Equation 2-5}$$

where, i is index of each set of applied load cycles at constant stress level $S_{i,}$,D_i is damage fraction accumulated during the load cycles of interval i at constant stress level $S_{i,}$, and X is damage criterion (a constant).

The Linear Damage Rule states that the damage fraction at a given constant stress level S_i is equal to the number of applied cycles n at stress level S_i divided by the fatigue life N at stress level S_i. (Equation 2-6)

$$D_i = \frac{n_i}{N_i} \qquad \textbf{Equation 2-6}$$

where, D_i is damage fraction accumulated during the load cycles of interval i at constant stress level S_i , Ni is number of applied load cycles at constant stress level S_i , and Ni is fatigue life at constant stress level S_i, obtained from the S-N curve.

For Miner's Rule, the damage criterion X is assumed to be equal to 1.0, and failure is predicted to occur when the damage fraction reach at 1. (Equation 2-7)

$$\sum_{i=1}^{I} \frac{n_i}{N_i} \geq 1 \qquad \textbf{Equation 2-7}$$

Considerable test data has been generated in an attempt to verify Miner's Rule. Most

test cases use a two step load history. This involves testing at an initial stress level S_1 for a certain number of cycles, and then the stress level is changed to a second level S_2 until failure occurs. If $S_1 > S_2$, it is called a high-low test, and if $S_1 < S_2$, a low-high test. The results of Miner's original tests showed that the damage criterion X corresponding to failure ranged from 0.61 to 1.45. Other researchers have shown variations as large as 0.18 to 23.0, with most results tending to fall between 0.5 and 2.0. In most cases, the average value is close to Miner's proposed value of 1.0.

One problem with two-level step tests is that they do not accurately represent many service load histories. Most load histories do not follow any step arrangement and instead are made up of a random distribution of loads of various magnitudes. However, tests using random histories with several stress levels show good correlation with Miner's rule. Even so, for conservative estimates of the life of a structure an X value of less than 1.0 is usually used.

The Linear Damage Rule has two main shortcomings when it comes to describing observed material behavior. First, load sequence effects are ignored. The theory predicts that the damage caused by a stress cycle is independent of where it occurs in the load history. An example of this discrepancy was discussed earlier regarding high-low and low-high tests. Second, the rate of damage accumulation is independent of the stress level. This trend does not correspond to observed behavior. At high strain amplitudes cracks will initiate in a few cycles, whereas at low strain amplitudes almost all the life is spent initiating a crack (i.e., very little propagation fatigue).

Despite these limitations, the Linear Damage Rule is still widely used. This is due both to its simplicity and the fact that more sophisticated methods do not always result in better predictions.

2.3 End Plate Connections

One of the common connection types in moment resisting frame building is end plate moment connection (EPMC). From the early 1960's, EPMC has been used to connect beam to column or beam to beam. Originally, it was developed from the tee stub connection study. EPMC is composed of a steel plate welded to the end of the beam section with attachment to an adjacent member using rows of high strength bolts. There are two types of end plate moment connections: flush type, Figure 2.3 (a), and extended type, Figure 2.3 (b). The main differences are the position of bolt and end plate geometry. In the flush end plate connection, the bolt is located inside of beam flange wide and the end plate does not extended beyond the beam cross section. In the extended end plate connection, the bolt can be located outside of beam flange wide and the end plate does extend beyond the beam cross section.

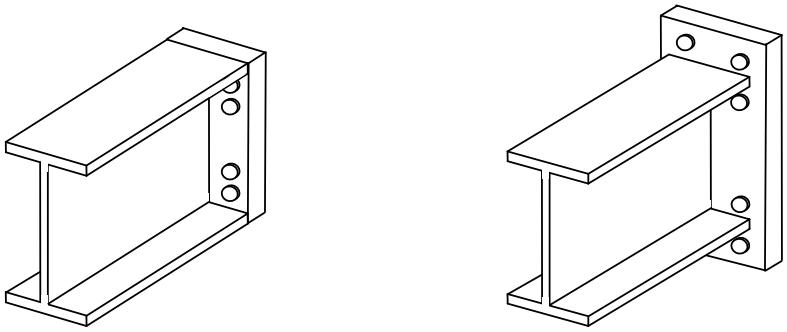

(a) Flush type (b) Extended type

Figure 2.3 End plate moment connections

2.3.1 EPMC Design

Certain configurations of end plate moment connection design procedures are presented in the AISC Manual of Steel Construction (AISC, 2005), AISC Steel Design Guide Series number 16 (AISC, 2002), and AISC Steel Design Guide Series

number 4 (AISC, 2003). The AISC manual includes four-bolt extended and the eight-bolt extended stiffened end plate moment connection configurations design procedures under static loading. The AISC design guide number 16 includes nine types of end plate connections configurations. The AISC manual and design guide number 16 covered only static loading but the AISC design guide number 4 is developed to cover seismic loading.

The two main limit states controlling the design of end plate in EPMC are end plate flexural yielding and bolt tension rupture. Extensive studies have been conducted in the past on the analysis and design of EPMC using these limits states. The early studies neglected the prying action in the end plate design procedure. After Kennedy et al. (1981) introduced the "split-tee analogy" to determine the bolt forces including prying action, numerous design procedures adopted and further developed Kennedy's method. From these studies, Srouji et al. (1983) reported the unification design procedure using the yield line theory for end plate yielding and Kennedy method for bolt failure. Hendrick et al. (1984), Morrison et al. (1985), Murray (1993), Borgsmiller (1995), Meng (1996), and Sumner (2000) developed the design procedure to variety type of EPMC and loading type. These results were used to develop the AISC design guides.

Yield line theory was first introduced to analyze plate or slab structure. The yield line theory is similar with a plastic design theory because the elastic deformations are negligible compared to the plastic deformations. With this procedure it is assumed that the yield lines divide the plate or slab into rigid plane regions. Therefore a yield line is a continuous formation of plastic hinges along an expected collapse mechanism line. The failure mechanism is assumed to exist when the yield lines form a

kinematically valid collapse mechanism, and this mechanism lines form is called by yield line pattern. Srouji (Srouji et al. 1983) suggests three guidelines to establish the yield line in the steel plate.

1. Axes of rotation generally lie along lines of support.
2. Yield lines pass through the intersection of the axes of rotation of adjacent plate segments.
3. Along a yield line, the bending moment is assumed to be constant and equal to the plastic moment of the plate.

The analysis of a yield-line mechanism can be performed by two different methods. One is the equilibrium method and the other is virtual work (energy method). For a specified yield-line pattern and loading, a certain plastic moment will be required along the hinge lines. To determine the required plastic moment capacity or the failure load, an arbitrary succession of possible yield-line mechanisms must be selected. The internal energy stored by a yield-line mechanism can be written as Equation 2-8 (Srouji et al., 1983).

$$W_i = \sum_{n=1}^{N} (m_{px}\theta_{nx}L_x + m_{py}\theta_{ny}L_y) \qquad \textbf{Equation 2-8}$$

Where N is the number of yield lines in the mechanism θ_n is the relative rotation of line n, and L is the element length of line n.

The external work done due to a unit displacement at the top of the beam flange

$$W_e = M_u\theta \qquad \textbf{Equation 2-9}$$

Figure 2.4 shows the example of yield line pattern and virtual displacement of EPMC.

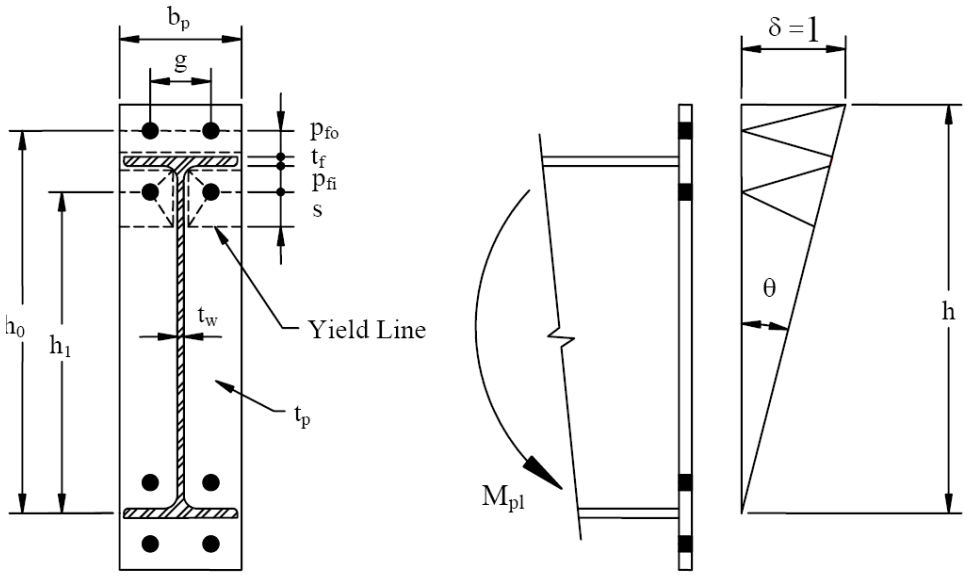

Figure 2.4 Yield line pattern and virtual displacement of a four bolt extended unstiffened connection (Sumner, 2003)

The yield line analysis procedures do not include the bolt forces if prying action is to be considered. Therefore, it was necessary to use a different method to obtain the desired bolt forces. Kennedy et al. (1981) introduced a method to predict bolt forces with prying action for tee stub connections. The basic assumption in the method is that the end plate identifies three stages behavior (Figure 2.5). In the first stage, the plastic hinge does not form into the plate and the prying action does not occur. Its behavior is termed **thick** plate behavior and the prying force, Q, is assumed to be zero. As the applied load increases, two plastic hinges form in the base of loading plate. Its behavior is termed **intermediate** plate behavior and the prying forces are present. The third stage begins when a second plastic hinge forms at the bolt line. The plate in that stage is called **thin** plate behavior and the prying forces are at a maximum.

Srouji (1983), Hendrick (1984, 1985), Morrison (1984, 1985), and Borgsmiller (1995) use a modified Kennedy approach to predict the bolt forces in different type of EPMC.

And their analytical results and experimental result showed good correlation.

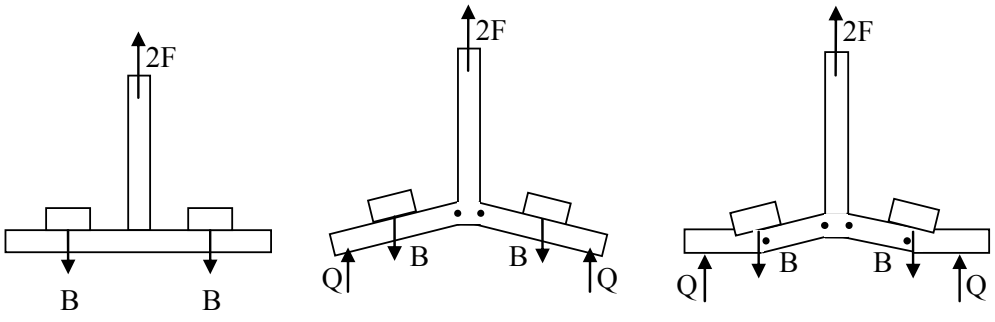

(a) Thick (b) Intermediate (c) Thin

Figure 2.5 Three stages of plate behavior

2.3.2 Finite element analysis

End-plate connections usually fail due to plate plasticity in plate bending and shear, bolt or weld fracture, column web shear failure, and/or excessive plasticity of the column flange in bending. Therefore the behavior of the connection represents a complex and indeterminate analytical problem with a large number of parameters affecting its structural behavior. Due to the limitation of the computer resource, the finite element analysis started with simply 2-D model and linear material properties with static loading. From the late 1970s, the finite element analysis adopted 3-D model to predict accurate the nonlinearity of material and structural behavior. A large number of studies were conducted to develop the accurate finite element model using different type of modeling concept.

Krishnamurthy and Graddy (1976) compared the 2-D analysis and 3-D analysis result to check the correlation characteristic to predict 3-D values form corresponding 2-D results. They reported the results of thirteen finite element analyses of 2-D and 3-D end plate connections that showed reasonable correlations. Rothert and Gebbeken

(1992) reported the study of the numerical tool, finite element modeling method, considering plastic behavior of the end plate moment connection. This study conducts the material nonlinearity, pretension effect, multi-body contact problem, and example of end plate connection. The load-deformation result showed good relationship with experimental result. Sherbourne and Bahaari (1994) developed 3-D finite element model of end plate connections using commercial code "ANSYS". The end plate, beam, column, and stiffeners were represented as plate, plastic quadrilateral shell, elements. The bolt shank was modeled using six spar elements. Bose, Wang, and Sarkar (1997) reported the results of an investigation devoted to the analysis of unstiffened flush end-plate bolted connection using the finite element technique. They used the commercial program "LUSAS" to analyze the nonlinear 3-D finite element model. The study included six experimental tests and its results showed good relationship with numerical test results. Bursi and Jaspart (1997) used the finite element method to analyze four bolt unstiffened extended moment end plate connections under static loading. The finite element results were compared to an experimental study. The bolt and bolt head were modeled using beam element. The end-plate and beam element were eight node brick elements which included plasticity. Contact elements were adopted to describe the interaction between the end plate and the column flange. The finite element model was validated by experimental testing. Bahaari and Sherbourne (2000) conducted 3-D finite element analysis devoted to the analysis of eight bolt extended end plate connections. They used plate, brick and truss elements to create the 3-D finite element model using the commercial program "ANSYS". The model was examined for three experimental case studies in the literature and the results compare well with experimental data in terms of both

strength and stiffness. Mays (2000) developed a design procedure for the sixteen bolt extended stiffened end plate connections using the finite element method. The study included a parametric study of the four bolt wide connection to better understand the complex interaction between end plate bending, prying forces, and bolt behavior. Sumner (2003) conducted twenty experimental tests and conducted finite element analysis to develop design procedures for eight extended end plate moment connection configurations subject to seismic loading. The finite element model used two element types. The solid eight node brick elements were used to model the beam flanges and web and solid twenty node brick elements were used to model the end plate and column flange, and bolts. The analysis considered plasticity effects but the bolt pretension effect was neglected. The finite element results correlated well with the experimental results. Adany and Dunai (2004) discussed the finite element modeling and analysis technique of end plate joints in steel frames, under monotonic and cyclic loading conditions. This study didn't include the low cycle fatigue effect but suggested some of modeling guideline for cyclic loading analysis.

2.3.3 EPMC Cyclic tests

End plate moment connections (EPMC) have several advantages over the conventional connections. One of the primary advantages is that the end plate to beam flange weld is performed in the fabrication shop. This typically results in higher quality control of the welding process. Many research studies have investigated the strength of end plate moment connections (EPMC) subject to monotonic static loading. However, a very limited number of studies have been conducted on the behavior of EPMC subject to cyclic loading.

The early research studies on EPMCs were conducted to verify moment capacity prediction, overall connection behavior, bolt prying forces, bolt behavior, and weld behavior. As the focus moving on seismic behavior, end plate connection was first tested under cyclic loading in the late 1980's. Popov and Tsai (1989) reported that the fully welded connection (web welded and flange welded) and the extended end plate moment connection had similar hysteretic moment rotation behavior. Both connection types exhibited more ductility, beam plastic rotation, than the bolted web welded flange connection. In addition, they concluded that the EPMC exhibited excellent energy dissipation characteristics. Korol, Ghobarah and Osman (1990) found that excessive yielding of the column flange, relatively thin column flange, made more prone to low-cycle fatigue and result in severe damage. They showed the end plate moment connection had enough energy dissipation without substantial loss of strength for seismic loading and proposed quantitative procedures for the design of seismic end-plate connections. Adey, Grondin and Cheng (1997) reported the use of extension stiffeners and relaxed bolt provided more energy dissipation and connection ductility. Several proposed end plate thickness prediction equation were evaluated by comparing test results and proposed new prediction equation. Ballio, Calado, and Castiglioni(1997) conducted experimental study of low cycle fatigue behavior of steel beam and column member . One of the seven type specimens was extended end plate moment connection. The study showed the proposed approach, S-N curve fatigue model using Minor's rule, could be used to predict the behavior of the low cycle fatigue behavior of structure connection member. The European project dealing with the "Reliability of moment resistant connections of steel building frames in seismic areas" reported eight countries co-work final report between 1997 and 1999 within the

INCO-Copernicus joint research projects of the 4th Framework Program. (RECOS, 2000) The project conducted extensive analytical and laboratory investigations to improve their seismic codes (Eurocode 8). The research reported the overall cyclic behavior of end plate moment connection (such as the influence of the strain rate on the cyclic behavior of end plate moment connection, low cycle fatigue approach, ductility, etc) and the results showed the end plate moment connection could be used in seismic area. Sumner and Murray (2002) conducted seven full-size extended end-plate moment connection tests under cyclic loading using six bare steel beam-to-column connections and one composite slab beam-to-column connection. They reported extended end-plate moment connections can be designed to be suitable for use in seismic force resisting moment frames, Bursi, Ferrario, and Fontanari (2002) focused on the low-cycle fracture behavior of Tee stub connections that are same elemental components of extended end plate connection with partial fillet welds. It showed good correlation between experimental results and FE model simulation results.

2.4 Other Bolted Connection LCF

A significant amount of research has been conducted on the bolted web welded flange moment connections since it has been widely used in construction industry since the late 1950s. The unexpected connection failures due to the Northridge earthquake brought about a large amount of additional research related to the BWWF connection. Krawinkler and Popov (1982) suggested developing mathematical models that permit the prediction of low cycle fatigue life for random deformation histories. It used the Miner rule, linear damage accumulation theory, and Manson-Coffin equation;

prediction of the low cycle fatigue life. Kuwamura and Suzuki (1992) conducted seven beam-to-column connection tests to verify a heat-treated 600-MPa tensile-strength grade steel ductile characteristic using low cycle fatigue test protocol. Kuwamura and Suzuki formulated energy dissipation capacity equation using least squares method. Kaufmann, Fisher, Julio, and Gross (1997) evaluated the damage of welded steel moment frame connection in the Northridge earthquake. They conducted sample connection test using simulated ground motion spectra for each building site and compared to the fracture analysis model. Richard, Allen and Partridge (2001) evaluated the fracture modes and the accumulated seismic connection damage of three different type connections, Slotted Web (SW), Dog bone (RBS) and Pre-Northridge (pre-N) connection, using stress concentration factors and accumulated damage model. It was same procedure what Krawinkler and Popov (1982) suggested. They modeled the mathematical model (Manson-Coffin equation) using experimental results, a series of constant-displacement low-cycle fatigue test, and applied linear damage accumulation theory (Miner rule) to predict seismic fatigue life. Stojadinovic (2002)

Recent years, variety bolted connection tests have been conducted to evaluate LCF behavior. These research studies have utilized different types of connections but the failure mechanism and analysis procedures were similar. Schneider and Teeraparbwong (2002) classified four different mechanism of stable inelastic behavior: panel zone distortion, bolt-slip, flange plate hinging, and girder hinging. The test result reported that the bolted flange plate connection absorbed a significant amount of inelastic energy, i.e. it had sufficient energy dissipation. And bolt slip was generally the first source of inelastic energy dissipation. Garlock, Ricles and Sause (2003) determined how the parameters, angle size, gage length, and washer plate,

were affect the connection stiffness, strength, energy dissipation capability, and resistance to low-cycle fatigue. They determined that the ratio of gage length per plate thickness was governed the low-cycle fatigue resistance. Smaller ratios dissipate more energy for a given deformation i.e. less resistance to low-cycle fatigue. Xu and Kasai, (2003) verified inelastic cyclic behavior of bolted T-stub connections. They compared with deformation based and energy based low cycle fatigue models based on Miner's rules using different displacement loading; constant peak displacement loading, shifted peak displacement loading, increased loading, reversed loading, and decreased loading. The deformation-based Miner's rule was applicable to the increased loading case only, but the energy-based Miner's rule was suitable for all load cases. Matteis, Corte, Mandara, and Mazzolani (2004) conducted tests on welded aluminum alloy T-stubs. They found that when the bolt strength was large enough, the failure mechanism occurred at the root of the weld in the plate section. They reported that the cyclic tests generally gave rise to a structural performance lower than the monotonic tests due to low cycle fatigue. And the damaging effect due to low cycle fatigue was limited for specimens collapsing due to bolt failure.

2.5 Need for Future Research

The low cycle fatigue concept has been developed through the extensive research and it has been used to predict the life of structures subject the cyclic load. In the design of a few structural connections, the low cycle fatigue concept has been adopted. However, very little research has been conducted on the bolted connections LCF strength life like the end plate moment connection.

Because the lack of research on end plate moment connection LCF behavior, further

research of the LCF behavior that determine the general LCF behavior on EPMC is needed. The need for developing the LCF model that utilizes a damage prediction of end plate moment connections is apparent.

The literature shows the recent three dimensional finite element method can be used to simulate the cyclic end plate moment connection accurately. Parametric study can adopt the FEM for researching that characterized the low cycle fatigue behavior on end plate moment connection. Developing the accurate FEM model that simulates the end plate moment connection is needed.

Chapter 3 Experimental Program I: T-stub Model

3.1 Introduction

The structural steel moment resisting frame system is one of the most popular and efficient building structural systems. If the beam to column connections are engineered to induce ductile behavior, the system can provide resistance lateral movements. However, during the Northridge earthquake in 1994 almost 150 structural steel buildings were seriously damaged and several exhibited brittle failures. (FEMA, 2000a) After extensive investigation of the unanticipated brittle failure, the SAC Joint Venture concluded that the discontinuity of material, stress concentration, and low cycle fatigue was the main reason for the failures. To address the observed failures, several alternative connection methods were investigated as a part of the SAC steel project.

The end plate moment connection (EPMC) is one of the selected alternative connections. Much of the previous work on EPMCs analyzed the failure of the entire connection and it made difficult to determine the detail connection performance. Therefore, the T-stub model which has widely used for reduced end plate moment connection from 1975 (Murray, 1988). Because the most LCF fracture occurred into the end plate (Bursi 2000, Garlock 2003, Kasai 2003), also the T-stub is a reasonable reduced end plate moment connection for low cycle fatigue analysis. Figure 3.1 illustrates the adopted specimen for this research.

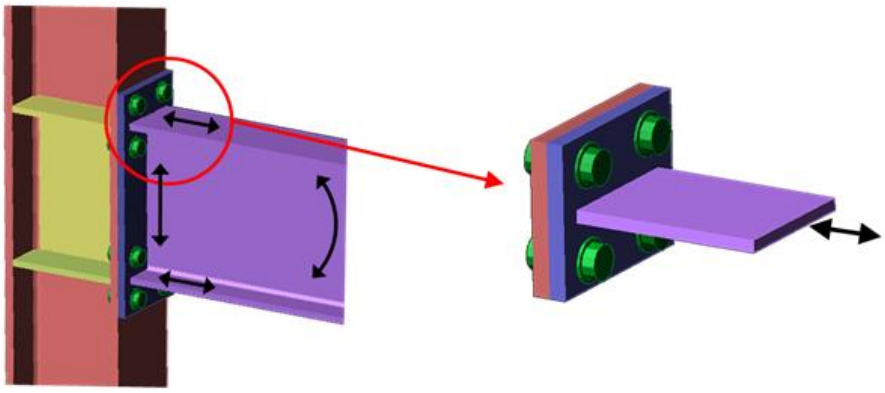

Figure 3.1 Reduced end plate moment connection (T-stub)

The study presented in this paper is part of a larger ongoing research program conducted at the NCSU CFL in Raleigh, NC. to investigate the LCF behavior of the four bolts extended unstiffened EPMC. The research program was divided into three primary tasks; i) validate analytical tools to predict the structural response of reduced EPMC (T-stub); ii) investigate the cyclic LCF behavior of EPMC through experimental tests and analytical modeling; iii) evaluate the accumulation of low cycle fatigue damage so that the structure life can be predicted. The focus of this paper is on details and results of the first task of the larger research program.

The bolted T-stub connections can fail due to plate plasticity in bending and shear, bolt or weld fracture and/or excessive plasticity of the stem plate in bending. Another potential failure mode is low cycle fatigue of the stem or flange plate when subjected to cyclic loading.

The objective of the study is to verify the reduced end plate moment connection model through analytical and experimental study. The analytical investigation included numerical (Finite element) and theoretical (yield line) analysis. In the first part, theoretical analysis will be conducted to determine the yield level of the structure.

In the second part, finite element models will be developed to simulate the experimental test and to verify the theoretical analysis. An experimental investigation will be conducted to validate the theoretical analysis and FEM analysis.

In this study, the component of the shear wall system, T-stub, was tested to define the reduced end plate moment connection behavior characteristic. The tested T-stub specimen is pre-engineered steel shear wall components for use in the StiffWall® Shear Wall System manufactured by The Steel Network, Inc. (TSN). Shear wall components Figure 3.2, are used in light gauge (cold-formed) steel framing to provide lateral strength and stiffness to the structure. The boot, T-stub, in the assembly connects to the vertical framing member, which is a cold-formed stud, while the track connects to the straps that run diagonally across the structure. Then both are anchored together to the floor, slab, or foundation. Acting together, the boot and the track can transfer the lateral forces in a structure to the next component in the load path.

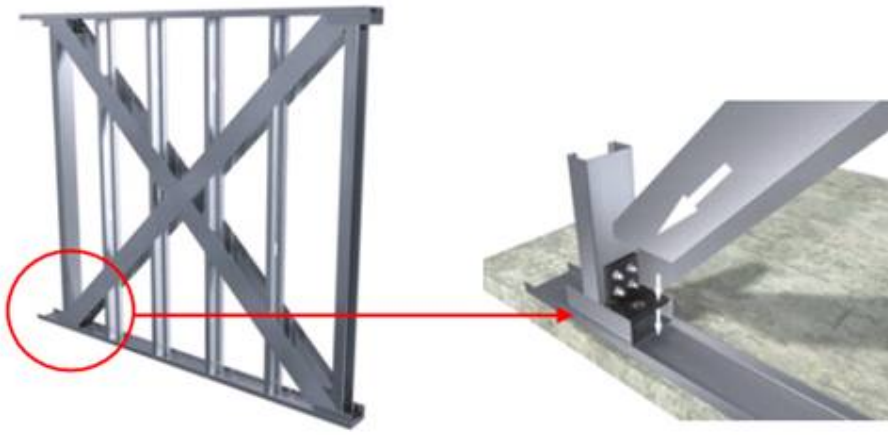

(a) StiffWall® Shear Wall System (b) Boot and Track Assembly

Figure 3.2 Test components

3.2 Theoretical Analysis

The two main limit states controlling the design of end plate are end plate flexural yielding and bolt tension rupture. Extensive studies have been conducted in the past on the analysis and design of EPMC using these limits states. The early studies neglected the prying action in the end plate design procedure. After Kennedy et al. (1981) introduced the "split-tee analogy" to determine the bolt forces including prying action, numerous design procedures adopted and developed Kennedy's method. From these studies, Srouji et al (1983) reported the unification design procedure using the yield line theory for end plate yielding and Kennedy method for bolt failure. Hendrick et al. (1984), Morrison et al. (1985), Murray (1993), Borgsmiller (1995), Meng (1996), and Sumner (2000) developed the design procedure for a variety of EPMC configurations and loading types. These results were used to develop the AISC design guides (AISC, 2002).

3.2.1 Yield line theory

Yield-line theory was first introduced to analyze reinforced concrete slabs. A yield-line is a continuous formation of plastic hinges along a straight or curved line. The failure mechanism of the slab is assumed to exist when the yield-line form a kinematically valid collapse mechanism. Since the elastic deformations are negligible compared to the plastic deformations, it has been proven acceptable to assumed that the yield-lines divide the slab into rigid plane region. Most of the development of this theory is related to reinforced concrete; however, the principles and findings are applicable to steel plates.

The analysis of a yield-line mechanism can be performed by two different methods.

One is the equilibrium method and the other is virtual work (energy method).

For a specified yield-line pattern and loading, a certain plastic moment will be required along the hinge lines. To determine the required plastic moment capacity or the failure load, an arbitrary succession of possible yield-line mechanisms must be selected.

The internal energy stored by a yield-line mechanism

$$W_i = \sum_{n=1}^{N} (m_{px}\theta_{nx}L_x + m_{py}\theta_{ny}L_y) \qquad \textbf{Equation 3-1}$$

Where, m_p is moment capacity per unit length of yield-line, θ_n is the relative rotation of plate on either side of yield-line and L is the length of yield lines.

The external work done due to a unit displacement at the top of the beam flange

$$W_e = F \times Disp.(unit) \qquad \textbf{Equation 3-2}$$

Therefore the equilibrium equation is

$$F \times Disp = \sum_{n=1}^{N} (m_{px}\theta_{nx}\ell_n + m_{py}\theta_{ny}\ell_n) \qquad \textbf{Equation 3-3}$$

One of the important assumptions in the yield line theory is the yield line pattern. Figure 3.3 shows the chosen yield line pattern of T-stub. The yield line pattern was developed based upon the observed behavior in the experimental investigation of the T-stub.

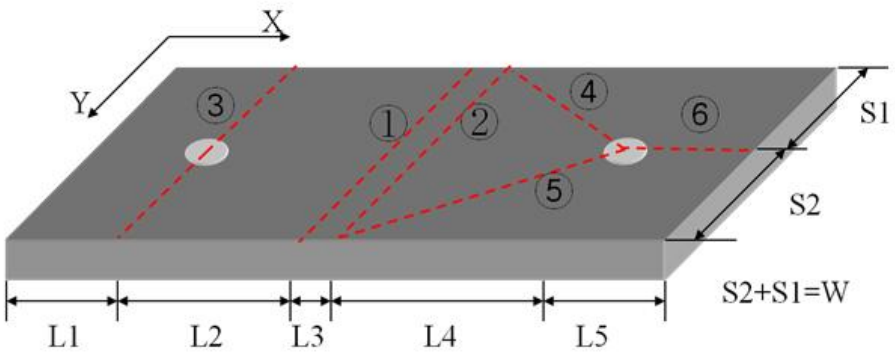

Figure 3.3 Yield-line pattern of T-stub

The final equation of the internal and external work equilibrium is

$$F = m_p \times \left(\frac{2W}{L_2} + \frac{2W}{L_4} + \frac{4L_4}{W} + \frac{4L_5}{W} \right) \qquad \textbf{Equation 3-4}$$

Where $m_p = Z\sigma_y = \frac{t_p^{\,2}}{4}\sigma_y$

t_p is the thickness of the plate and σ_y is the yield strength of plate. The calculated force F, which corresponds with the formation of the yield line mechanism, was calculated with the current research specimen's geometries using Equation 3-4.

3.2.2 Kennedy method

Basic yield-line analysis procedures define the flexural response of the end plate and do not produce any prediction of bolt forces within the connection. Therefore, it was necessary to use the method suggested by Kennedy (1981) estimate the bolt forces due to the applied force and to the effects of prying action. The basic assumption in the method is that the end-plate goes through three different stages of behavior (Figure 3.4). Q is the prying force, the B is bolt resisting force, and F is the loading. During the first stage, plastic hinges have not developed and the plate is referred to as

"thick". The prying force is taken as zero in this stage. When the plastic hinge forms at the beam flange, the plate becomes "intermediate" and the prying force is somewhere between zero and the maximum prying force that can occur. The last stage begins when a second plastic hinge forms at the bolt line. The end-plate in that stage is called "thin" and the prying force is at its maximum.

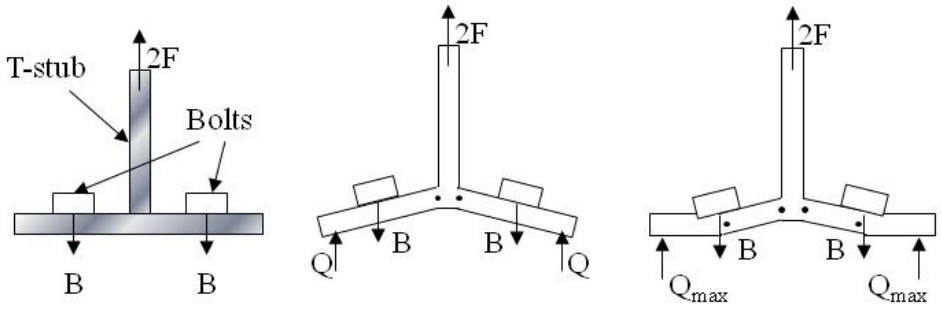

(a) Thick (b) Intermediate (c) Thin

Figure 3.4 Three stages of plate behavior according to Kennedy (Kennedy, 1981)

For the example, if the plate has a thin plate behavior, the Figure 3.5 is the static of the system. M1 and M2 is the moment at the plastic hinge position. Therefore the equations of the moment of equilibrium for the system are in Equation 3-5, Equation 3-6, and Equation 3-7.

$$M_1 = B \times b - Q(a+b) - M_b$$ **Equation 3-5**

$$M_2 = Q \times a$$ **Equation 3-6**

$$F_b \times b - M_b = M_1 + M_2$$ **Equation 3-7**

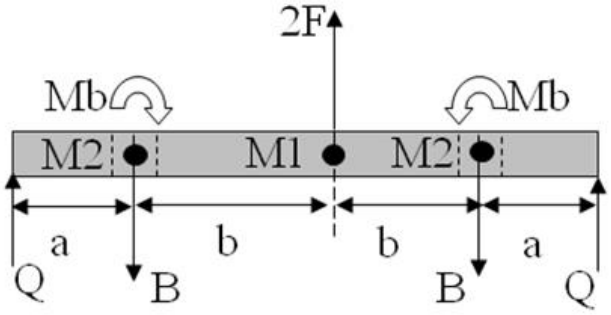

Figure 3.5 Static state of the prying effect on the plate

The general equation for the thin plate behavior plate is

$$F_b \times b - M_b = \frac{wt_p^{\,2}}{4}\sqrt{\sigma_y^{\,2} - 3\left(\frac{F}{wt_p}\right)^2} + \frac{w't_p^{\,2}}{4}\sqrt{\sigma_y^{\,2} - 3\left(\frac{F}{w't_p}\right)^2} \qquad \textbf{Equation 3-8}$$

Where the w is the plate width, w' is the net plate width, t_p is the plate thickness, F is the plate yielding force, σ_y is the strength of the plate.

Therefore, maximum prying force equation is

$$Q_{\max} = \frac{M_p}{a} = \frac{w't_p^{\,2}}{4a}\sqrt{\sigma_y^{\,2} - 3\left(\frac{F}{w't_p}\right)^2} \qquad \textbf{Equation 3-9}$$

3.2.3 Specimen strength predictions

Based on the previous theory, yield line theory and Kennedy method, the strength of T-stub specimen was calculated. Figure 3.6 shows the specimen and its dimensions.

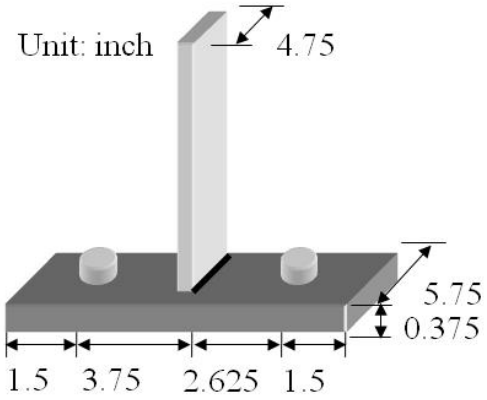

Figure 3.6 T-stub specimen

The plate yield limit was calculated by the Equation 3-4. The plate material was ASTM A572 Grade50 steel and the yield strength of material (σ_y) was 50 ksi. Table 3-1 presents the dimension of plate for Figure 3.3.

Table 3-1 The plate dimension

	L_1	L_2	L_3	L_4	L_5	S_1	S_2	W	t_p
Length (in)	1.5	3	0.75	2.625	1.5	2.875	2.875	5.75	0.375

Therefore, the plate yield force (F) is 19.48 kips as shown Equation 3-10.

$$F = \frac{0.375^2}{4}(50)\times\left(\frac{2(5.75)}{1.5}+\frac{2(5.75)}{2.625}+\frac{4(2.625)}{5.75}+\frac{4(1.5)}{5.75}\right)=19.48 kips \quad \textbf{Equation 3-10}$$

The bolt resisting strength was calculated using Equation 3-4. The bolt resisting strength (F_b) was determined by subtracting the maximum prying force (Q_{max}) from the tensile strength of the bolts (B). The bolts were ASTM A490 high strength structural bolt and the diameter of bolt stud was 7/8 inch. The tensile strength of bolt (B) was 68 kips per bolt based on the bolt material property. Equation 3-11 shows the maximum prying force (Q).

$$Q_{\max} = \frac{4.875(0.375)^2}{4(1.5)}\sqrt{50^2 - 3\left(\frac{8.632}{4.875 \times 0.375}\right)^2} = 8.45 kips \qquad \textbf{Equation 3-11}$$

Therefore the bolt resisting strength (Fb) is 59.5 kips per bolt. The specimens had two bolts so the bolt resisting strength is 119 kips.

3.3 Numerical Analysis

3.3.1 Modeling

To simulate the experiment, the 3-D solid model, shown in Figure 3.7, was developed and solved with the FE analysis program ANSYS. The nominal specimen dimensions were used to define the model geometry. Figure 3.8 identifies the different element type used to create the model. SOLID45 8 node solid elements were used for the plates. The bolt shanks were defined by PREST179 to allow the application of pretension. There were two contact areas in the FE model. The first area was in between top and bottom plate surface. And second area was in between bolt shank and the inside surface of the bolt hole of the top and bottom plate. CONTA175 and TARGE170 elements were used to define the contact condition between the two plates and between the bolts and plates. The mesh size is 0.1875 inch which was selected through a mesh convergence study. A total of 8,547 elements were used to represent one half of the specimen. The model consists of three different parts, top plate, bottom plate, and bolt. Because the focus of the analysis was plate behavior, the stem plate was not explicitly modeled. The properties of the bolt were configured to take into account the rectangular shape of bolt stud. . Since the project is focused on the plastic behavior of the system, the analysis options included contact, plasticity,

pretension and large displacements.

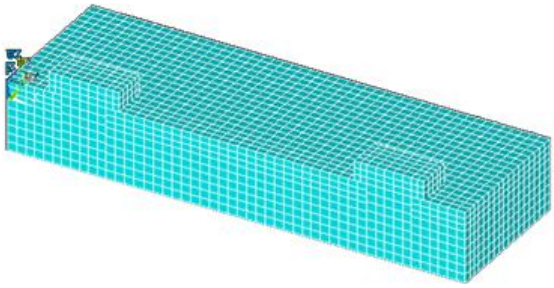

Figure 3.7 Half section 3-D FEM model

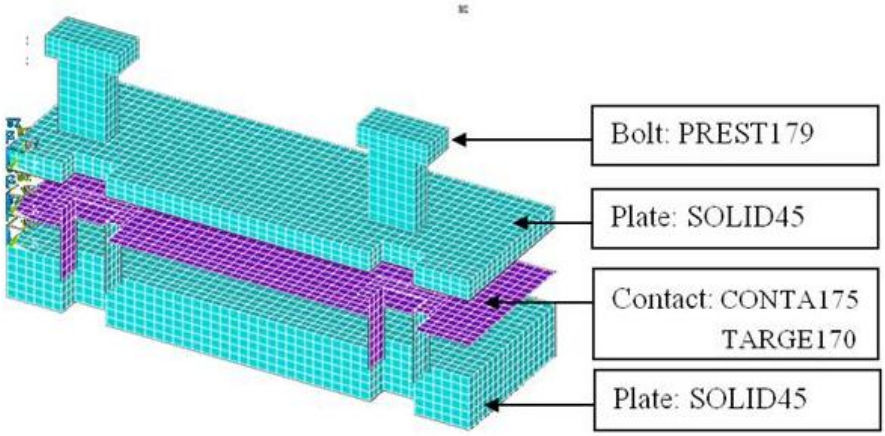

Figure 3.8 Element type of FEM model

3.3.2 Boundary conditions and material properties

Symmetric boundary condition was applied to the half surface and a fixed boundary condition applied through entire bottom plate and bottom of bolt stud. The bolt pretension was applied with 8 kips pretension to simulate the hand tightened condition of the bolts. The loading was applied on the top plate where the stem plate was connected. The maximum applied load was 36 kips. The measured material properties were utilized within the model properties. The tri-linear material models used for the plate and bolt elements are shown in Figure 3.9.

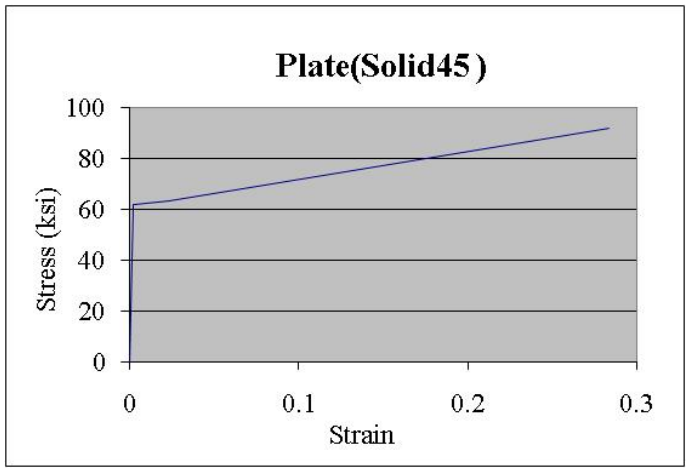

(a) Plate stress-stain curve

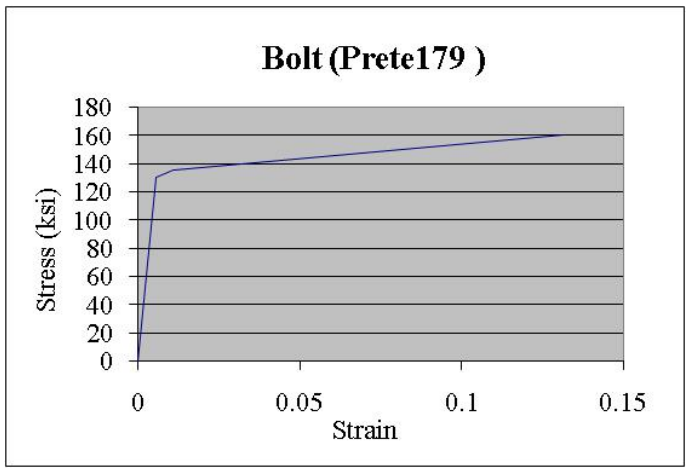

(b) Bolt stress-strain curve

Figure 3.9 Element material properties

3.3.3 Results

Figure 3.10 (a) shows the deformed shape and von-mises stress contours at the max applied load (36 kips) loading. To check the general behavior of the system, prying effects and contact effects were checked by stress contour view. The prying force was observed at the bottom plate edge as indicated by the concentrated stresses at the point

of contact. The contact effect between bolt shank and bottom plate hole were also observed (Figure 3.10 (b)).

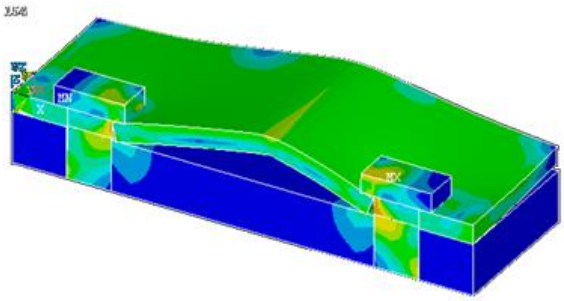

(a) Von-mises stress contour at 36kips loading

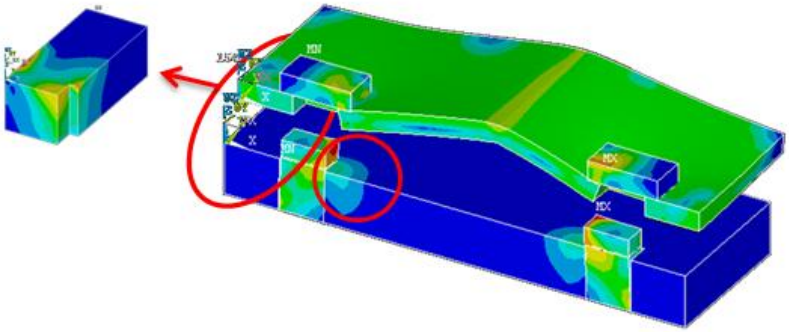

(b) Prying effect and contact effect

Figure 3.10 Behavior of FEM analysis

The maximum displacement occurred in the top plate at the location of the applied loading line. The load-displacement response of the T-stub specimen is shown in Figure 3.11. The top plate started to yield approximately 17 kips and the system had a large displacement as load continued to increase beyond this point. The observed response was essentially bi-linear as it exhibited two distinct stiffnesses.

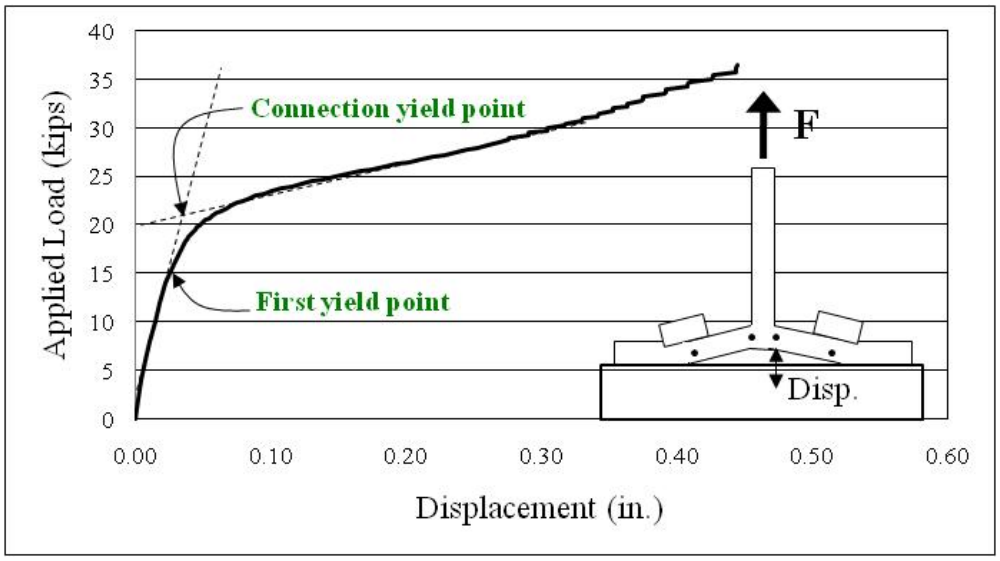

Figure 3.11 Load displacement graph (Center of loading line)

The propagation of stresses through the system is illustrated in Figure 3.12 as the load increases. The contour is the von-mises stress and the deformation is real scale. The development of the plate yield line mechanism is apparent.

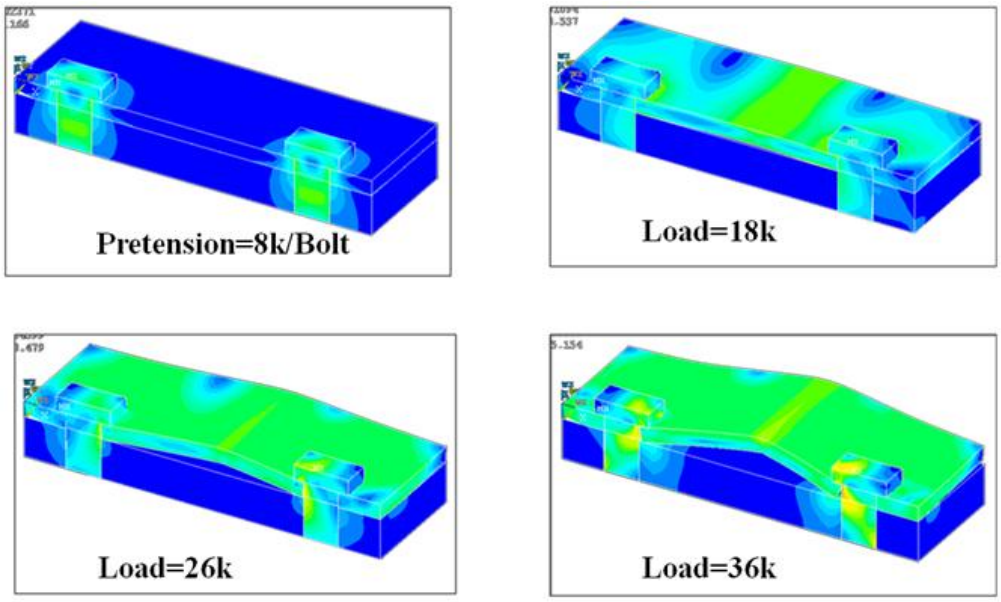

Figure 3.12 Von-mises contour and deformation

3.4 Experimental Investigation

3.4.1 Specimens

Four full-scale T-stub tests were conducted to verify the analytical procedures presented as a part of this paper. The same test specimen geometry and test setup were utilized for all tests. However, the bolt strength was varied to isolate the plate and bolt failure modes. Test phase one used D7/8×L4½ A325 bolts and the test phase two used D7/8×L4½ A490 bolt. All of test bolts were hand tightened wrench and the hand tightening bolt tension was measured using skid-more bolt calibrator to be approximately 8 kips/bolt. Figure 3.6 shows the specimen configuration and geometry. The specimen was fabricated with a base plate and stem plate using A572 Grade 50 steel. The base plate was welded to stem plate with 3/4" fillet weld using Metal Arc or similar welding and E70xx electrodes at only one side.

3.4.2 Test setup

For the experimental tests, a fixture was fabricated to hold the boot and track assembly level so that the stem of the T-stub was vertical. The stem of the T-stub was attached to a two-inch thick steel loading plate, using ½" x 3" A325 bolts, designed to simulate the column in a building. To ensure that the stem and loading plate remained vertical and did not have any out-of-plane movement, the steel plate was laterally braced using rollers. One roller was placed at the bottom of the steel plate in the middle of the bolt pattern that connected it to the boot stem. A ¾" plate with oversized holes in it was used to offset the roller from the plate to ensure that it did not bear on the bolts. Another roller was placed approximately 12" higher on the plate and on the other side. These rollers were supported and braced against the test fixture. A computer controlled hydraulic tack was used to apply the vertical load through the load plate.

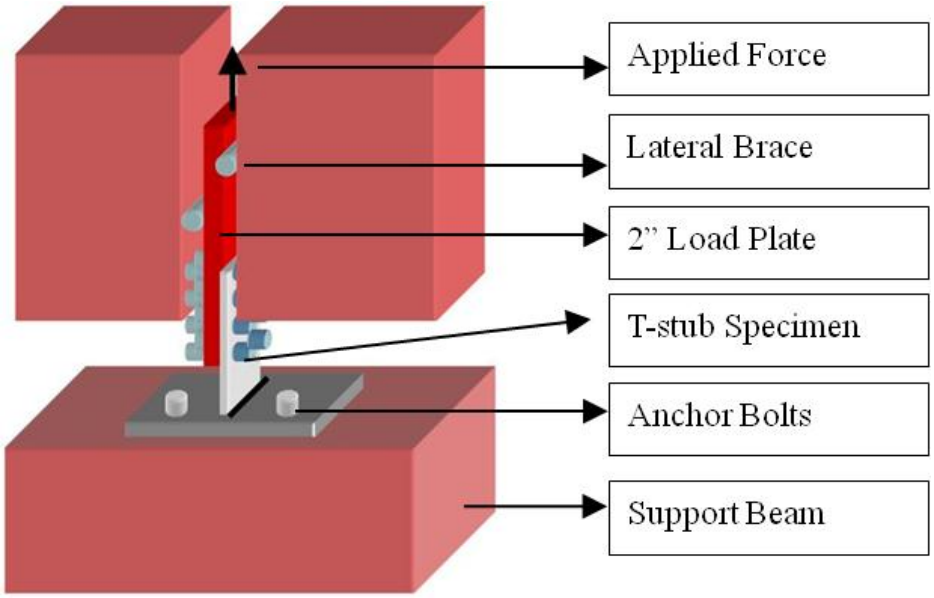

Figure 3.13 Test setup

3.4.3 Instrumentation

Ten linear potentiometers were used to measure specimen displacements for this test (Figure 3.14). A computer controlled Vishay data acquisition system was used to record the load and displacement data points. Six linear potentiometers (#1, 2, 5, 6, 7 and 9) were placed on the surface of the T-stub specimen to measure the vertical deflection. Three linear potentiometers (#3, 4, and 10) were used to measure the test setup movement for vertical direction. One linear potentiometer (#8) was placed at the stem surface to measure the lateral displacement of specimen.

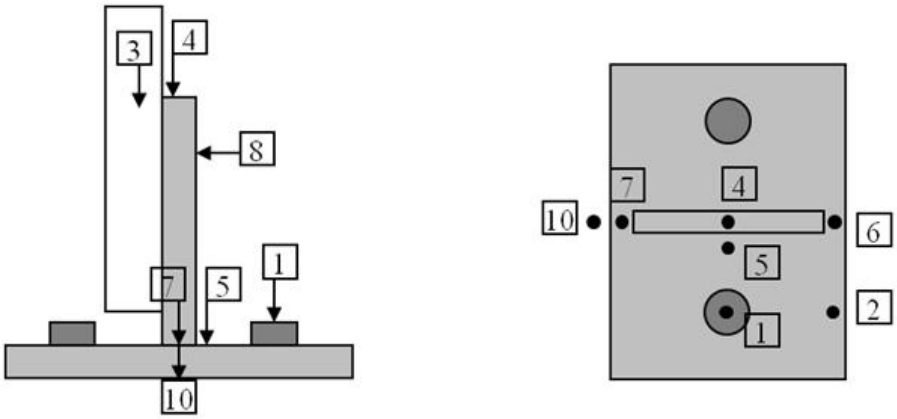

Figure 3.14 Instrumentation of specimens

3.4.4 Loading procedures

At the beginning of each test a small pre-load was applied to check the behavior of the test setup and instrumentation. The test load was applied in displacement control and a displacement rate of 0.1in/min was used.

3.4.5 Result

Load-deflection response of the four tests is shown in Figure 3.15. Linear potentiometer No. 5 (as shown in Figure 3.14) is used as the reference displacement. All of tests were performed exhibited similar behavior. However the second phase tests showed slightly stiffer behavior and higher ultimate load. A summary of results is presented in Table 3-2

.

Table 3-2 Test summary

Phase	Specimen ID	Failure modes	Max. Applied Load
1	Tstub01	Bolt Fracture	54.39k
	Tstub02	Bolt Fracture	52.75k
2	Tstub03	Base plate Tearing	66.35k
	Tstub04	Base plate Tearing	63.79k

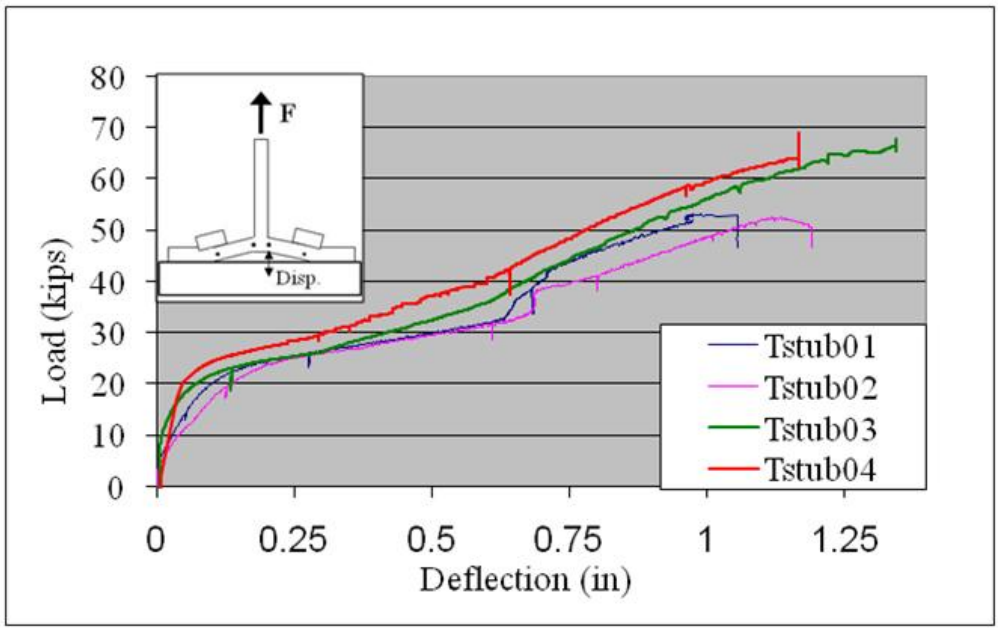

Figure 3.15 Center point vertical displacement

Figure 3.16 shows the ultimate failure mode of the test. Due to the large deflection and prying effect, the first phase ultimate failure mode was bolt tension rupture. However the ultimate failure mode of second phase was base plate bolt hole tear out. This ultimate failure mode change was anticipated since the tests used the stronger A490 strength bolts.

(a) Phase 1 (b) Phase 2

Figure 3.16 Ultimate failure modes

3.5 Comparison of Results

The Figure 3.17 shows the yield line pattern sketched on the experimental test photograph and FEM analysis result. The observed yield line pattern in both cases was similar to the selected yield line pattern.

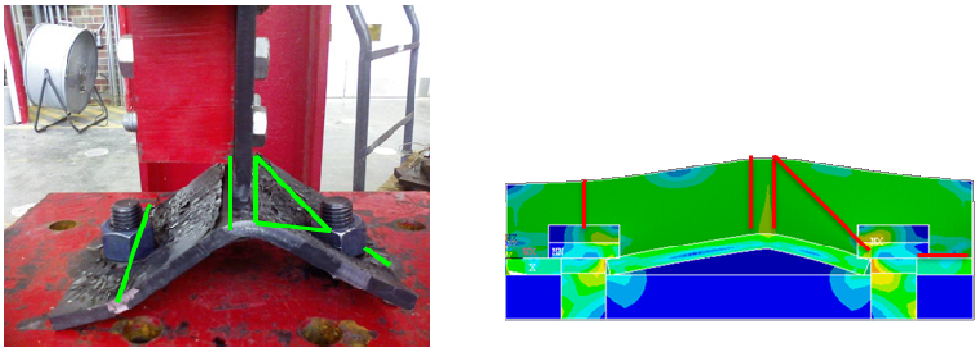

(a) T-stub04 at end of test (b) Von-mises stress at 36kips

Figure 3.17 Experimental and FEM yield line pattern

A comparison of the load displacement response of the experimental test (Tstub03 and Tstub04), FEM and yield line is shown in Figure 3.18. The force-displacement curves obtained from the numerical analysis show a rather good agreement with the

experimental results. In particular, the yielding limit of the theoretically obtained line is very close to both the experimental and numerical yielding level.

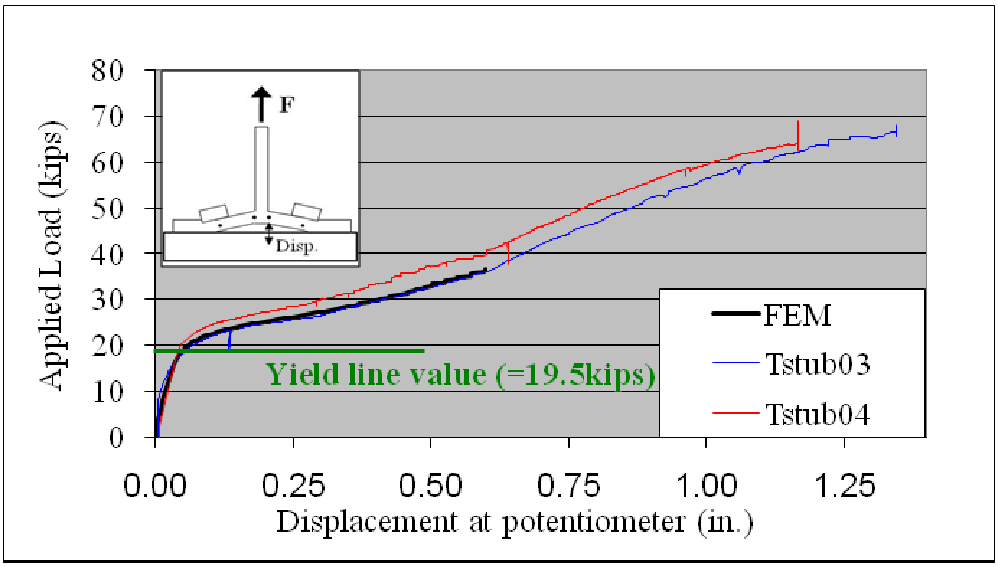

Figure 3.18 Comparison of test, FEM, and yield line results

3.6 Conclusions

As a part of alternative seismic moment resisting frame connection, the end plate moment connection was focused after Northridge earthquake (1994). To simplify the connection analysis, the T-stub was used as the reduced end plate moment connection. The objective of the study is verification of the reduced end plate moment connection characteristic with various analysis methods. Three different approaches were adopted to analyze the reduced end plate moment connection (T-stub). The yield line analysis defined the yield limit of system. The numerical analysis (FEM) verified the theoretical result and simulated the behavior of the experimental test. Based on the result of this comparative study, the following conclusions can be made.

- The yield line theory can be use to predict the end plate flexural yield force with correct yield line pattern.
- The numerical model (FEM) can accurately simulate the behavior of end plate.
- The yield line theory and numerical model can be used as the pre-analysis tool for simulate the end plate moment connection experimental test behavior.

3.7 Future Work

- Additional cyclic testing is necessary to establish the T-stub specimen as simplify the full scale end plate moment connection.
- An experimental study needed to investigate the simplified LCF modeling protocol.

3.8 Acknowledgement

This research was supported by The Steel Network, Inc. (TSN).

3.9 References

AISC (2002), "AISC Design Guide 16: Flush and Extended Multiple-Row Moment End-Plate Connections", American Institute of Steel Construction, Chicago.

Borgsmiller, J., (1995). "Simplified Method for Design of Moment-End-Plate Connections", M.S. Thesis, Virginia Polytechnic Institute and State University, Blacksburg, VA.

Bursi, O. S., Ferrario, F., Fontanari, V., (2002) "Non-linear Analysis of the Low-cycle Fracture Behaviour of Isolated Tee Stub Connections", Computers & Structures, 80, 2333-2360.

FEMA. (2000a), FEMA 350 Recommended Seismic Design Criteria for New Steel Moment-Frame Buildings, FEMA, Washington, DC.

Garlock, M. M., Ricles, J. M., Sause, R., (2003). "Cyclic Load Tests and Analysis of Bolted Top-and-Seat Angle Connections", Journal of Structural Engineering.

Hendrick, D., Kukreti, A. R., Murray, T. M., (1984). “Analytical and Experimental Investigation of Stiffened Flush End-Plate Connections with Four Bolts at The Tension Flange”, Research Report FSEL/MBMA 84-02, Fears Structural Engineering Laboratory, University of Oklahoma, Norman, OK.

Kasai, K., Xu, Y., (2003). “Cyclic behavior and low-cycle fatigue of semi-rigid connections (Part II: bolted T-stub connections)”, Behaviour of Steel Structures in Seismic Areas, STESSA 2003, Balkema, pp. 321–327

Kennedy, N.A., Vinnakota, S., Sherbourne, A.N., (1981). “The Split-Tee Analogy in Bolted Splices and Beam-Column Connections”, Joints in Structural Steelwork, John Wiley & Sons, London-Toronto, pp. 2-138-2.157.

Meng, R. L. (1996), "Design of Moment End-Plate Connections for Seismic Loading", Ph.D. Dissertation, Virginia Polytechnic Institute and State University, Blacksburg, VA.

Morrison, S. J., Astaneh-Asl,, A., Murray, T. M., (1986). “Analytical and Experimental Investigation of the Multiple Row Extended 1/3 Moment End-Plate Connection with Eight Bolts at the Beam Tension Flange,” Report No. FSEL/MBMA 86-01, University of Oklahoma, Norman, Oklahoma.

Murray, T.M., (1988). "Recent Developments for the Design of Moment End-Plate Connections", Construction Steel Research 10 133-162

Srouji, R., Kukreti, A., Murray, T. M., (1983). “Yield-Line Analysis of End-PlateConnections with Bolt Force Predictions”, Report No. FESL/MBMA 83-05, University of Oklahoma, Norman, Oklahoma.

Sumner, E. A. and Murray, T. M. (2002). "Behavior of Extended End-Plate Moment Connections Subject to Cyclic Loading", Journal of Structural Engineering, ASCE, vol. 128, no. 4, pp. 501-508.

Chapter 4 Experimental Program II&III: Full Scale Model

4.1 Introduction

In 1994, unanticipated brittle structure failures were occurred at California urban area by Northridge earthquake. Especially, the various structure connections got severe damage. The Federal Emergency Management Agency (FEMA) leaded the urgent research for the examination of the failure. As the results, one of the failure reasons was "Low cycle fatigue (LCF) originated from strain concentration" (FEMA, 2000a). To address the observed failure, several alternative connection methods were investigated as a part of the project. In this paper, one of the alternative connections, the four bolts extended unstiffened end plate moment connection, is studied to evaluate the Low Cycle Fatigue (LCF) behavior.

The early research studies on End Plate Moment Connections (EPMC) were conducted to verify moment capacity prediction, overall connection behavior, bolt prying forces, bolt behavior, and weld behavior. As the focus has moved on to seismic behavior, the first end plate connection test under cyclic loading was conducted in the late 1980's. Since then, a number of investigations have studied the cyclic behavior of EPMC. In the limited LCF studies, the LCF fractures were observed to occur in the end plate. (Garlock 2003, Kasai 2003, Sumner 2000) In the fillet welded joints, the cracks appeared at the weld toe and then propagate through the end plate in a direction perpendicular to the applied principal stresses. This observed behavior is logical since the maximum principal stress and maximum plastic deform action both occurred near the weld area. Figure 4.1 shows the initial crack location and common LCF failure in EPMC.

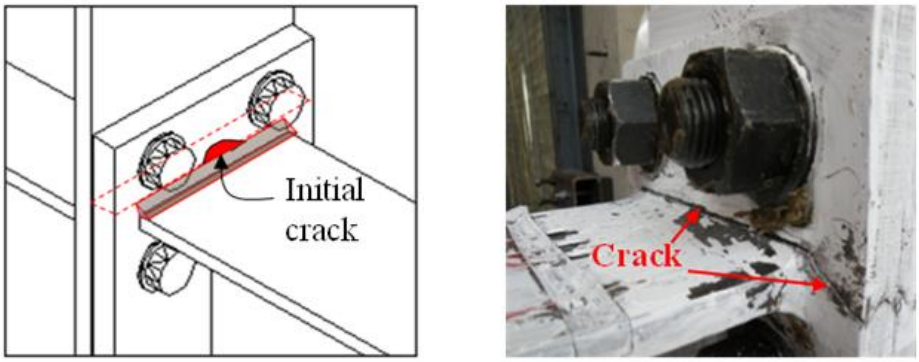

(a) FEM Illustration (b) Experimental test

Figure 4.1 Low cycle fatigue fracture in EPMC

Ballio, Calado, and Castiglioni(1997) conducted experimental study of low cycle fatigue behavior of a steel beam to column connection. One of the seven types of specimens was the extended end plate moment connection. The study concluded the proposed approach, S-N curve fatigue model using Minor's rule, could be used to predict the behavior of the low cycle fatigue behavior of structural member connections. The European collaborative project conducted extensive analytical and laboratory investigations to improve their seismic codes (Eurocode 8). The research reported the overall cyclic behavior of end plate moment connection (such as the influence of the strain rate on the cyclic behavior of end plate moment connection, low cycle fatigue approach, ductility, etc).

The primary objectives of this study are to develop the low cycle fatigue model, to estimate the life of connection assembly in the inelastic range with the LCF model, and to investigate critical geometric and material parameters for four bolts unstiffened EPMCs on LCF.

To accomplish these objectives, a four part research plan was developed. In the first part, pre-analysis was conducted with FEM analysis to design the test specimens and

to predict the specimen response. In the second part, four experimental tests were conducted with three constant peak cyclic loading and one random loading. In the third part, the post analysis was conducted to develop the low cycle fatigue model with experimental results. In the last part, the post analysis was conducted to verify the fatigue model and life estimating method.

4.2 Background

The two main design concepts were adopted in the design and two theories were adopted in the post analysis. The yield line theory and Kennedy method were used in the connection design. The Coffin-Manson theory and Miner's rule were used to analysis of results.

In the design of the test specimens, yield line theory was used to verify the flexural yield limit of end plate and Kennedy split-tee analogy (Kennedy, 1988) was used to determine the bolt strength considering the prying effect. Extensive studies have been conducted in the past on the analysis and design of EPMC using these limits states. The early studies neglected the prying action in the end plate design procedure. After Kennedy et al. (1981) introduced the "split-tee analogy" to determine the bolt forces including prying action, numerous design procedures adopted and developed Kennedy's method. From these studies, Srouji et al. (1983) reported the unification design procedure using the yield line theory for end plate yielding and Kennedy method for bolt failure. Hendrick et al. (1984), Morrison et al. (1985), Murray (1993), Borgsmiller (1995), Meng (1996), and Sumner (2000) developed the design procedure to variety type of EPMC and loading type. These results were used to develop the currently available AISC design guides (AISC 2002).

4.2.1 End-Plate flexural strength

Yield-line theory was first introduced to analyze reinforced concrete slabs and has been adopted for use with steel plates in recent years. A yield-line is a continuous formation of plastic hinges along a straight or curved line. The failure mechanism of the plate is assumed to exist when the yield-line form a kinematically valid collapse mechanism. Since the elastic deformations are negligible compared to the plastic deformations, it has been proven acceptable to assumed that the yield-lines divide the plate into rigid plane region.

The analysis of a yield-line mechanism can be performed by two different methods. One is the equilibrium method and the other is virtual work (energy method).

For a specified yield-line pattern and loading, a certain plastic moment will be required along the hinge lines. To determine the required plastic moment capacity or the failure load, an arbitrary succession of possible yield-line mechanisms must be selected.

The one of the important assumption in the yield line theory is the yield line pattern. The critical (controlling) pattern is the one that requires the least energy to form. Figure 4.2 shows the chosen yield line pattern of 4 bolts extended end plate moment connection and virtual displacement as presented by Sumner (2003).

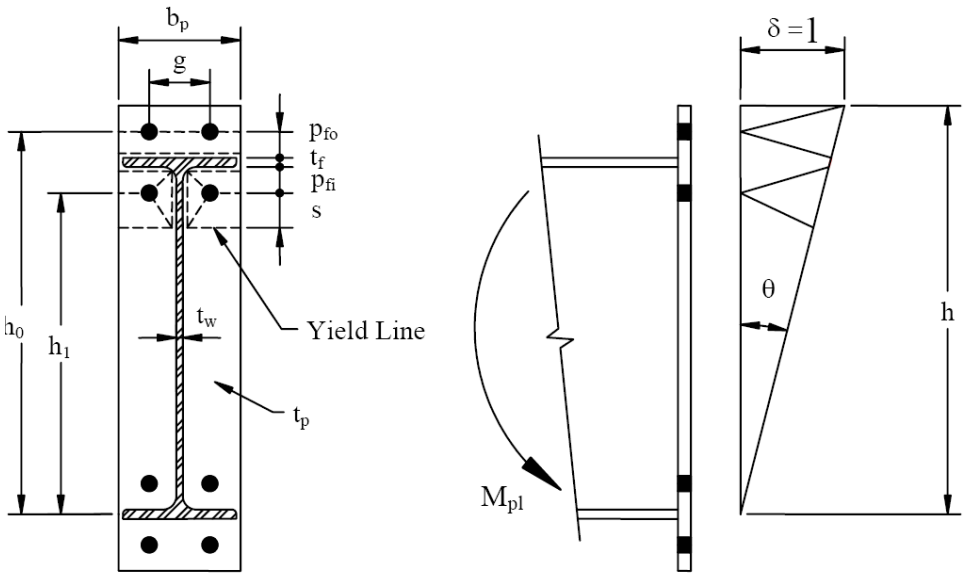

Figure 4.2 Yield line pattern and virtual displacement of 4E EPMC (Sumner, 2003)

The yield line solution is determined by equating the external work with the internal work solving for the resulting applied connection moment. Using the yield line pattern presented in Figure 4.2, the connection final equation of the work equilibrium is

$$M_{pl} = F_{yp} t_p^2 \left[\frac{b_p}{2} \left[h_1 \left(\frac{1}{p_{fi}} + \frac{1}{s} \right) + h_0 \left(\frac{1}{p_{f0}} \right) - \frac{1}{2} \right] + \frac{2}{g} \left[h_1 \left(p_{fi} + s \right) \right] \right] \quad \textbf{Equation 4-1}$$

where M_{pl} is the EPMC strength based on the flexural yielding of the end plate.

4.2.2 Bolt force predictions

The effect of Kennedy split-tee analogy was used to estimate the bolt forces due to applied force and prying action. The basic assumption in the method is that the end-plate goes through three different stages of behavior (Figure 4.3); Thick, Intermediate, Thin. Q is the prying force, the B is bolt resisting force, and 2F is the applied flange

tension loading. During the first stage, plastic hinges have not developed and the plate is referred to as “thick”. The prying force is taken as zero in this stage. When the plastic hinge forms at the beam flange, the plate becomes “intermediate” and the prying force is somewhere between zero and the maximum prying force that can occur. The last stage begins when a second plastic hinge forms at the bolt line. The end-plate in that stage is called “thin” and the prying force is at its maximum.

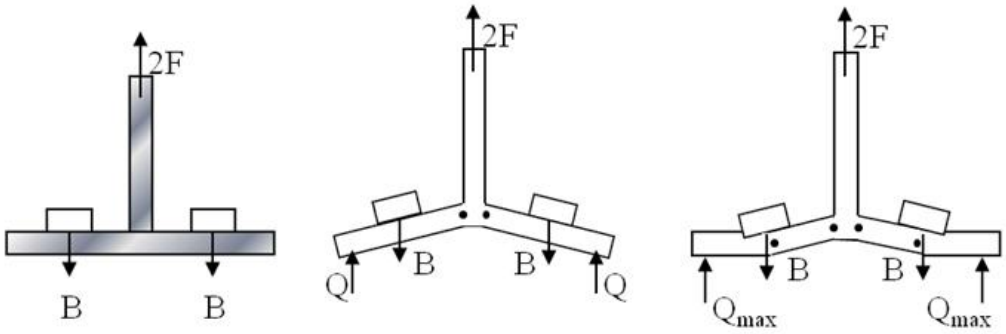

(a) Thick (B=F) (b) Intermediate (B=F+Q) (c) Thin (B=F+Q_{max})

Figure 4.3 Three stages of plate behavior

The Kennedy method was modified by Srouji (1983), Hendrick (1984), and Morrison (1985) to adjust the applied prying force position and the distribution of the flange tension force. The resulting bolt force prediction procedure is known as the “Modified Kennedy Method”. The modified Kennedy method was used to predict the bolt forces within the test connections.

4.2.3 Low cycle fatigue model

Strain-life equation was work done by Morrow (Morrow, 1965) and Landgraf (Landgraf, 1969). It combined and improved the Basquin, elastic range, and Coffin-Manson, plastic range, equation.

$$\frac{\Delta\varepsilon}{2} = \frac{\sigma'_f}{E}(2N_f)^b + \varepsilon'_f(2N_f)^C \qquad \textbf{Equation 4-2}$$

Where $\Delta\varepsilon/2$ is strain amplitude (load parameter). $2N_f$ is fatigue life in reversals. E is modulus of elasticity. σ'_f is fatigue strength coefficient. b is fatigue strength exponent. ε'_f is fatigue ductility coefficient. c is fatigue ductility exponent.

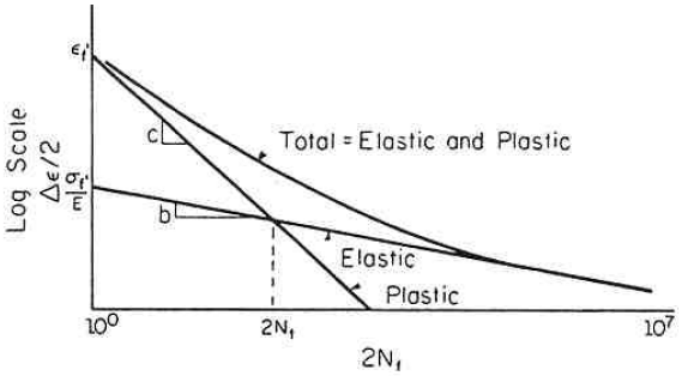

Figure 4.4 Total elastic and plastic strain components strain-life curves (Fuchs 1980)

Figure 4.4 presents the total elastic and plastic components strain-life curves. At a given life N, the total strain is the sum of the elastic and plastic strains. Both the elastic and plastic curves can be approximated as straight lines. At short fatigue lives, low cycle fatigue, plastic stains dominate and at long fatigue lives, high cycle fatigue, elastic strains dominate the fatigue life. This method allows for the characterization of fatigue properties for a material throughout the entire life range. However, the focus of this current research is the LCF (short life) behavior and life prediction.

Three constant amplitude load tests were used to develop the LCF model and Manson-Coffin relation equation was adopted. (Equation 4-3)

$$N_f = C(\Delta S)^{-b} \qquad \textbf{Equation 4-3}$$

Where C and b are positive constants and ΔS is deformation range or dissipated

hysteretic energy.

Figure 4.5 shows how three different constant cyclic loading tests are used to make the Manson-Coffin LCF model. Figure 4.5 (a) plots Force-deformation hysteretic curve for each cyclic loading. N is the reversal number and ΔS is deformation range or dissipated hysteretic energy when the specimen gets to failure. Figure 4.5 (b) shows the LCF model using the test result; the graph is a log scale plot.

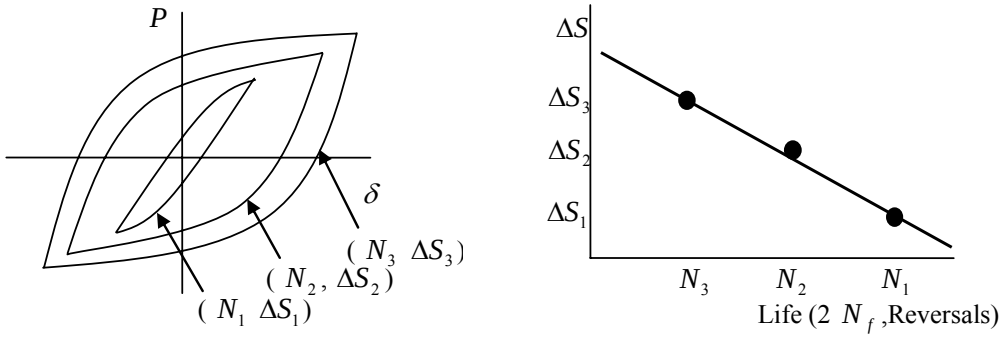

(a) Force-Deformation Hysteretic loop (b) LCF Model

Figure 4.5 Low Cycle Fatigue model

Using the developed S-N curve, the LCF life of a component can be determined for any given range of deformation.

4.2.4 Low cycle fatigue life prediction

To verify the damage of the system under variable loading, the Linear Damage Rule was first proposed by Palmgren (Palmgren, 1924) and was further developed by Miner (Miner, 1945). Today the method is commonly known as Miner's Rule. The Linear Damage Rule is based on the concept of fatigue damage (Equation 4-4). A damage fraction, D, is defined as the fraction of life used up by an event or a series of events. Failure is predicted to occur when the sum of D_i reach unity.

$$\sum_{i=1}^{I} D_i = X \leq 1.0$$ **Equation 4-4**

where, i is index of each set of applied load cycles at constant stress level $S_{i,}$,D_i is Damage fraction accumulated during the load cycles of interval i at constant stress level $S_{i,}$, and X is Damage criterion (a constant).

The Linear Damage Rule states that the damage fraction at a given constant stress level S_i is equal to the number of applied cycles n at stress level S_i divided by the fatigue life N at stress level S_i. (Equation 4-5)

$$D_i = \frac{n_i}{N_i}$$ **Equation 4-5**

where, D_i is damage fraction accumulated during the load cycles of interval i at constant stress level S_i , N_i is number of applied load cycles at constant stress level S_i , and N_i is fatigue life at constant stress level S_i, obtained from the S-N curve.

$$\sum_{i=1}^{I} \frac{n_i}{N_i} \geq 1$$ **Equation 4-6**

Considerable test data has been generated in an attempt to verify Miner's Rule. Most test cases use a two step load history. This involves testing at an initial stress level S_1 for a certain number of cycles, and then the stress level is changed to a second level S_2 until failure occurs. If $S_1 > S_2$, it is called a high-low test, and if $S_1 < S_2$, a low-high test. The results of Miner's original tests showed that the damage criterion X corresponding to failure ranged from 0.61 to 1.45. Other researchers have shown variations as large as 0.18 to 23.0, with most results tending to fall between 0.5 and 2.0. In most cases, the average value is close to Miner's proposed value of 1.0.

One problem with two-level step tests is that they do not accurately represent many service load histories. Most load histories do not follow any step arrangement and

instead are made up of a random distribution of loads of various magnitudes. However, tests using random histories with several stress levels show good correlation with Miner's rule. Even so, for conservative estimates of the life of a structure an X value of less than 1.0 is usually used.

The Linear Damage Rule has two main shortcomings when it comes to describing observed material behavior. First, load sequence effects are ignored. The theory predicts that the damage caused by a stress cycle is independent of where it occurs in the load history. An example of this discrepancy was discussed earlier regarding high-low and low-high tests. Second, the rate of damage accumulation is independent of the stress level. This trend does not correspond to observed behavior. At high strain amplitudes cracks will initiate in a few cycles, whereas at low strain amplitudes almost all the life is spent initiating a crack (i.e., very little propagation fatigue).

Despite these limitations, the Linear Damage Rule is still widely used. This is due both to its simplicity and the fact that more sophisticated methods do not always result in better predictions.

4.3 Experimental Test

4.3.1 Specimens

The AISC design guide 4 “Extended End-Plate Moment Connections Seismic and Wind Applications” (AISC 2002) was used to design the four bolts extended unstiffened end plate moment connection (4E EPMC). Previous studies have shown that the end plate exhibited the highest degree of LCF behavior (Sumner, 2000). To ensure LCF behavior, the end plate was designed as the weak link in the connection

system. The selected components and materials for the test specimens are shown in Table 4-1. The test specimen and end plate geometry are shown in Figure 4.6 and Figure 4.7.

Table 4-1 Design section

Component	Selection	No.	Material
Beam	W12x48	1	A992
Column	W14x74	1	A992
Plate	1”x10”x25.375”	1	A572 GR50
Bolt	Dia.1.25”x3.25”	8	A490
Doubler P	1/2”x10 7/8”x16”	1	A572 GR50

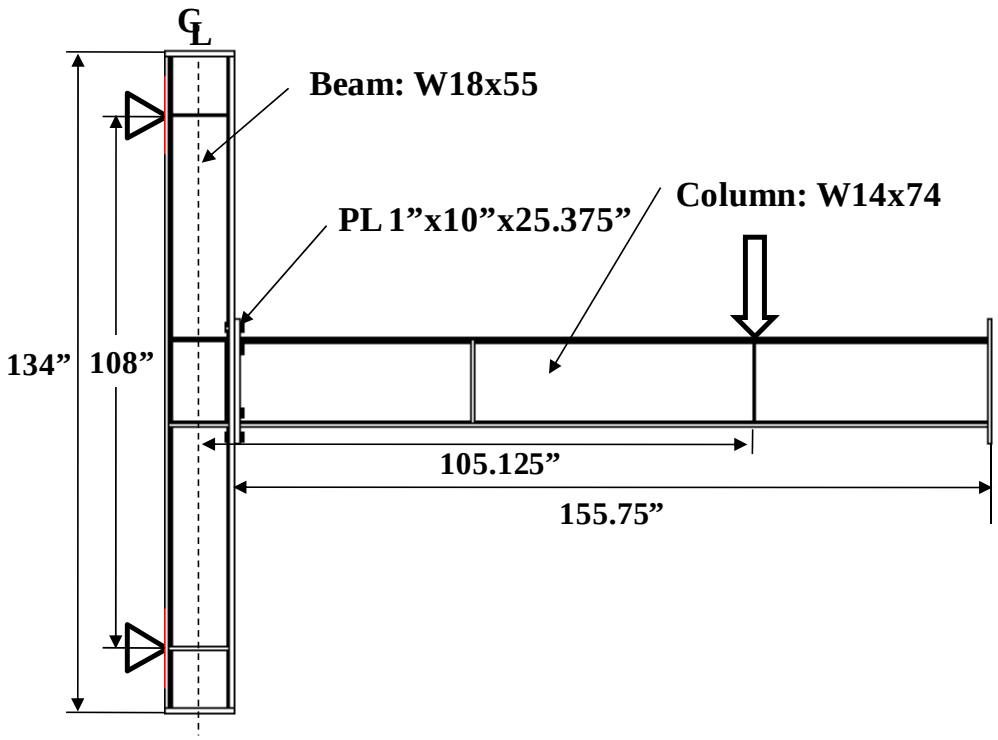

Figure 4.6 End plate moment connection test specimen

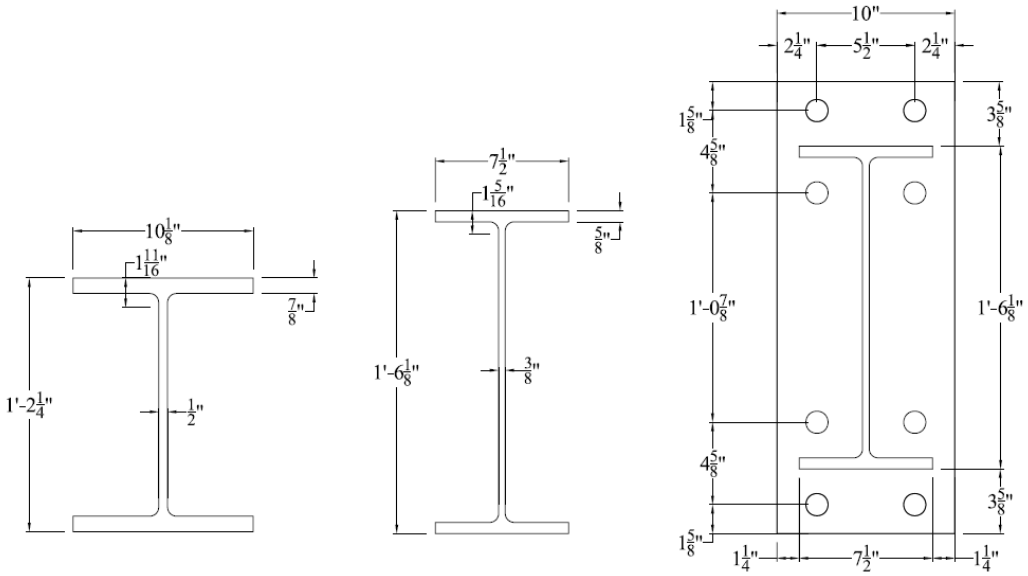

(a) Column (b) Beam (c) End plate

Figure 4.7 EPMC components geometry

The calculated design strength for each component is summarized in Table 4-2.

Table 4-2 Design limit state strength

Section	limit state	Design Strength (kips-ft)
End plate	Plate yielding	411
Beam	Flexural	513
		451
Column	Flexural	701
	Local web yielding	488
	Web crippling	491
	Buckling of the web	484
	Panel-zone shear	623
Bolt (A490)	No prying	809
	Max prying	547

Four full scale tests were conducted with varying loading type. Test LCF01, LCF02, and LCF03 utilized constant amplitude cyclic loading and test LCF04 utilized random loading as summarized in Table 4-3.

Table 4-3 Test matrix

Name	Beam	Column	Loading
LCF 01	W18×55	W14×82	1.75” constant peak cyclic
LCF 02	W18×55	W14×82	2.5” constant peak cyclic
LCF 03	W18×55	W14×82	2.25” constant peak cyclic
LCF 04	W18×55	W14×82	Random cyclic

The specimens were fabricated at Apex Steel Company in Raleigh, North Carolina in accordance with AISC and AWS specifications. The weld quality was inspected by MACTEC Engineering & Consulting, Inc. AWS certified weld inspector using ultrasonic scan and magnetic particle method. The welding procedure specified in “AISC steel design guide 4 (AISC 2003)” was used to install the beam end to end-plate welds.

4.3.2 Test setup

The basic assumption was all tests were exactly same except the level of constant loading. All four tests were used same test setup as shown Figure 4.8. The beam-to-column EPMC sub-assembling was attached to laboratory. The support frame mounted on the strong wall with high strength threaded rods. The testing-frame was located on the loading position. The MTS 440kips capacity dynamic hydraulic actuator and load reaction frame were positioned above the load point on the test

specimen. To prevent unexpected behavior of the specimen, the lateral support was provided to the beam at the load point. The end plate-beam assembly was bolted in the middle of the column flange with eight 1 1/4 inch diameter ASTM A490 bolts. All the test setup bolts were fully tightened with air impact wrench. Bolt of 110kips pretension was applied in the end plate connection.

Figure 4.8 Test setup

4.3.3 Instrumentation

The test assembly was instrumented with fourteen strain gages, four calibrated calipers, and linear potentiometers to measure the specimen's response. The instrumentation was connected to a Vishay data acquisition system to record the data. Figure 4.9 illustrates the layout of instrumentation on the test specimens. As shown in Figure 4.9, five strain gages were located on the top of beam flange surface and one strain gage was located in the middle of bottom flange surface. Two linear potentiometers were mounted on the column panel zone to measure the column panel zone behavior. Two linear potentiometers were used to measure the beam and column

horizontal movement at the top and bottom and at the level of beam flanges. The beam tip displacement was measured using a string potentiometer attached under the bottom of beam flange in the loading point. To measure the bolt force, calibrated instrumented bolts were used in the specimen connection.

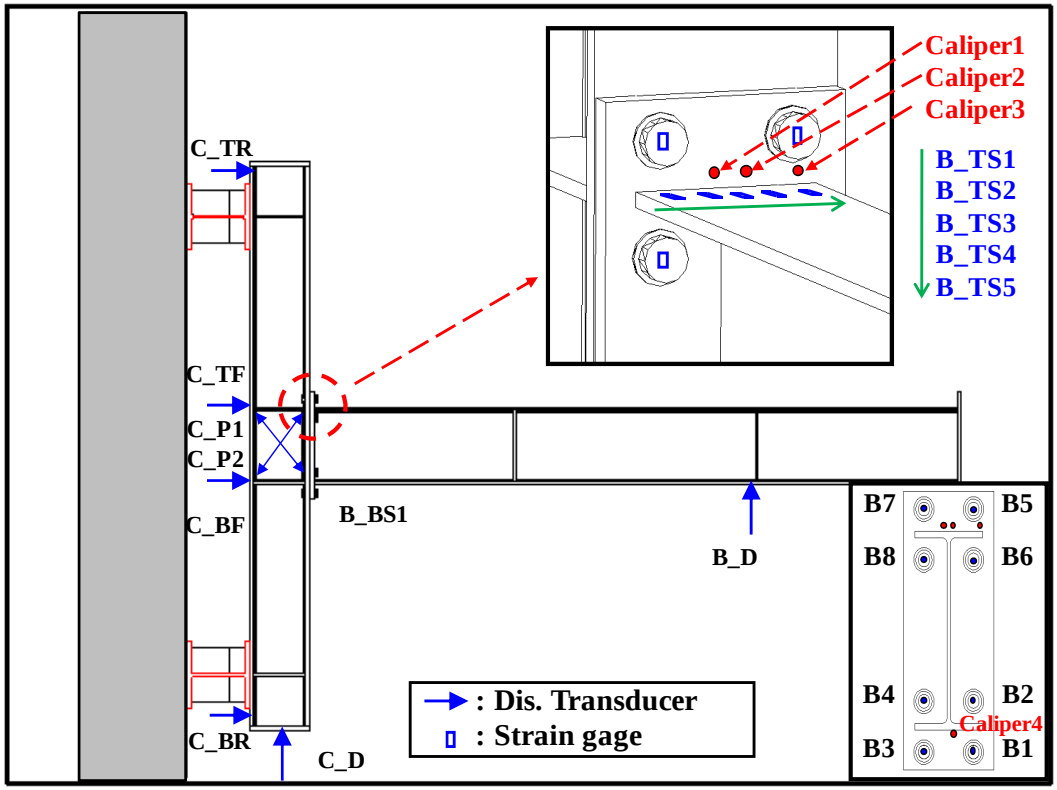

Figure 4.9 Specimen instrumentation

4.3.4 Loading procedures

At the beginning of each test a small pre-load was applied to the test specimen to check the test setup and instrumentation. The test load was applied with the actuator in displacement control. The first cycle was start with 0.15in/min load rate and then changed to 20min/cycle. The cycle load was sinusoidal loading. Figure 4.10 shows three tests displacement load history. The history for LCF01 is plotted for every 10th

cycle. To develop the LCF model, three different constant peak cyclic loads were applied as summarized in Table 4-4. Three different displacement load levels which were used in previous tests were selected to apply for the random load test. The displacement was applied in groups of six cycles. The load was started with the lowest level and the N increased two load steps and then decreased. After two cycle of load level changing, the middle constant load level was applied until the system failure.

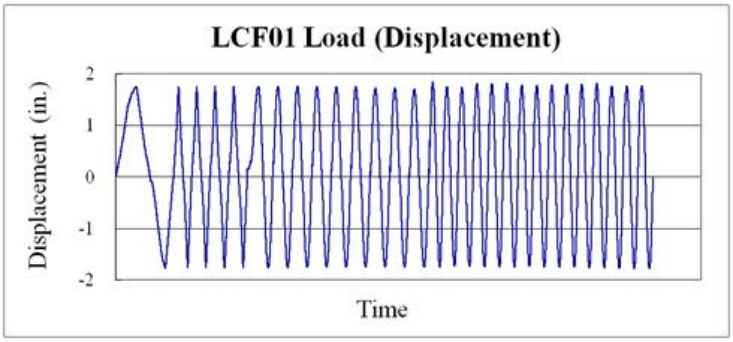

(a) LCF01 1.75in constant (every 10th cycle)

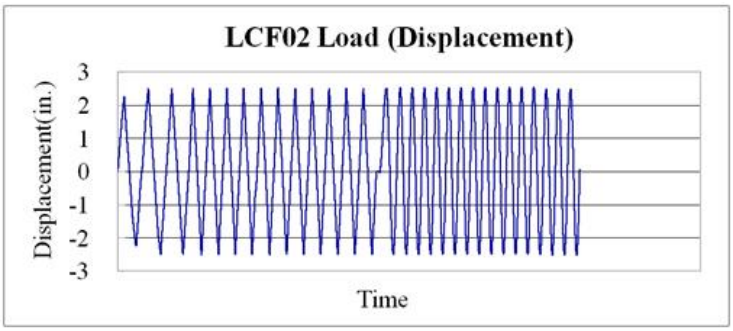

(b) LCF02 2.5in constant peak load

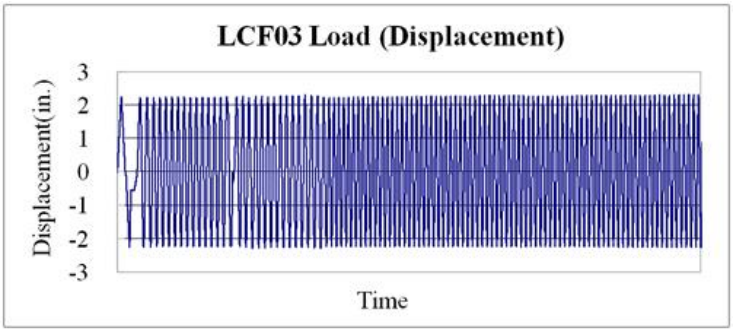

(c) LCF03 2.25in constant peak load

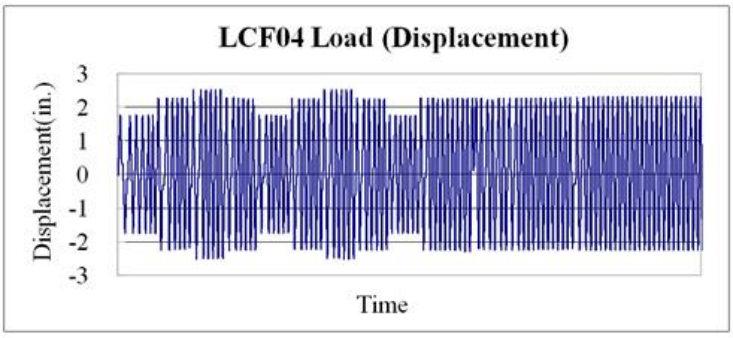

(d) LCF04 random load

Figure 4.10 Loading history

4.3.5 Results

The expected failure mode was end plate low cycle fatigue failure because it was designed with weak end plate concept. All of tests failure mode were end plate low cycle fatigue failure at the beam flange location. The observed failure mode was ductile because the test was conducted in displacement control. A summary of results is presented in Table 4-4. LCF01 and LCF02 had a symmetric low cycle fatigue behavior. However LCF03 and LCF04 had an asymmetric cyclic behavior after some amount of cycles because the top of beam flange got a crack at the top of beam flange. The crack was developed from the right edge of beam flange next to the weld point to the beam web. The cycles were counted by reversal.

Table 4-4 Test summary

Test ID	Observed Failure mode	Applied Disp.	No. Failure
LCF01	End plate LCF failure at top flange	±1.75 in.	276
LCF02	End plate LCF failure at bottom flange	±2.5 in.	50
LCF03	End plate LCF failure at bottom flange	±2.25 in.	158
LCF04	End plate LCF failure at bottom flange	±2.5 in.	121

Figure 4.11 shows the ultimate failure mode of the tests. All tests had clear crack shape in both top and bottom flange area. LCF01 was failed at the top beam flange area of end plate. The crack was fully penetrated through the end plate cross section. LCF02 was failed at the bottom flange area of end plate. The crack was fully penetrated through the end plate cross section. LCF03 and LCF04 were failed at the bottom beam flange area of end plate. The crack was formed following the weld edge.

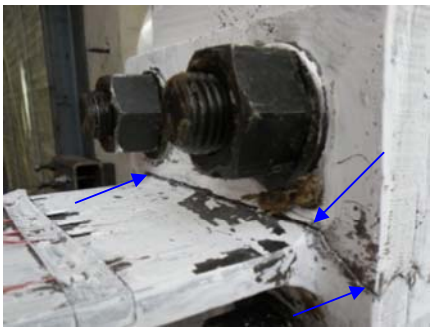

(a) LCF01

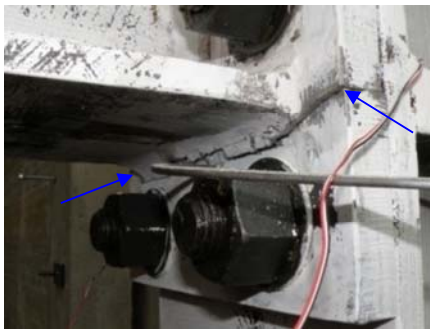

(b) LCF02

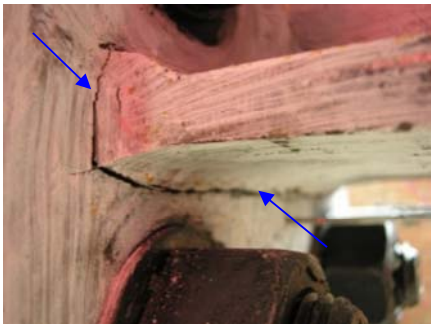

(c) LCF03

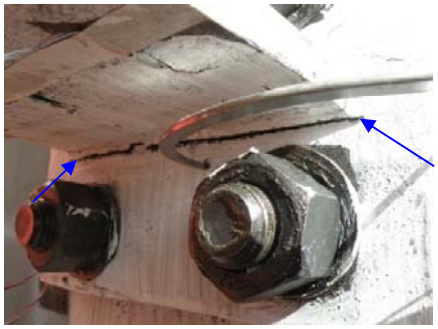

(d) LCF04

Figure 4.11 Ultimate failure mode

All of tests had same failure mode. After several cycles, initial crack was recognized at the end plate. As increase the cycle number, the crack was propagated through end plate cross section. The crack propagation (failure) procedure is showed in Figure 4.12.

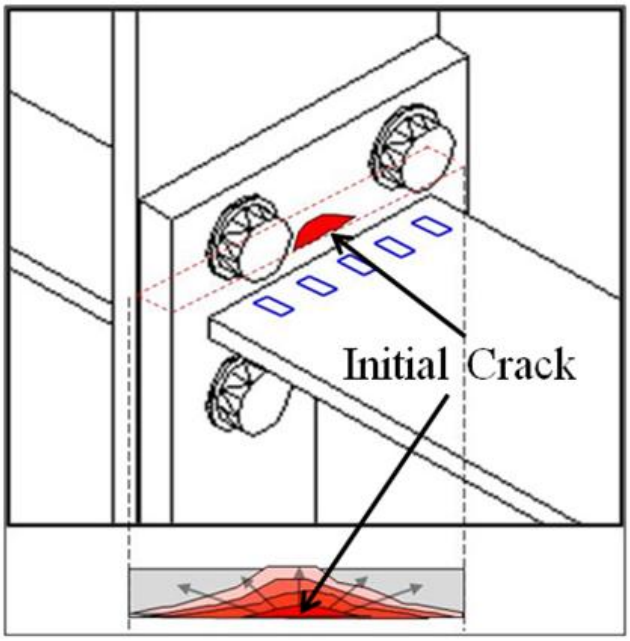

Figure 4.12 End plate cross section and crack propagation

The load-deflection response of the test assembly is illustrated in Figure 4.13. The load was measured at the loading point with MTS load cell. The plotted deflection is the net deflection which is the displacement measured at the loading point with the rigid body displacements of the test rigid subtracted. For clarity, LCF01 and LCF03 graph are plotted with every 10^{th} cycle and LCF06 graph is plotted with every 6^{th} cycle.

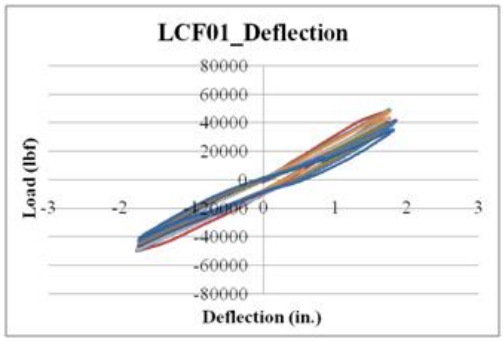

(a) LCF01 Hysteresis loop

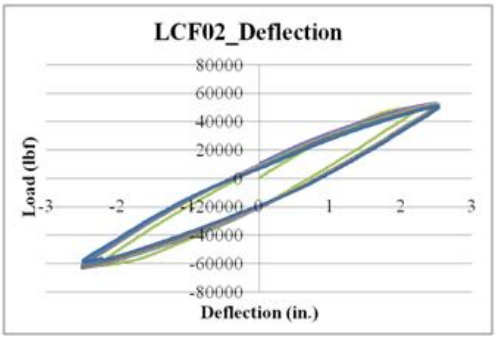

(b) LCF02 Hysteresis loop

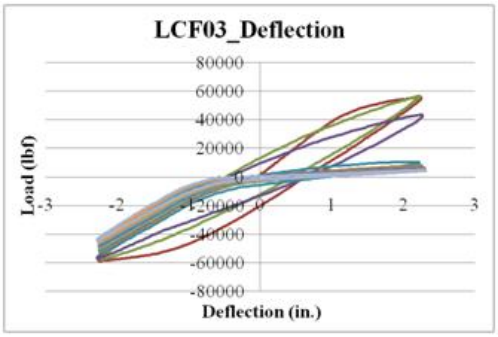

(c) LCF03 Hysteresis loop

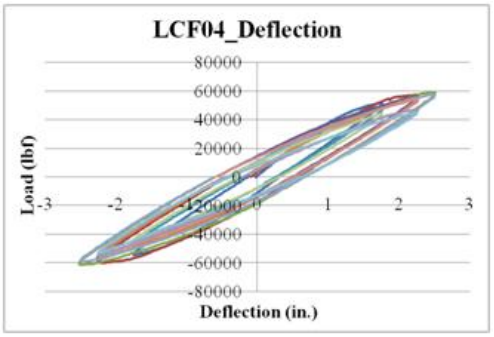

(d) LCF04 Hysteresis loop

Figure 4.13 Tests load deflection response

It is hard to evaluate the end plate behavior because the joint between end plate and beam flange weld had complex stress field. The beam flange strain was one of critical parameter of the test since the flange had a uni-axial stress profile. The bolt tension force was also one of the critical parameter because the failure of the end plate was induced losing the bolt resistance force. Figure 4.14 present the center of beam flange strain in failure side.

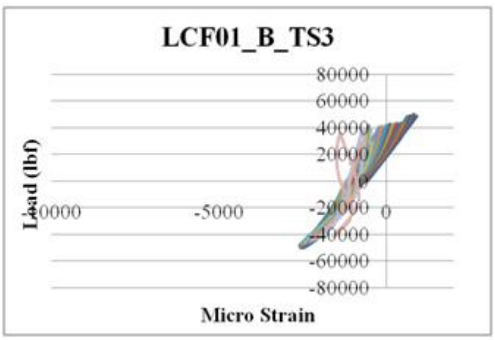

(a) LCF01 Top flange

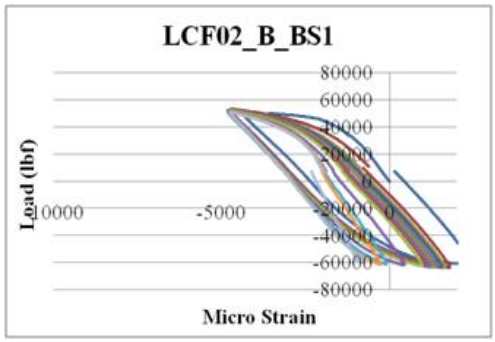

(b) LCF02 Bottom flange

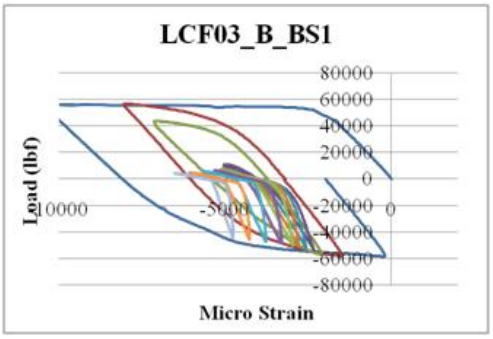

(c) LCF01 Bottom flange

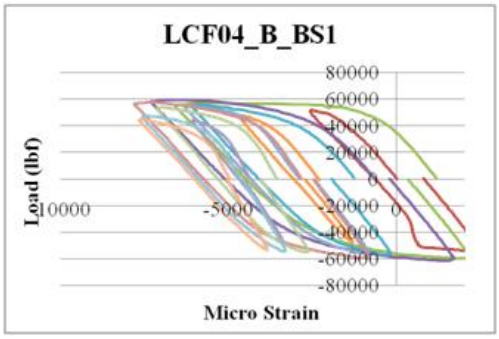

(d) LCF04 Bottom flange

Figure 4.14 Center of beam flange strain

4.3.6 Failure Criteria

Even all collected data shows the system got degradation as the cycles increased like as Figure 4.13 and Figure 4.14, it is hard to define the exact failure number on the connection system because test load was controlled by displacement control and the connections were failed in ductile manner. Therefore the specific failure criteria were needed to define the exact number of system failure.

All of test failure modes were end plate low cycle fatigue failure at the beam flange area and the initial crack was occurred at the center of end plate. The center of beam flange strain is the base of the criteria because it presents the isolated end plate-beam flange interaction. The system failure criteria are revealed by the slope of strain-load

graph. In this paper, we call the slope of strain-load graph by “strain stiffness”. As shown in Figure 4.14, the center beam flange strain stiffness is increased as the cycle number increased because the effect of interaction between end plate and beam flange is decreased. To analyze the strain stiffness, the history of strain stiffness and the time history of reduction percentage of strain stiffness are plotted in Figure 4.15. The reduction percentage is calculated based on the initial strain stiffness. The failure number which based on two criterions is summarized in Table 4-5. When the structure failed, the stiffness of strain reached 70l and the stiffness reduction reached -100%.

Table 4-5 Failure number

Test ID	Stiffness based Failure No. cycles	Reduction based Failure No. cycles
LCF01	148	**138**
LCF02	26	**25**
LCF03	140	**138**
LCF04	84	**84**

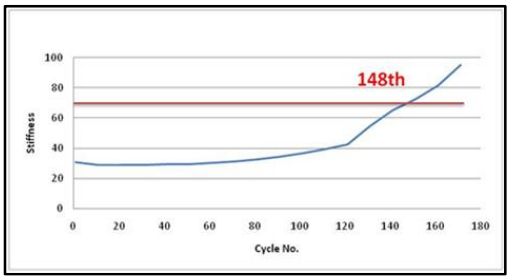

(a) LCF01 Strain stiffness

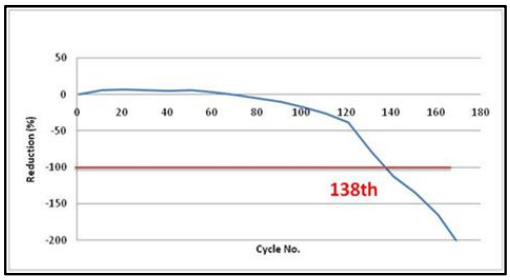

(b) LCF01 Strain reduction

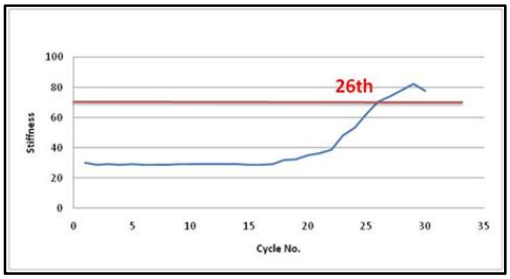

(c) LCF02 Strain stiffness

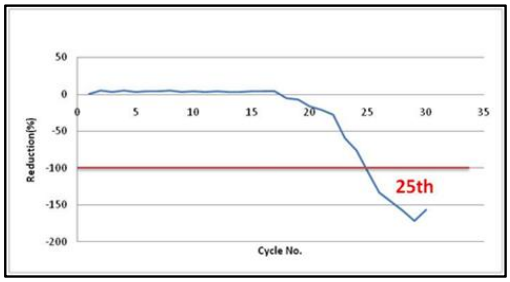

(d) LCF02Strain reduction

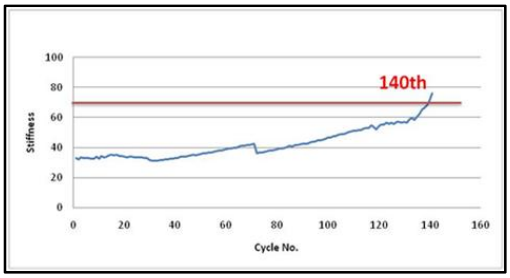

(e) LCF03 Strain stiffness

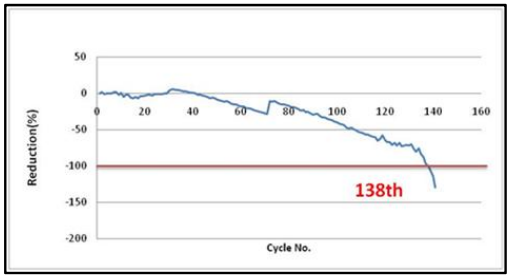

(f) LCF03 Strain reduction

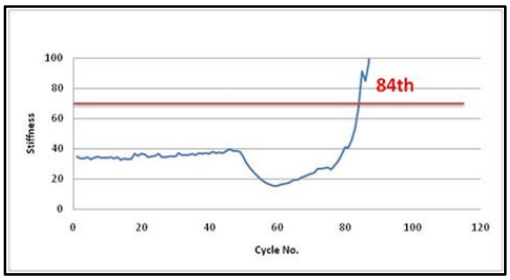

(g) LCF04 Strain stiffness

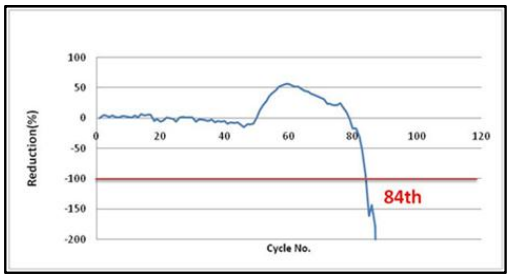

(h) LCF04 Strain reduction

Figure 4.15 Strain stiffness history

4.4 Numerical Analysis

To develop the three dimensional FEM model for beam-column connection, the modeling procedure form an earlier phase of this research was employed. The simplified end plate moment connection (Tstub) was modeled using 3-D solid element and gave a reasonable result. In this study, the FEM model was built with nominal geometric data. Solid element, contact element, target element, and pretension element were used to reduce the calculation load, the simplified modeling concept was used to develop the FEM model. As shown in Figure 4.16, half section of the column flange, end plate, bolts, and beam were modeled with symmetric boundary condition. And the length of the beam section was reduced from 8' 9⅛" inch to 8 inches. At the end of the reduced section, a stiffener was inserted at the end of beam to prevent large distortion of beam flange when the model loading was applied.

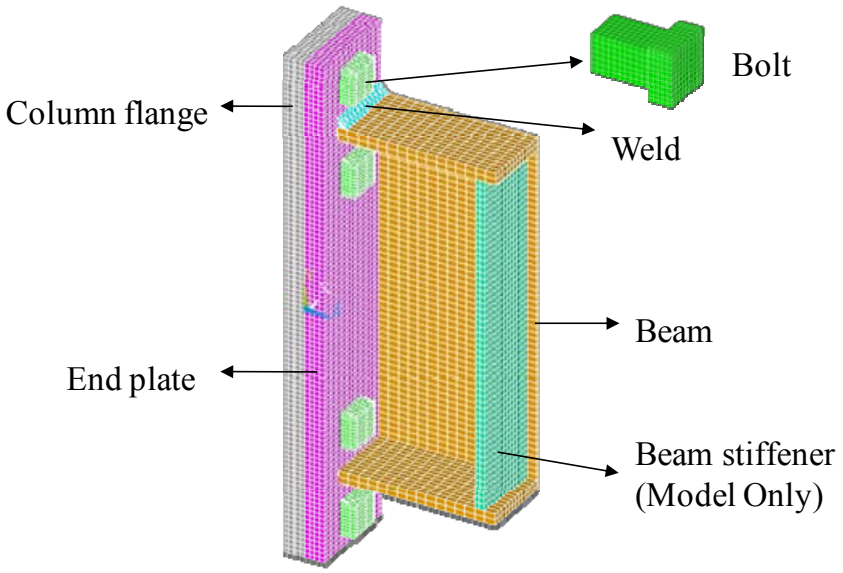

Figure 4.16 Half section 3-D FEM model

To use the simplified FEM model, the point load (F) was transformed into a shear (F)

and a moment load (Me). The loading was applied on the beam cross section by pressure and shear force. The pressure load was simulated the moment loading. Therefore the distributed pressure was applied at the cross section. Figure 4.17 shows the concept of the loading. This concept was validated using a full scale model with no significant difference in results.

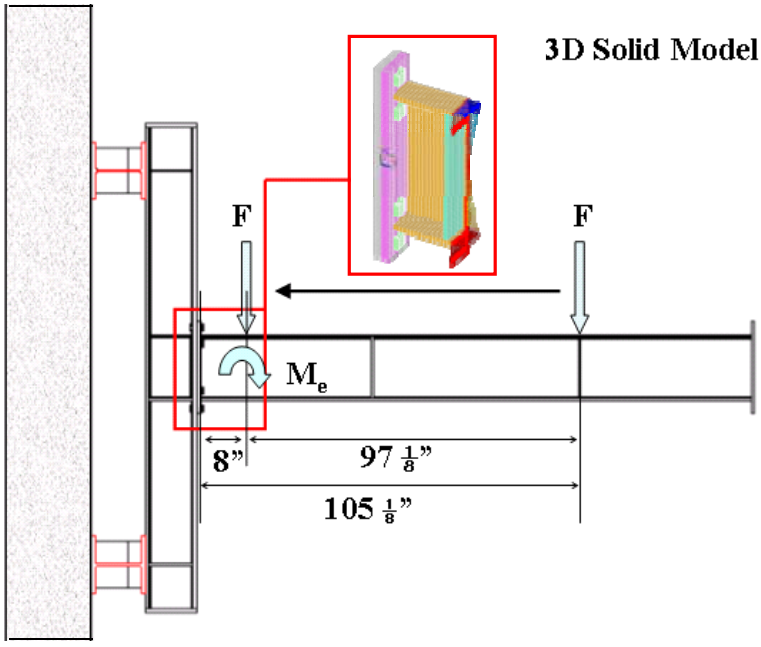

Figure 4.17 FEM modeling concept

The column flange, end plate, beam, and beam stiffener was defined by SOLID45 8 nodes solid element. The weld was defined with SOLID92 20 nodes solid element. The bolts were defined by SOLID92 and PREST179 to apply pretension. There were two contact areas in the FE model. The first area was in between the column flange plate and end plate surface. And second area was in between bolt stud and hole of the column flange and end plate. CONTA175 and TARGE170 elements were used to define the contact condition. The mesh size is 0.1875 inch which chooses through mesh size analysis. A total of 30736 elements were used to represent a half of the

specimen. The properties of the bolt were properly adjusted in order to take into account the rectangular shape of bolt stud. Since the project is focused on the plastic behavior of the system, the analysis options included contact, plasticity, pretension and large displacements.

4.4.1 Boundary condition and material properties

As shown in Figure 4.18, symmetric boundary condition was applied to the half surface. To simulate the column boundary condition, fixed boundary conditions were applied to column flange at the column web and stiffener location. Another boundary condition was the bolt boundary condition which has a fixed boundary condition at the bottom of the stud.

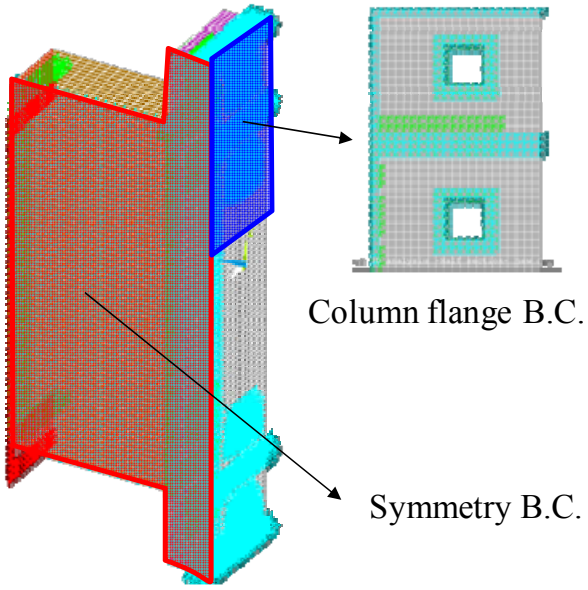

Figure 4.18 Boundary condition of FEM model

Three different materials were used to develop the FEM model. The beam and column were used the measured material property. And the bolt was adopted the previous

research (Wade, 2006) material property. To evaluate the property of the end plate, supplementary tensile coupon tests were conducted in accordance with ASTM A370 "Standard Test Methods and Definitions for Mechanical Testing of Steel Products". Three tension coupon samples were taken from the end plate part included in the test program. An average of the stress-strain curve was derived from the three coupon tests. Figure 4.19 showed the plate and bolt material property.

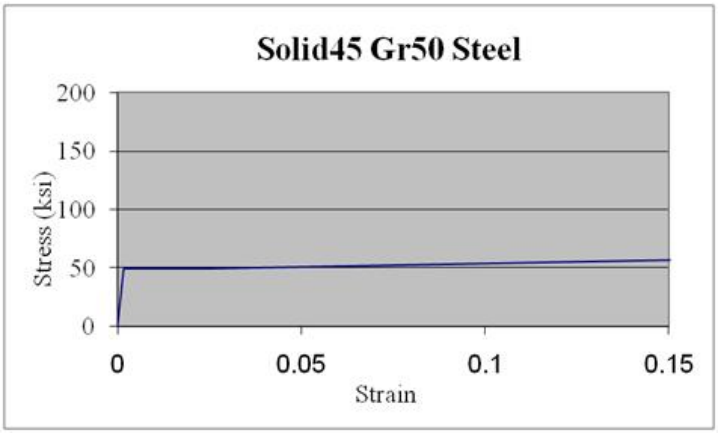

(a) Plate stress-stain curve

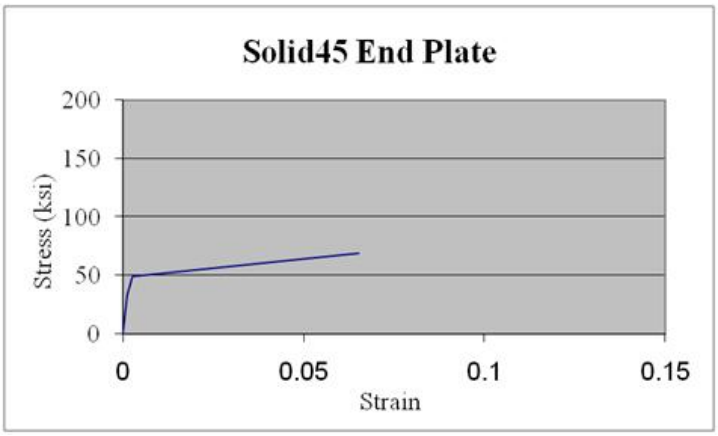

(b) Plate stress-stain curve

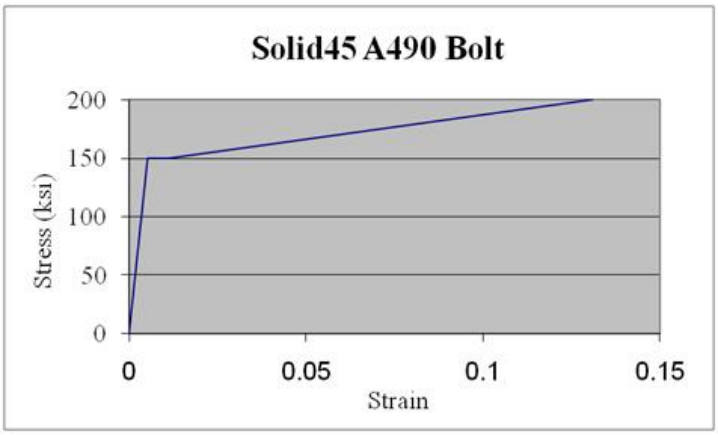

(c) Bolt stress-strain curve

Figure 4.19 Element material properties

4.4.2 Loading

In the first load step, the bolt pretension force was applied with 100kips pretension to simulate fully tightened moment connection. The Figure 4.20 (a) shows the pretension deformed shape and the von-misses stress contour. The distributed pressure was applied through the beam cross section to apply the moment loading. Since the beam cross section had a symmetric shape, the maximum pressure was applied top and bottom with opposite direction. At the same time, the shear load was applied through the beam cross section. (Figure 4.20 (b)) The maximum applied moment force was 530 kips-ft.

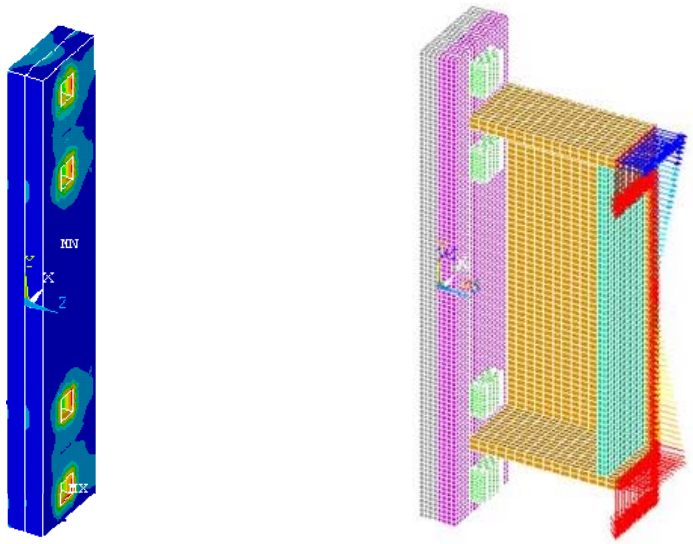

(a) Pretension force (Von-mises) (b) Applied force and pressure load

Figure 4.20 Loading

4.4.3 Result

The performance of the system is present to the Figure 4.21 as the load increase. The contour is the von-mises stress and the deformation is real scale. As shown Figure 4.21, the four stages of deformed shapes with von-mises stress contour were used to

check the general behavior of the FEM model. Figure (a) present the pretension stage. The end plate and column flange had a large compression stress; it shows all the contact element and pretension member work properly. Figure (b) and (c) shows the Von-mises stress contour at each loading point. Figure (d) presents the maximum load stage. Due to the shear force, stress concentration effect occurred at the contact surface between the bolt stud and bolt hole. Similar with previous study, the beam flange position had a maximum deformation at the end plate. The beam had a symmetric stress contour because symmetric pressure load was applied. The top of the beam flange had a tension stress and the bottom of the beam flange had a compression stress.

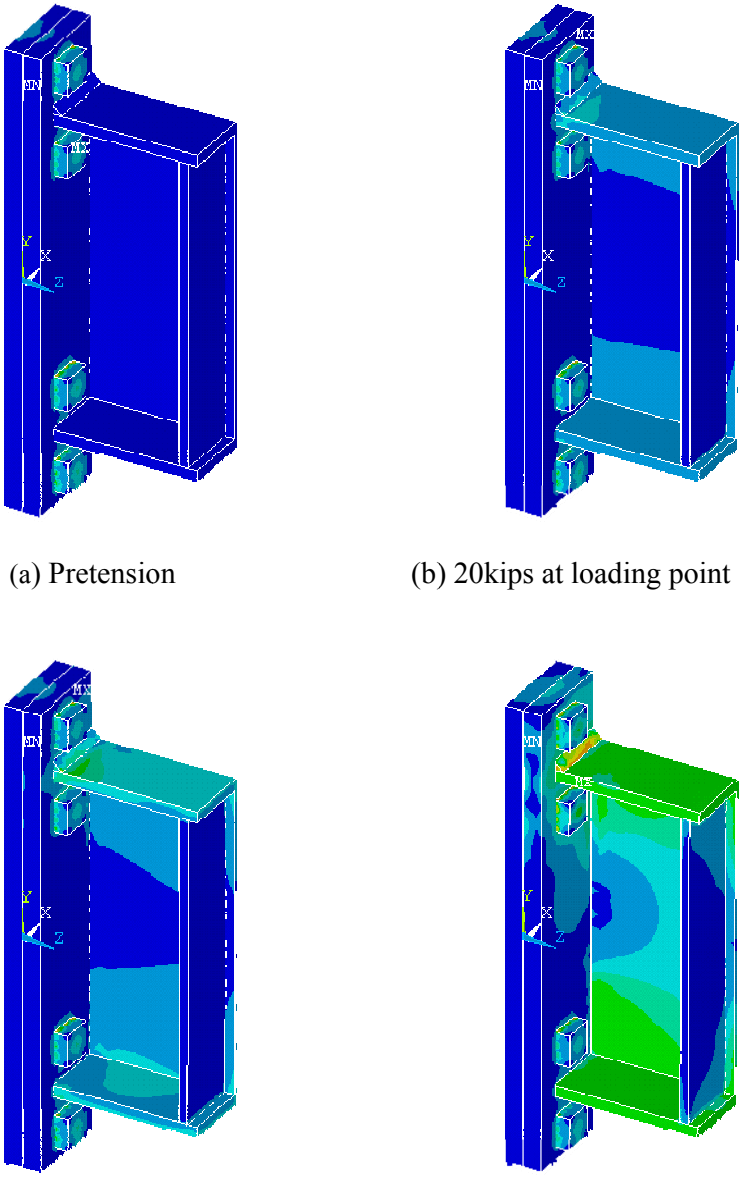

(a) Pretension (b) 20kips at loading point

(c) 30kips at loading point (d) 50kips at loading point

Figure 4.21 Behavior of FEM analysis (Von-mises contour)

In the end plate, the maximum displacement occurred through the beam flange line. Figure 4.22 presents the load-displacement curve at the center of loading line with z-direction deformation of end plate. The end plate started to yield at about 200kips-ft

and the system had a large displacement as load increasing.

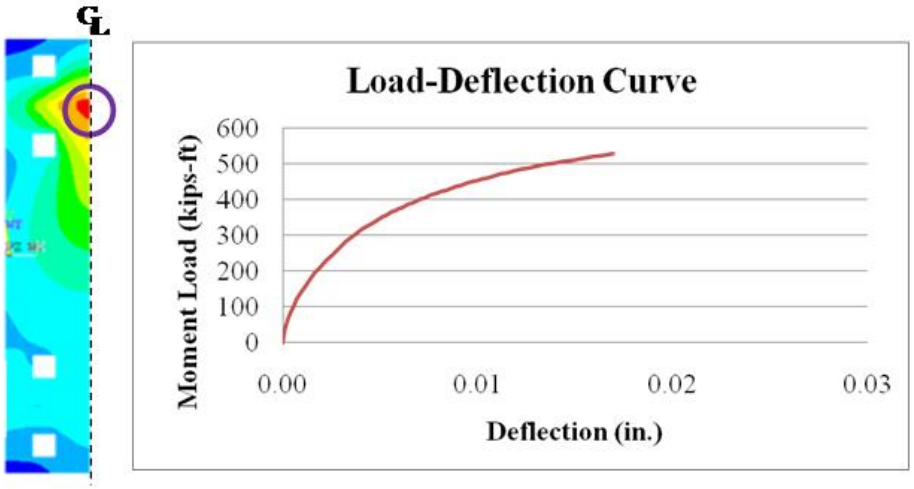

Figure 4.22 Load displacement response of FEM

4.5 Analysis of Results

4.5.1 General behavior

To compare the experimental result with FEM analysis result, the center of base plate point was selected as shown Figure 4.23. As shown in Figure 4.24, the load-strain curves obtained from the numerical analysis show a rather good agreement with the experimental results. In particular, the yielding limit of the theoretically obtained line is very close to both the experimental and numerical yielding level. The FEM model was adopted LCF01 test information and the results were compared with experimental programs. The end plate expected yield limit was calculated by yield line theory. The yield line limit was similar with the theoretical assumption. Therefore three approaches, theoretical, numerical, and experimental, have good relationship among each other.

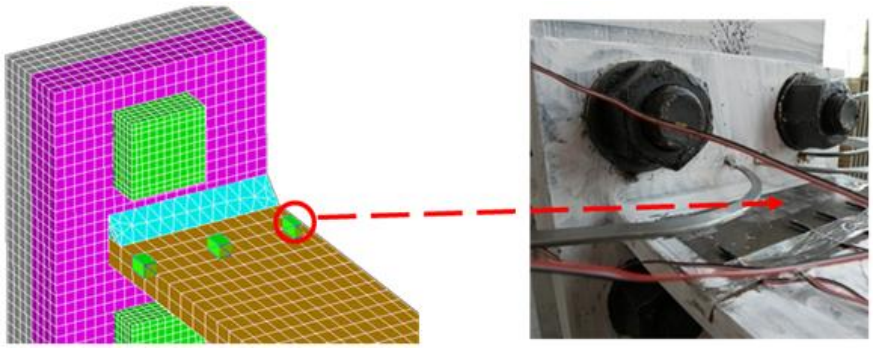

(a) LCF01 Data collect point

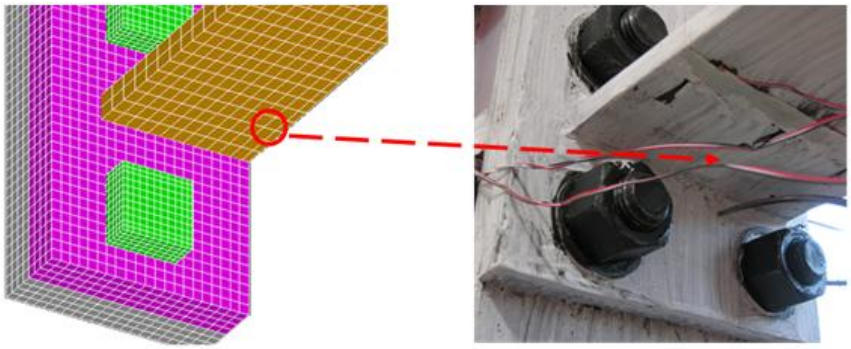

(a) LCF04 Data collect point

Figure 4.23 Data collection point

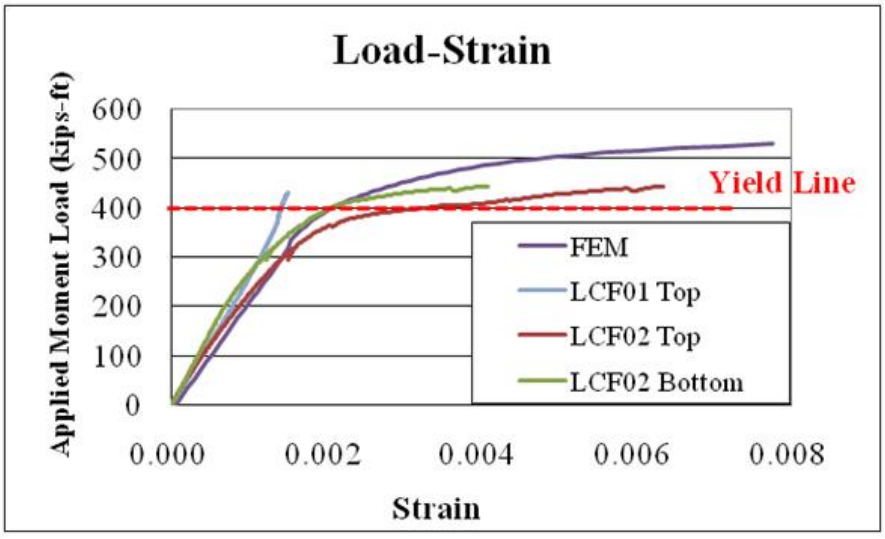

Figure 4.24 Comparison of results

In this study, the S is the displacement load and N is the reversal number. Table 4-6

was present the S-N data. LCF03 test used half cycle after 20 full cycles because the early crack development. The low cycle fatigue model can be draw as Figure 4.25.

Table 4-6 S-N Curve data

Test ID	Applied Disp.(S)	Failure No.(N)	log S	log N
LCF01	1.75	276	0.243	2.441
LCF03	2.25	158	0.352	2.199
LCF02	2.5	50	0.398	1.699

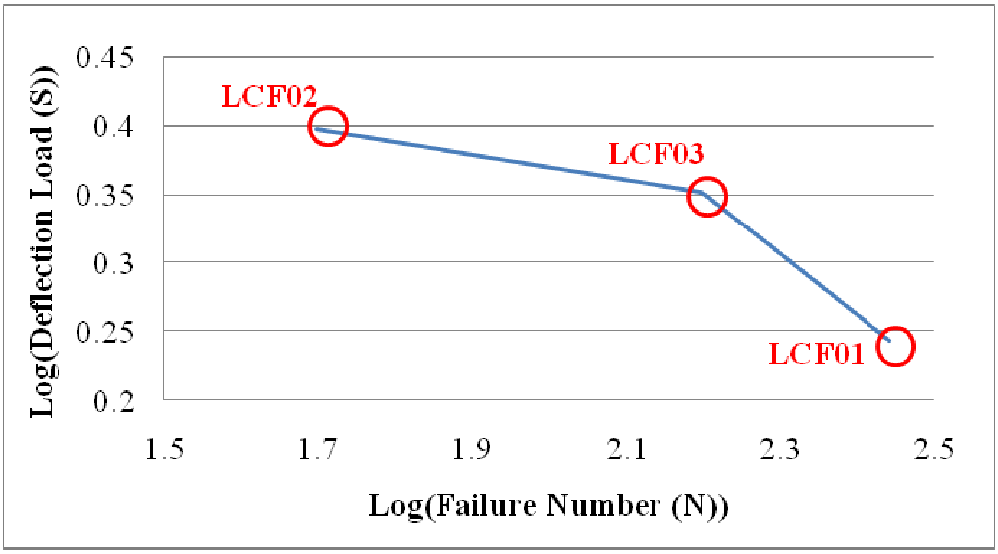

Figure 4.25 Low cycle fatigue model

Each different level of the peak constant displacement load brought different failure number of cycles and different crack initiation number of cycles. After the crack developed in the connection system, the displacement load was not changed but the system responses were changed.

4.5.2 Life prediction

Previous result developed the LCF model for 4E EPMC. Three constant peak cyclic loads were used to develop the LCF model. Because LCF life prediction test used exactly same test specimen and test setup, the LCF model can be used without any change. Figure 4.25 presents the LCF model. The Manson-Coffin relation equation, Equation 4-3, was used to develop the LCF model. Equation 4-7 presents the 4E EPMC LCF model for current geometry.

$$N_f = 4020(\Delta S)^{-4.787} \qquad \textbf{Equation 4-7}$$

However, the LCF model, Equation 4-7, used only two test result. As shown in Figure 4.26, the S-N curve is not the straight line. Therefore this study used the trend line considering three data point. Figure shows the trend line equation on log-log plot graph.

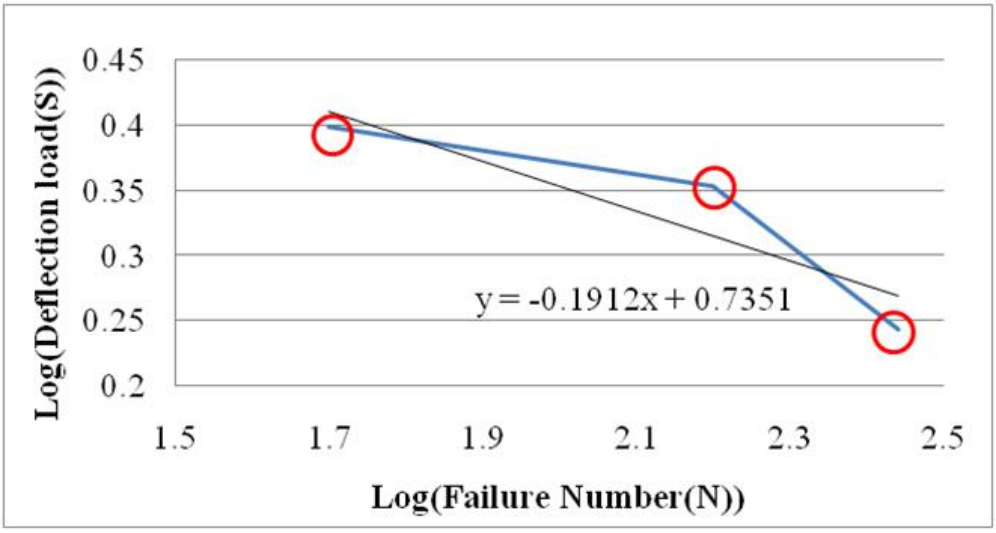

Figure 4.26 Trend line equation on log-log plot graph

Base on the trend line S-N curve, the Equation 4-7was changed to Equation.

$$N_f = 6978(\Delta S)^{-5.227} \qquad \textbf{Equation 4-8}$$

In order to anticipate the LCF failure in the 4E EPMC system, the Miner's rule was adopted. (Equation 4-4) The damage fraction, D_i was calculated using Equation 4-5. Each damage fraction presents the life reduction from the total structure life. In this study, the damage criterion X is assumed to be equal to 1.0, and failure is predicted to occur when the damage fraction reach at 1. (Equation 4-6) Table 4-7 and Figure 4.27 presents the test result and damage history. The anticipated failure number is 110 reversal based on the Miner's rule. It is 9% difference with experimental failure number.

Table 4-7 Damage history

Load	ΔS	n_i	N_i	D_i	X_i	Reversal
G1	1.75	12	374.5812	0.0320	0.0320	12
G2	2.25	12	100.6637	0.1192	0.1512	24
G3	2.5	12	57.99481	0.2069	0.3582	36
G4	2.25	12	100.6637	0.1192	0.4774	48
G5	1.75	12	374.5812	0.0320	0.5094	60
G6	2.25	12	100.6637	0.1192	0.6286	72
G7	2.5	6	57.99481	0.1035	0.7321	78
G8	2.25	6	100.6637	0.0596	0.7917	84
G9	1.75	6	374.5812	0.0160	0.8077	90
G10	2.25	6	100.6637	0.0596	0.8673	96
G11	2.25	6	100.6637	0.0596	0.9269	102
G12	2.25	6	100.6637	0.059604	0.986506	108
G13	2.25	6	100.6637	0.059604	1.04611	114

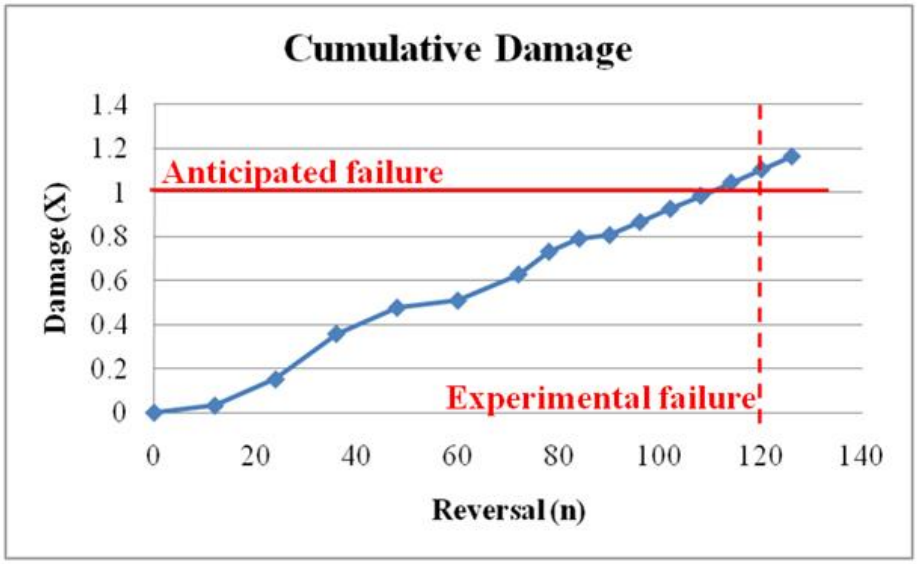

Figure 4.27 Damage history

4.6 Conclusion

The study presented in this paper is part of a research program which has three tasks to explain the LCF behavior of four bolts extended unstiffened EPMC; i) validate analytical tools to predict the structural response of reduced EPMC (T-stub); ii) investigate the cyclic LCF behavior of EPMC through experimental tests and analytical modeling; iii) evaluate the accumulation of low cycle fatigue damage so that the structure life can be predicted. This paper focuses on the results of the second and the third task of the large research objectives.

The Coffin and Manson equation is adopt to make the low cycle fatigue model with experimental result. The equation needs the constant peak cyclic loading test results to draw a linear line in log-log plot graph. Because the test loading range is in plastic behavior range, the pre-analysis is conducted to confirm the level of constant cyclic loading. Total 3 different level of constant cyclic loading levels are choose to develop

the low cycle fatigue model. Three different approaches were adopted to analyze the 4E EPMC. The theoretical analysis defined the yield limit of system. The numerical analysis verified the theoretical result and simulated the behavior of the experimental test. Shown as Figure 4.24, three different approaches show good relationship. Based on the three constant peak displacement load test results, low cycle fatigue model was developed to predict the low cycle fatigue failure. The LCF model was verified with the random load test by prediction of the connection life. Based on the result of the 4E EPMC tests, the following conclusions can be summarized.

- The yield line theory can be accurately predict the end plate flexural yield limit.
- The numerical modeling can accurately simulate the non-linear behavior EPMC with large deflections.
- The location of low cycle fatigue failure can be predicted by the numerical model. The weld root at the face of the end-plate is the most critical location for crack initiation.
- The LCF model can be use to predict the life of EPMCs.
- The displacement load can successfully be used as the LCF model index "S"

4.7 Future Work

- Additional full scale experimental cyclic tests are needed to verify the developed LCF model.
- LCF investigation program needed to determine the LCF behavior on beam flange.

- Additional theoretical analysis needed to apply different LCF modeling method.
- Parametric study needed to determine the LCF geometric characteristic.

4.8 References

AISC (2003). "Steel Design Guide 4 Extended End-Plate Moment Connections Seismic and Wind Applications", Chicago

AISC (2002), "AISC Design Guide 16: Flush and Extended Multiple-Row Moment End-Plate Connections", American Institute of Steel Construction, Chicago.

ASTM (2001). "Standard Specification for General Requirements for Rolled Structural Steel Bars, Plates, Shapes, and Steel Piling, ASTM A6.

ASTM (1998) , ASTM E606: Standard Practice for Strain-Controlled Fatigue Testing, Philadelphia, PA, vol. 03.01, pp. 525-539.

AWS (2002). "Structural Welding Code - Steel", American Welding Society, AWS D1.1-98, Miami

Adany, S., Dunai, L., (2004). "Finite Element Simulation of The Cyclic Behavior of End-Plate Joints", Computers & Structures, 82, 2131-2143

Adey, B.T., Grondin, G.Y., and Cheng, J.J.R. (1997). "Extended End Plate Moment Connections under Cyclic Loading", Department of Civil Engineering University of Alberta, Structural Engineering Report No. 216

Bahaari, M. R.,Sherbourne, A. N., (2000). "Behavior of eight-bolt large capacity endplate connections", Computers & Structures, 77, 315-325

Ballio, G., Calado, L., Castiglioni, C. A., (1997). "Low cycle Fatigue Behavior of Structural Steel Members and Connections", Fatigue & Fracture of Engineering Materials & Structures, vol. 20, no 8, 1129-1146

Barsom, J. M., Pellegrino, J. V., (2002). "Failure Analysis of Welded Steel Moment-Resisting Frame connections", Journal of materials in civil engineering.

Borgsmiller, J., (1995). "Simplified Method for Design of Moment-End-Plate Connections", M.S. Thesis, Virginia Polytechnic Institute and State University, Blacksburg, VA.

Bose, B., Wang, Z. M., Sarkar, S., (1997). "Finite-Element Analysis of Unstiffened Flush End-Plate Bolted Joints", Journal of Structural Engineering, Vol. 123, No. 12

Bursi, O. S., Jaspart, J. P., (1997). “Calibration of a Finite Element Model for Isolated Bolted End-Plate Steel Connections”, J. Construct. Steel Res. Vol. 44, No. 3, pp. 225-262

Bursi, O. S., Ferrario, F., Fontanari, V., (2002) "Non-linear Analysis of the Low-cycle Fracture Behaviour of Isolated Tee Stub Connections", Computers & Structures, 80, 2333-2360.

Coffin, Jr., C.F. (ed.) (1969). Manual on Low Cycle Fatigue Testing, ASTM, STP 465, American Society for Testing and Materials, Philadelphia

Coffin, L. F., Jr.,(1954). "A study of the Effects of Cyclic Thermal Stresses on a Ductile metal", Trans. ASME, Vol. 76 .p.p . 931-950.

Sumner, E. A., (2003). “Unified Design of Extended End-Plate Moment Connections Subject to Cyclic Loading”, Ph.D. Dissertation, Virginia Polytechnic Institute and State University, Blacksburg, VA.

Ewens, S., (1997). “Experimental Verification of A Simplified Method for Design of Structural Tee Hangers”, M.S. Dissertation, Virginia Polytechnic Institute and State University, Blacksburg, VA.

FEMA. (2000a), FEMA 350 Recommended Seismic Design Criteria for New Steel Moment-Frame Buildings, FEMA, Washington, DC.

FEMA. (2000b), FEMA 351 Recommended Seismic Evaluation and Upgrade Criteria for Existing Welded Steel Moment-Frame Buildings, FEMA, Washington, DC.

Garlock, M. M., Ricles, J. M., Sause, R., (2003). "Cyclic Load Tests and Analysis of Bolted Top-and-Seat Angle Connections", Journal of Structural Engineering.

Garlock, M. M., Ricles, J. M., Sause, R., (2005). "Experimental Studies of Full-Scale Posttensioned Steel Connections". Journal of Structural Engineering ASCE.

Ghobarah, A., Osman, A., Korol, R.M., (1990). "Behaviour of extended end-plate connections under cyclic loading", J. Struct. Engr. 12 1, pp. 15-27

Hendrick, D., Kukreti, A. R., Murray, T. M., (1984). “Analytical and Experimental Investigation of Stiffened Flush End-Plate Connections with Four Bolts at The Tension Flange”, Research Report FSEL/MBMA 84-02, Fears Structural Engineering Laboratory, University of Oklahoma, Norman, OK.

Kaufmann, E. J., Fisher, J. W.; DiJulio, R. M., Jr.; Gross, J. L., (1997). "Failure Analysis of Welded Steel Moment Frames Damaged in the Northridge Earthquake", NISTIR 5944; 175 p.

Kasai, K., Xu, Y., (2003). “Cyclic behavior and low-cycle fatigue of semi-rigid

connections (Part II: bolted T-stub connections)", Behaviour of Steel Structures in Seismic Areas, STESSA 2003, Balkema, pp. 321–327

Kennedy, N.A., Vinnakota, S., Sherbourne, A.N., (1981). "The Split-Tee Analogy in Bolted Splices and Beam-Column Connections", Joints in Structural Steelwork, John Wiley & Sons, London-Toronto, pp. 2-138-2.157.

Krawinkler, H., Popov, E.P., (1982). "Seismic Behavior of Moment Connections and Joints", Journal of Structural Division, ASCE 108 2 , pp. 373-391

Krishnamurthy, N., Graddy, D.E., (1976). "Correlation Between 2- and 30 Dimensional Finite Element Analysis of Steel Bolted End-Plate Connections," Computers & Structures, Pergamon, 6(4-5/6), 381-389

Kuwamura, H., (1997). "Transition between Fatigue and Ductile Fracture in Steel", Journal of Structural Engineering, Vol. 123, No. 7.

Kuwamura, H., and Suzuki, T. (1992). "Low-Cycle Fatigue Resistance of Welded Joints of High-Strength Steel under Earthquake Loading", Proceedings of the Tenth World Conference on Earthquake Engineering, Madrid, Spain, Vol.5, pp.2851-2856

Landgraf, R.W., Morrow, J., Endo, T., (1969). "Determination of the cyclic stress–strain curve", Journal of Materials, JMLSA, 4(1), pp.176-188

Mays, T. W., (2000). " Application of The Finite Element Method to The Seismic Design and Analysis of Large Moment End-Plate Connections", Ph.D. Dissertation, Virginia Polytechnic Institute and State University, Blacksburg. VA.

Manson, S.S., Freche, J.C., Ensign, C.R., (1967). "Application of a double linear damage rule to cumulative fatigue. Fatigue Crack Propagation", ASTM STP 415, pp. 384-41

Matteis, D., Mandara, A., Mazzolani, F.M. (2000). "T-stub Aluminium Joints: the Influence of Behavioural Parameters", Computers and Structures, Pergamon, ISSN 0045-7949, Oxford (UK),Vol. 78, No. 1-3, 311-327.

Matteis, G. De, (2004). "Experimental Behaviour of Aluminium T-stub Connections", Connections in Steel Structures V- Amsterdam

Mazzolani, F., (1999). "Moment Resistant Connections of Steel Frames in Seismic Areas", Taylor & Francis

Meng, R. L. (1996), "Design of Moment End-Plate Connections for Seismic Loading", Ph.D. Dissertation, Virginia Polytechnic Institute and State University, Blacksburg, VA.

Miner, M.A., (1945). Trans. ASME, J. Appl. Mech. 67, p. A159.

Morrison, S. J., Astaneh-Asl,, A., Murray, T. M., (1986). "Analytical and

Experimental Investigation of the Multiple Row Extended 1/3 Moment End-Plate Connection with Eight Bolts at the Beam Tension Flange," Report No. FSEL/MBMA 86-01, University of Oklahoma, Norman, Oklahoma.

Morrow, J., (1965). "Cyclic plastic strain energy and fatigue of metals", American Society for Testing and Materials, ASTM STP 378

Murray, T.M., (1988). "Recent Developments for the Design of Moment End-Plate Connections", Construction Steel Research 10 133-162

Neuber, H., (1961). "Theory of Stress Concentration for Shear-Strained Prismatical Bodies with Arbitrary Nonlinear Stress-Strain Laws," Journal of Applied Mechanics, Trans. ASME, Vol. E28, 544.

Partridge, J.C., Paterson S.R. and Richard R.M., (2000). "Low Cycle Fatigue Tests and Fracture Analyses of Bolt-Welded Seismic Moment Frame Connections"

Palmgren, A., (1924). "Die Lebensadauer von Kugellagern,", Z. Vereines Deutcher Ingenieure, Vol. 68, pp. 339-341

Rothert, H., Gebbeken, N., Binder, B., (1992). "Non-Linear Three-Dimensional Finite Element Contact Analysis of Bolted Connections in Steel Frames", International Journal for Numerical Methods in Engineering, Vol. 34, 303-3 18

RECOS, (2000). "Moment Resistant Connections of Steel Frames in Seismic Areas Design and Reliability", Taylor and Francis, ISBN: 978-0-415-23577-8.

SAC Joint Venture. (1997). "Protocol for fabrication, inspection, testing and documentation of beam-column connection tests and other experimental specimens", Rep. No. SAC/BD-97/02, Sacramento, Calif.

Schneider, S. P., Teeraparbwong, I. (2000). "Bolted flange plate con-nections", Rep. No. SAC/BD-00/05, Sacramento, Calif.

Sherbourne, A. N., Bahaari, M. R., (1994). "3D Simulation of End-Plate Bolted Connections", Journal of Structural Engineering, Vol. 120, No. 11

Srouji, R., Kukreti, A., Murray, T. M., (1983). "Yield-Line Analysis of End-PlateConnections with Bolt Force Predictions", Report No. FESL/MBMA 83-05, University of Oklahoma, Norman, Oklahoma.

Stojadinovic, B., (2003) "Stability and Low-Cycle Fatigue Limits of Moment Connection Rotation Capacity," Engineering Structures, Elsevier Science

Sumner, E. A. and Murray, T. M. (2002). "Behavior of Extended End-Plate Moment Connections Subject to Cyclic Loading", Journal of Structural Engineering, ASCE, vol. 128, no. 4, pp. 501-508.

Tsai, K.C., Popov, E.P., (1990). "Cyclic behaviour of end-plate moment connections",

Journal of Structure Engineering, 116 11, pp. 2917-2930

Wade, P., (2006). “Characterization of High-strength Bolt Behavior in Moment Connections”, Master’s Dissertation, North Carolina State University, Raleigh, NC.

Chapter 5 Parametric Study of LCF Geometries

5.1 Introduction

In past research related to the investigation of the cyclic behavior of the End Plate Moment Connection (EPMC), Low Cycle Fatigue (LCF) behavior was observed within the connection components. However, the study by Lim (Lim, 2009) was limited to a single EPMC geometric combination. Due to the large number of material and geometric parameters related to EPMCs, a study to investigate the sensitivity of the LCF behavior to changes in critical parameters is needed. To investigate the sensitivity a parametric study has been conducted at NCSU CFL using numerical (FEM) analysis. The study includes the variation of three critical geometric properties; end-plate thickness (t_p), inner and outer pitch distances (p_f), and the connection beam flange thickness (t_p) as defined in Figure 5.1. Figure 5.1 shows the detail geometric information of the end plate.

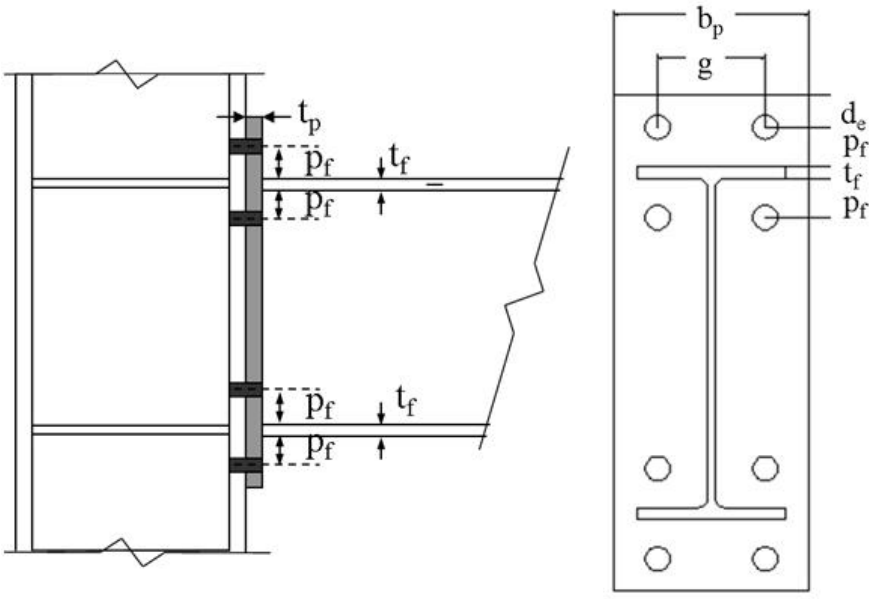

(a) Side view (b) Front view

Figure 5.1 Detail geometry of end plate

The primary objectives of this chapter are to investigate effect of the indentified geometric parameters on the LCF behavior of EPMCs and to apply propose appropriate modifications to the LCF model.

5.2 Critical Geometry

The low cycle fatigue effect is primarily related to the inelastic deformation of the connection. In the EPMC, the largest inelastic deformation typically occurs in the end plate beam flange connection region. Three main parameters directly affected to the end plate inelastic deformation. The first parameter is end plate thickness (t_p). Second is beam flange thickness (t_p) and the third is bolt location (p_f) between beam flange and bolt center.

The numerical models were created based on the original four bolt extended

unstiffened EPMC geometric parameters. Utilized in Lim (2009), this model is designated LCF-1-0625-2 in Table 5-1. The additional models were created with on critical parameter modified in each one. Table 5-1 presents the numerical analysis test matrix.

Table 5-1 Parametric numerical analysis matrix

Model ID	End plate THK(t_p)	Flange THK(t_f)	Bolt location(p_f)
LCF-1-0625-2 (original)	1	0.625	2
LCF-075-0625-2	0.75	0.625	2
LCF-125-0625-2	1.25	0.625	2
LCF-1-075-2	1	0.75	2
LCF-1-05-2	1	0.5	2
LCF-1-0625-225	1	0.625	2.25
LCF-1-0625-25	1	0.625	2.5

5.3 Parametric Study Model

The FEM model utilized in the parametric study was developed in previous phase of this research project. The model was previously used to anticipate general behavior of the experimental tests. The FEM model showed good relationship with experimental results and was used to validate the numerical results. Figure 5.2 shows the pre-developed 3D FEM model. The FEM model developed with simplified half section of specimen and it consists with 4 types of element; solid element, contact element, target element, and pretension element. And the beam section was reduced from 105.125 inch to 8 inch. In reduced section, stiffener was inserted at the end of beam to prevent large defection of beam flange. The applying load (F) is translated to

equivalent moment (Me) and shear force (F).

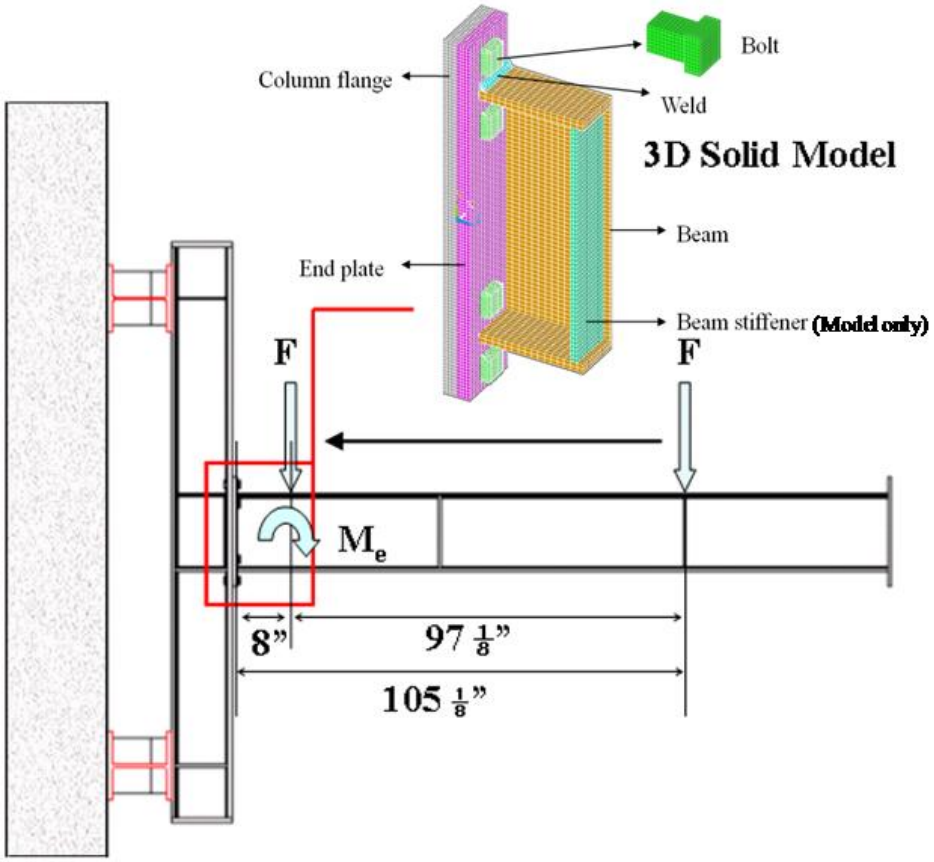

Figure 5.2 Half section 3-D FEM model

The column flange, end plate, beam, and beam stiffener was defined by SOLID45 8 nodes solid element. The weld was defined with SOLID92 20 nodes solid element. The bolts studs were defined by SOLID92 and PREST179 to apply pretension. There were two contact areas in the FE model. The first area was in between column flange plate and end plate surface. And second area was in between bolt stud and hole of the column flange and end plate. CONTA175 and TARGE170 elements were used to define the contact condition. The mesh size is 0.1875 inch which chooses through mesh size analysis. The properties of the bolt were properly adjusted in order to take

into account the rectangular shape of bolt stud. As shown in Figure 5.3, symmetric boundary condition was applied to the half surface. To simulate the column boundary condition, fixed boundary conditions were applied to column flange at the column web and stiffener location. Another boundary condition was the bolt boundary condition which has a fixed boundary condition at the bottom of the stud.

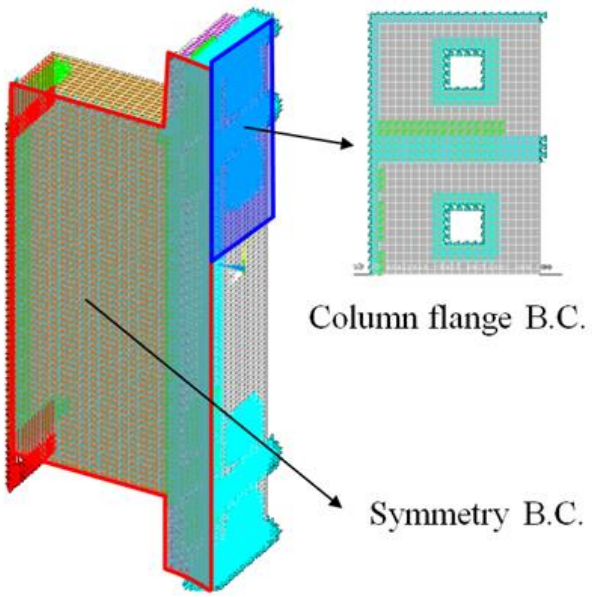

Figure 5.3 Boundary condition of FEM model

Three different materials were used to develop the FEM model. The beam and column were used the measured material property. And the bolt was adopted the previous research (Wade, 2006) material property. To evaluate the property of the end plate, supplementary tensile coupon tests were conducted in accordance with ASTM A370 “Standard Test Methods and Definitions for Mechanical Testing of Steel Products”. Three tension coupon samples were taken from the end plate part included in the test program. An average of the stress-strain curve was derived from the three coupon tests. The Figure 5.4 is showed the plate and bolt material property.

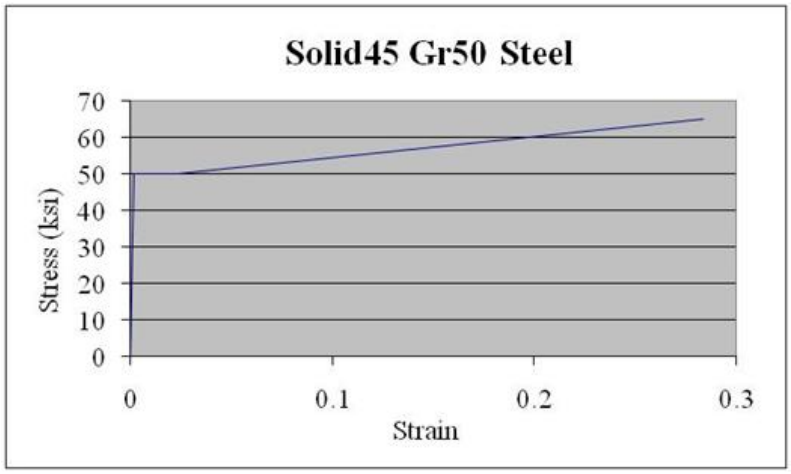

(a) Plate stress-stain curve

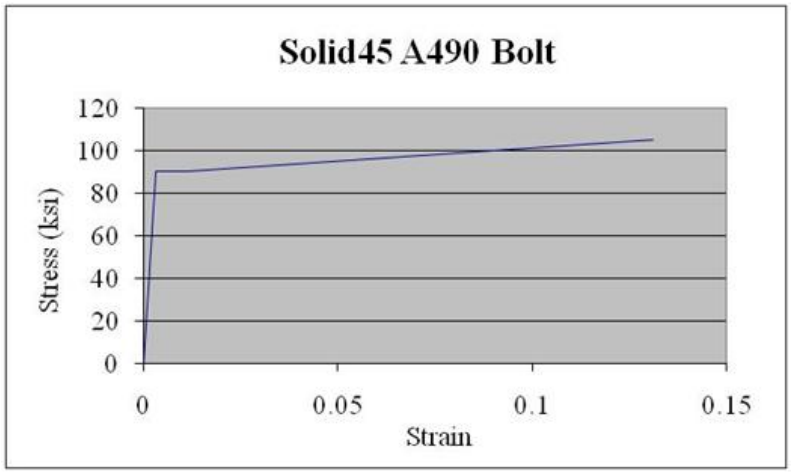

(b) Plate stress-stain curve

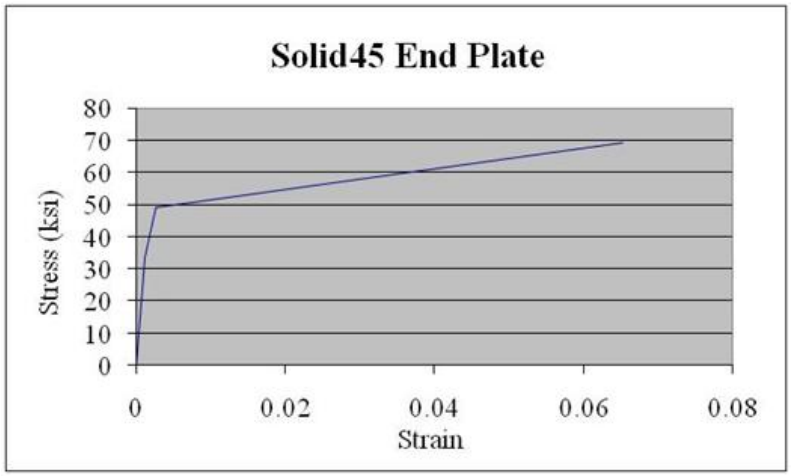

(c) Bolt stress-strain curve

Figure 5.4 Element material properties

The load was imposed through two steps. In the first load step, the bolt pretension force was applied with 100kips pretension to simulate fully tightened moment connection. The Figure 4.20 (a) shows the pretension deformed shape and the von-misses stress contour. The distributed pressure was applied through the beam cross section to apply the moment loading. Since the beam cross section had a symmetric shape, the maximum pressure was applied top and bottom with opposite direction. At the same time, the shear load was applied through the beam cross section. (Figure 4.20 (b)) The maximum applied moment force was 530 kips-ft.

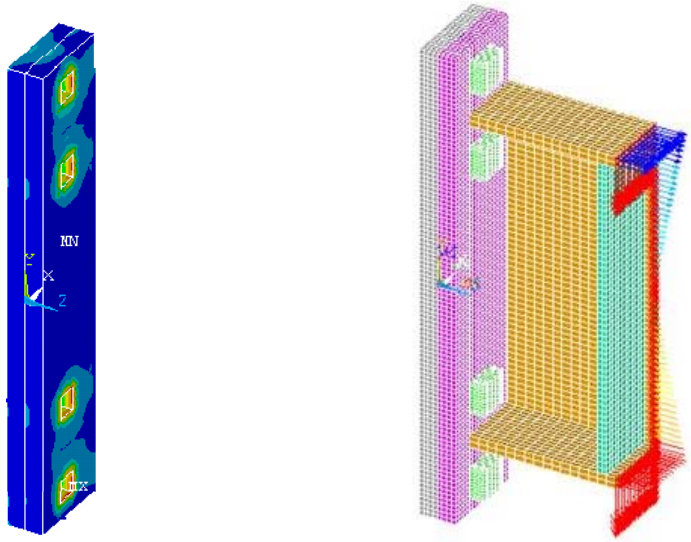

(a) Pretension force (Von-mises) (b) Applied force and pressure load

Figure 5.5 Loading

5.4 Analysis of Results

5.4.1 General behavior

The seven parametric FEM models were analyzed with the commercial code ANSYS. The models were classified into three categories based on the three critical parameters.

To understand the general behavior of the connection, the Von-mises stress contour was plotted in Figure 5.6 for all parametric models at the maximum load level (530 kips-ft). And the deformation which is end plate out of plane displacement of center of crack point response was plotted in Figure 5.7. Overall FE model behaviors were reasonable. Figure 6.7 shows all test model had symmetric response of the system and the maximum stress was generated at the connection between end plate and beam flange. The end plate thickness parameter group (Figure 5.6 (a)) shows the increase of the end plate thickness generated more response of the beam and the less deformation on the crack point (Figure 5.7 (a)). The thicker end plate gets more stiff response. The beam flange thickness parameter group (Figure 5.6 (b)) shows the increase of the beam flange thickness generated similar performance with end plate thickness parameter group. However the effect for the deformation of the end plate (Figure 5.7 (b)) is smaller than end plate thickness group. The bolt distance parameter group (Figure 5.6 (c)) shows the change of the distance doesn't give a significant effect to the beam performance. However the more distance induce more out of plane deformation as shown in Figure 5.7 (c).

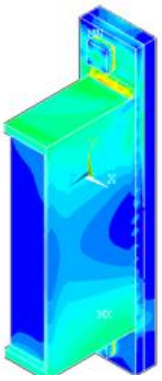
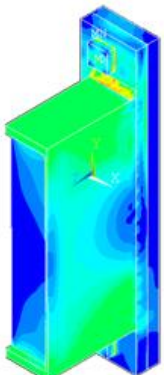
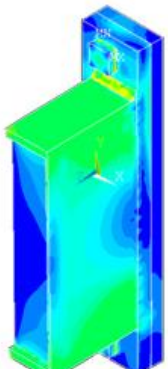

LCF-**075**-0625-2　　LCF-**1**-0625-2　　LCF-**125**-0625-2

(a) End plate thickness parameter group

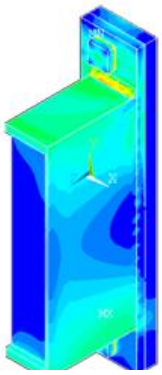
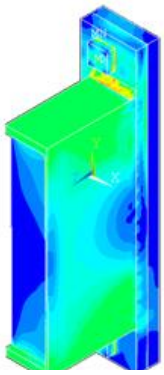
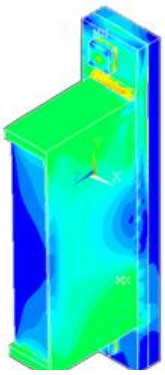

LCF-1-**05**-2　　LCF-1-**0625**-2　　LCF-1-**075**-2

(b) Beam flange thickness parameter group

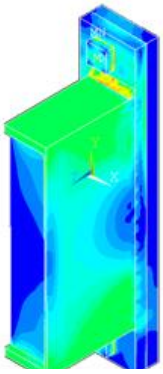
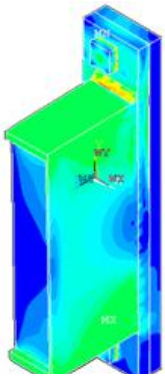
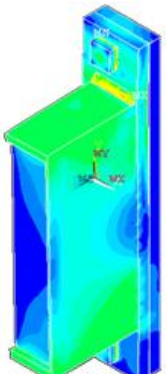

LCF-1-0625-**2**　　LCF-1-0625-**225**　　LCF-1-075-**25**

(c) Bolt distance parameter group

Figure 5.6 Von-mises stress contour

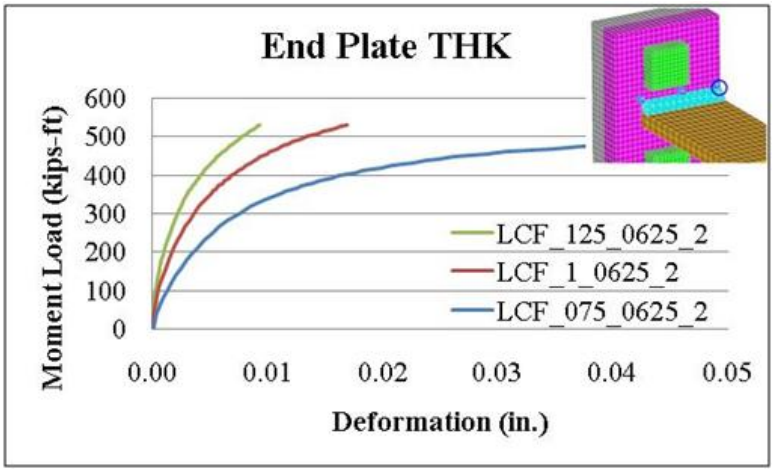

(a) End plate thickness group

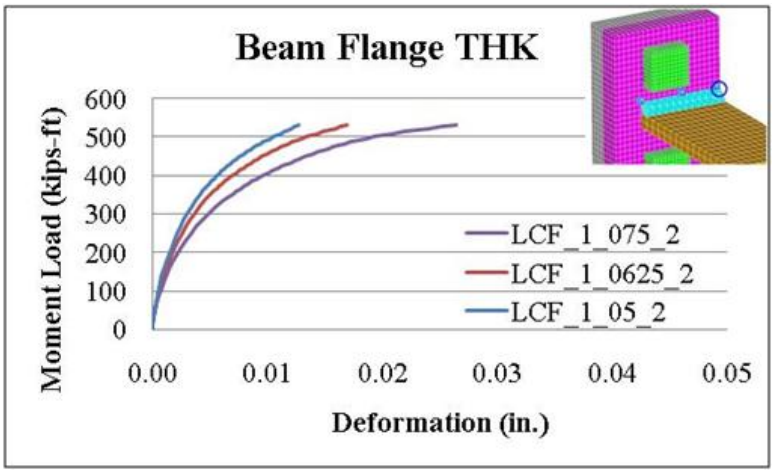

(b) Beam flange thickness group

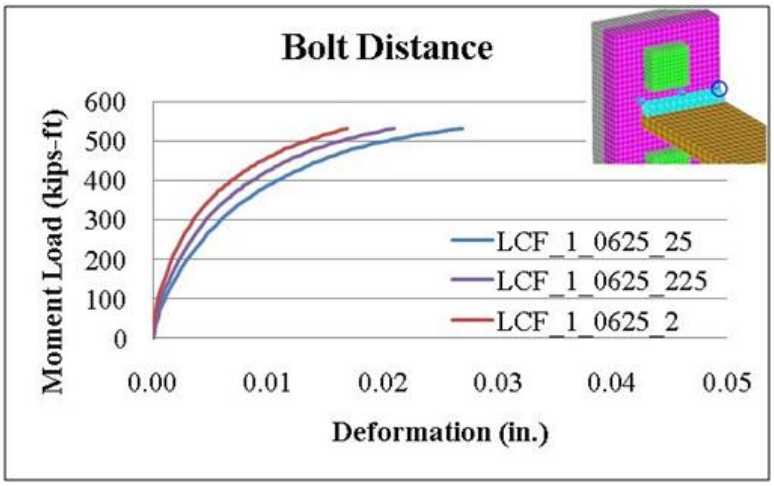

(c) Bolt distance group

Figure 5.7 Out of plane deformation

5.4.2 Local behavior

The deformation, strain and stress contours for the original model are presents in Figure 5.8. The figure shows that the maximum end plate out of plane displacement occurred at the center of beam flange area and that a large amount of the longitudinal strain and Von-mises stress was concentrated at adjacent to the weld root (Figure 5.8 (b), (c)). This correlates well with the experimental results reported in (Lim, 2009) since this is the location observed of the LCF crack as shown in Figure 5.9 (a).

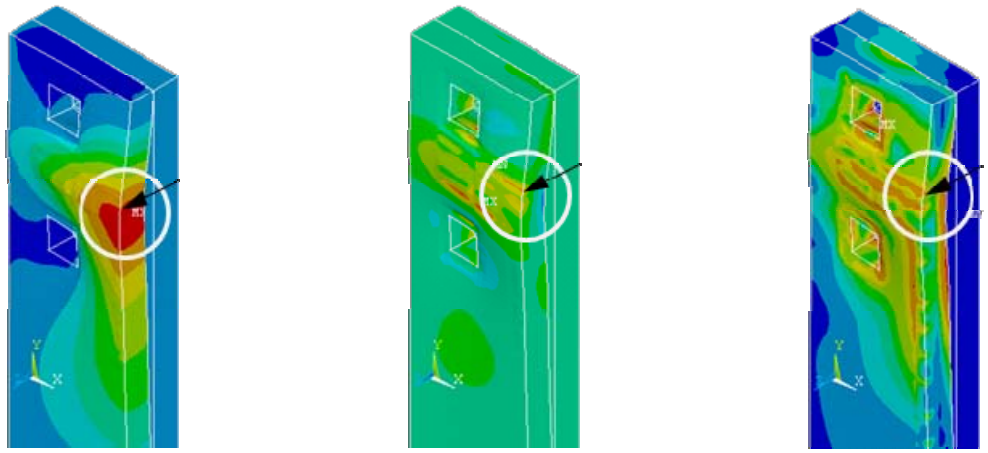

(a) Deformation (b) Longitudinal strain (c) Von-mises stress

Figure 5.8 Maximum response of system (LCF-1-0635-2)

In order to compare the FE analysis results, total six points were selected in each FEM analysis. In order to figure out the crack area strain level, three points were selected on the end plate along the crack line. Figure 5.9 (a) shows the crack level at real specimen and FE model. Another three points were selected on the beam flange surface which place is same line with strain gages were installed. Figure 5.9 (b) shows the strain gage and FE model.

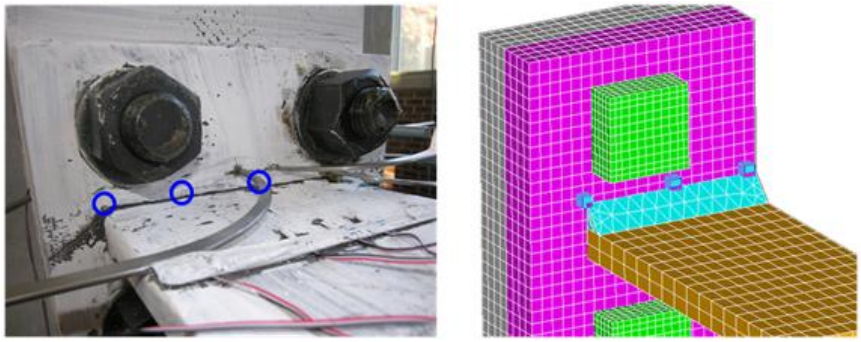

(a) End plate (crack line)

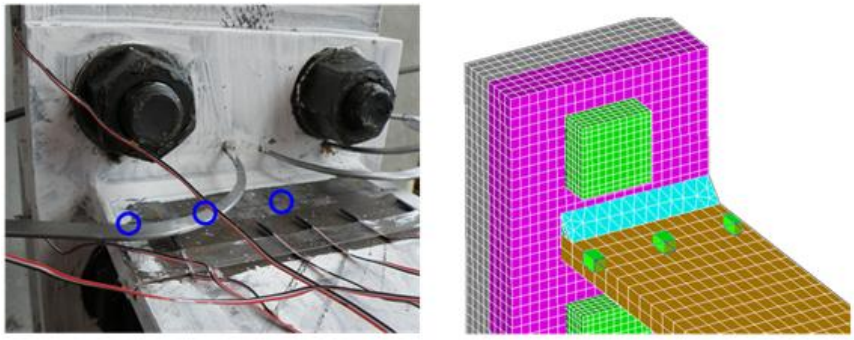

(b) Beam flange (strain gage line)

Figure 5.9 FEM data collection location

All of the parametric study results were compared with LCF-1-0625-2 FE model results. Figure 5.10 shows selected longitudinal direction stress and Von-mises stresses of LCF-1-0625-2 model. Figure 5.10 shows the pretension bolt effect. The 100kips pretension was applied to each bolt and the graph shows the end plate was not deformed until the load reached the pretension load level. In the Figure 5.10, the center stress (sy1637) was almost not affected by pretension since the distance from the bolt. Both the longitudinal stress and the Von-mises stresses show similar behavior because the longitudinal stress governs the stress status. Figure 5.10 shows the crack stress profile. The center of crack line stress is highest values and the point is selected the comparison data point in this paper.

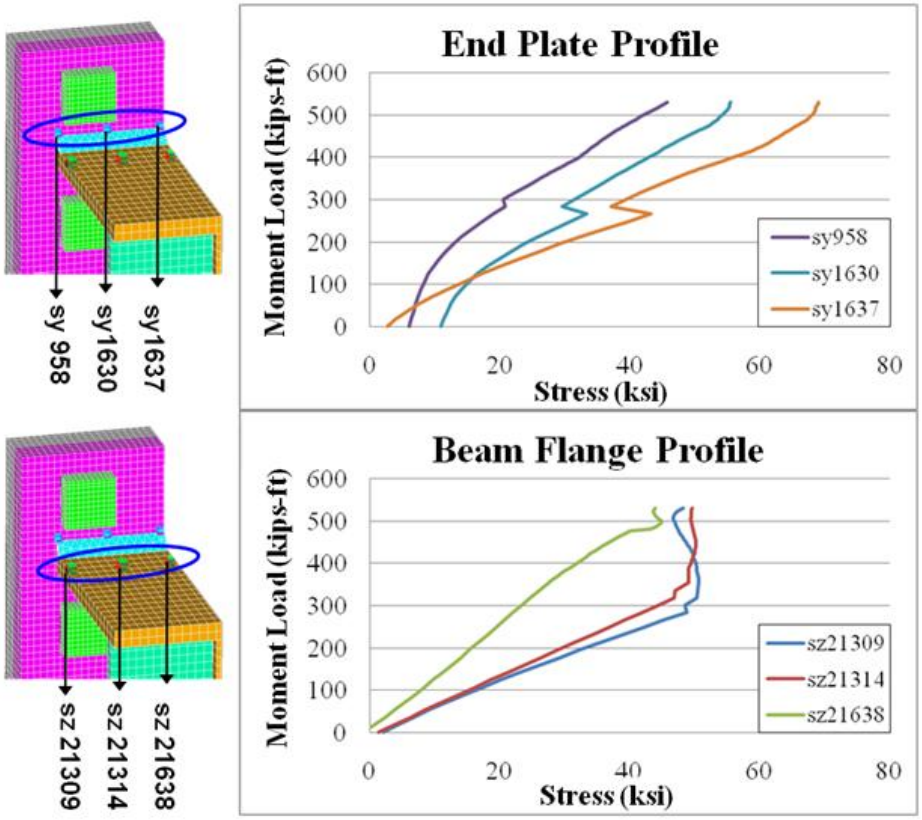

Figure 5.10 Longitudinal stress result of LCF-1-0625-2

The longitudinal direction strain which was perpendicular form the crack line was used to understand the LCF behavior because the strain result was generally used as the index of LCF fracture. (Rice 1969) Therefore all of parametric study groups were plotted the longitudinal direction strain and was compared the LCF behavior in Figure 5.11. In the Figure 5.11, the top guide line is the crack line which was observed at previous research program (Lim, 2009), the middle guide line is the weld material root and the bottom guide line is the beam flange bottom edge. The bottom guide line gives the geometric limit of applied loading. Although all model geometries were different, the large amount of strain was generated at adjacent to the weld root line as shown in Figure 5.11. Figure 5.11 (a) shows the thinner plate got more strain

concentration in the middle of crack line. In Figure 5.11 (b) and (c), it is hard to compare the difference among the group by the contour plot.

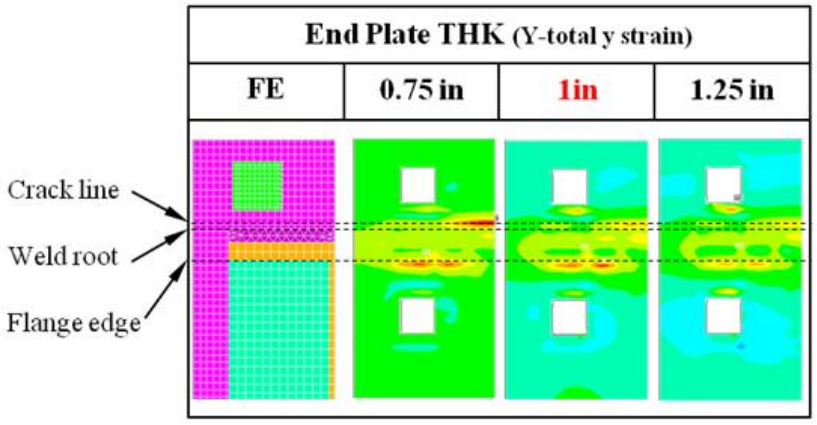

(a) End plate thickness group behavior

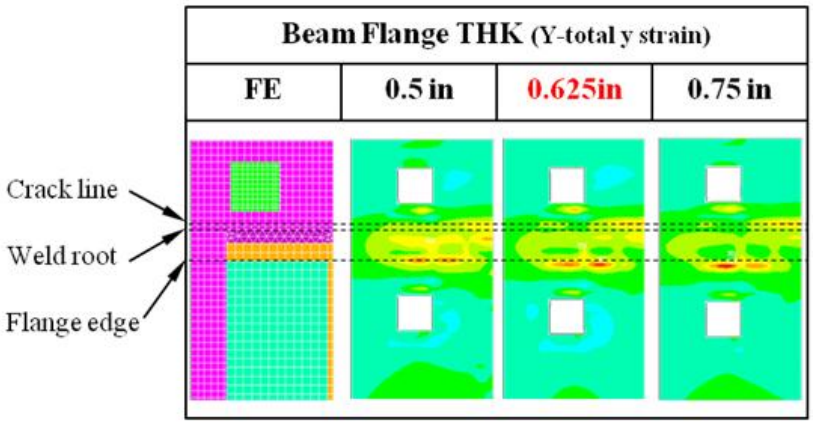

(b) Beam flange thickness group behavior

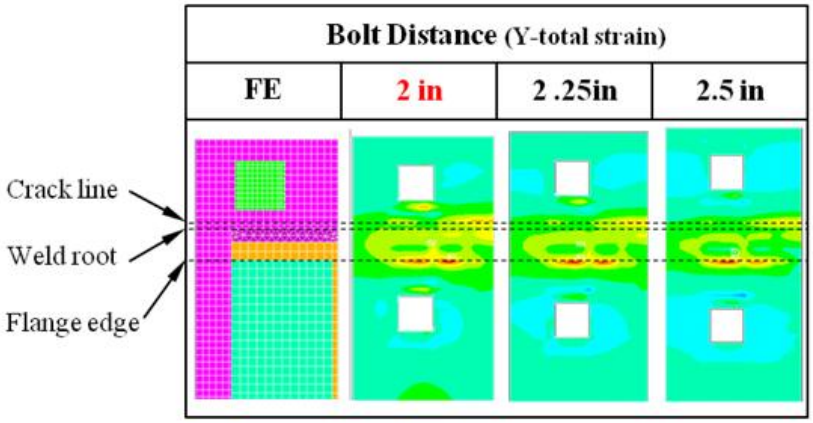

(c) Bolt distance group behavior

Figure 5.11 Location of maximum strain

5.5 LCF Model Modification

The LCF model for the original parametric model (LCF-1-0625-2) was developed in previous research program using full-scale experimental test results. Table 4-6 shows the summary of previous experimental test program results to generate the LCF model. In this chapter, the LCF model(S-N curve) was generated with applied moment load (S) and failure reversal number (N) by log-log plot. Figure 5.12 shows the equivalent LCF model of LCF-1-0625-2.

Table 5-2 LCF-1-0625-2 LCF model data

Test ID	Applied Load(S)	Failure No.(N)	log S	log N
LCF01	442	276	2.6451	2.441
LCF03	520	158	2.716	2.199
LCF02	557	50	2.745	1.699

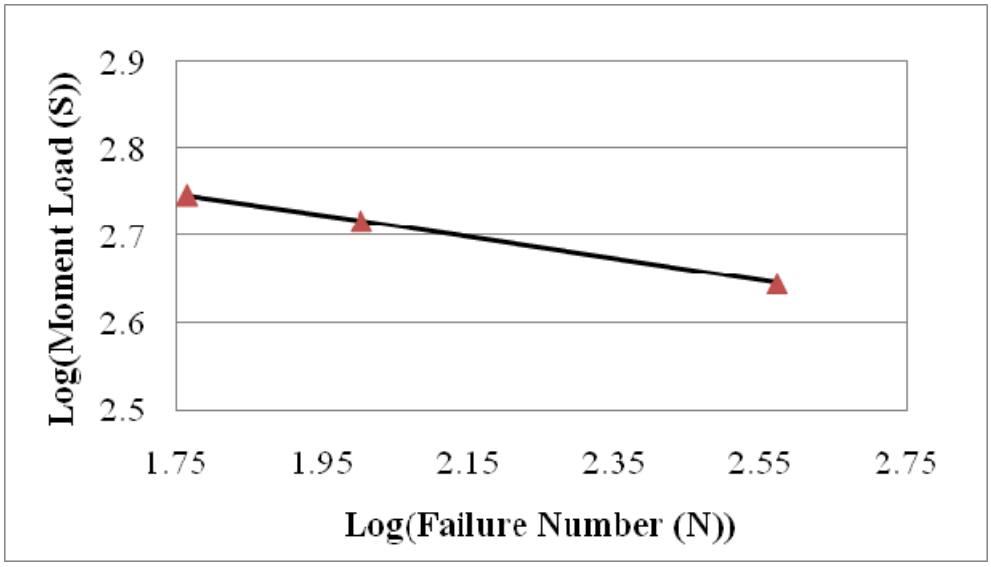

Figure 5.12 LCF-1-0625-2 LCF model

However, the LCF model has been developed with the stress or strain level and failure

number because the LCF crack propagation (LCF failure) directly affected by local stress or strain. Therefore the strain results of parametric studies gave an idea of LCF modification. As mentioned previously, the LCF model is generated with two data value. One is the applied moment load (S) and the other is the failure reversal. One premise needs to generate the modified LCF model for each parametric model. If a certain parametric model has same longitudinal strain value with LCF-1-0625-2 model at the center of crack line, the level of applied load is the LCF modeling data (S). In other word, the failure number is same with LCF-1-0625-2's failure number. Because the certain level of cyclic strain induced the system failure with certain number. The example of the modified LCF model for parametric tests is illustrated in Figure 5.13.

Followed the procedure of generating the modified LCF model for parametric study:

1. Determine the level of constant moment load (S1 and S2) when the LCF failure occurred in standard LCF experimental tests.
2. Determine the center of crack position longitudinal strain (ε1 and ε2) from the moment-strain graph using (S1 and S2). (Figure 5.13 (a))
3. Determine the level of moment load (S1' and S2') from the moment-strain graph for the P1 parametric test with ε1 and ε2 values. (Figure 5.13 (a))
4. Determine the failure number (N1 and N2) for the P1 parametric test based on the premise which the same strain level means same failure number. (Figure 5.13 (b))
5. Plot the modified LCF model for P1 parametric test using two data point, (log(N1), log(S1')) and (log(N2), log(S2')), in log-log plot graph. (Figure 5.13 (b))

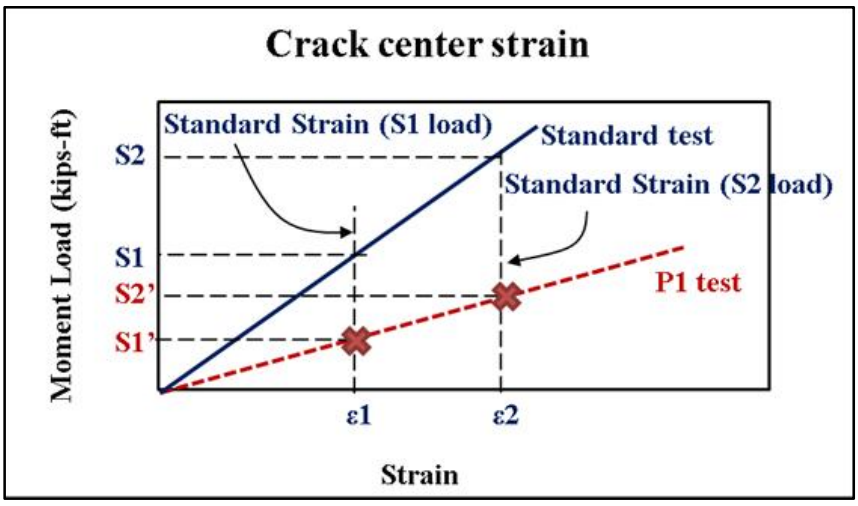

(a) End plate longitudinal strain in the center of crack line

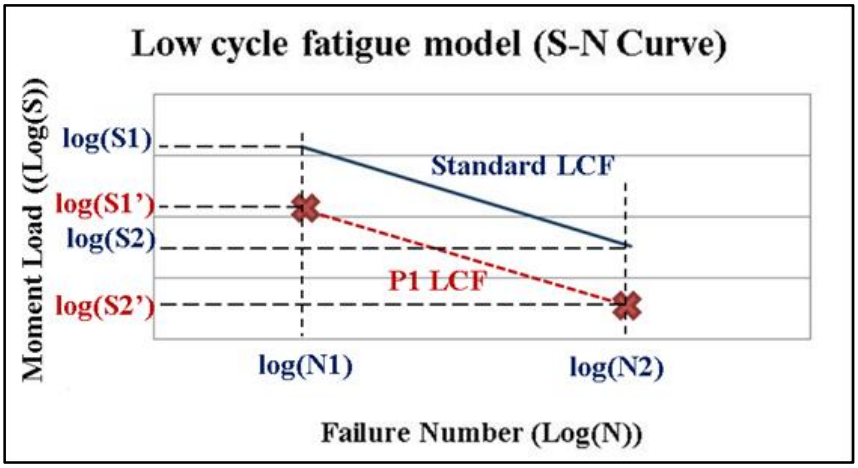

(b) Modified LCF model

Figure 5.13 Modified LCF model example

The longitudinal strain at the center of crack line is plotted into Figure 5.14, Figure 5.15, and Figure 5.16 by the parametric group. Vertical dot guide lines are the level of end plate longitudinal strain which were used to generate the LCF model. The blue circle indicates the cross point with parametric test strain result and the vertical guide lines. Horizontal dot guide lines are the applied moment load level for parametric test which has same strain value with LCF model strain level. The limits of strain are

determined from the standard LCF model using numerical (FEM) model based on the level of constant moment load level. The lower limit of strain is 0.00256 and higher limit of strain is 0.005.

As shown Figure 5.14, the end plate thickness gave a most significant effect to the crack strain result in parametric study. The thin plate (0.75in THK) shows less stiff and has significant non-linear behavior. The thick plate (1.25in THK) shows stiff behavior. However, the beam strains are almost same behavior.

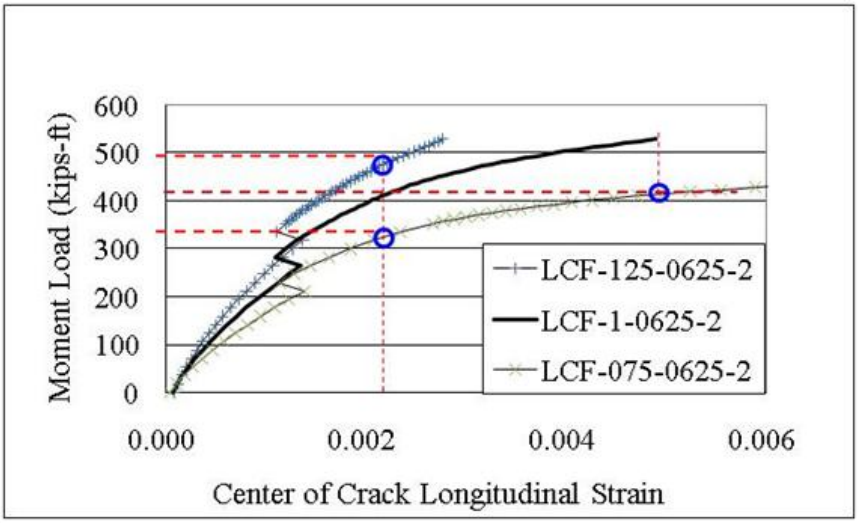

Figure 5.14 End plate thickness group strain result

As shown Figure 5.15, the beam flange thickness gave a less effect to the crack strain result comparing with end plate thickness. However the larger flange thickness (0.75in THK) gives more non-linear deformation in the system. The beam strain is almost same until elastic range of material property. The think flange (0.5in THK) got more beam strain.

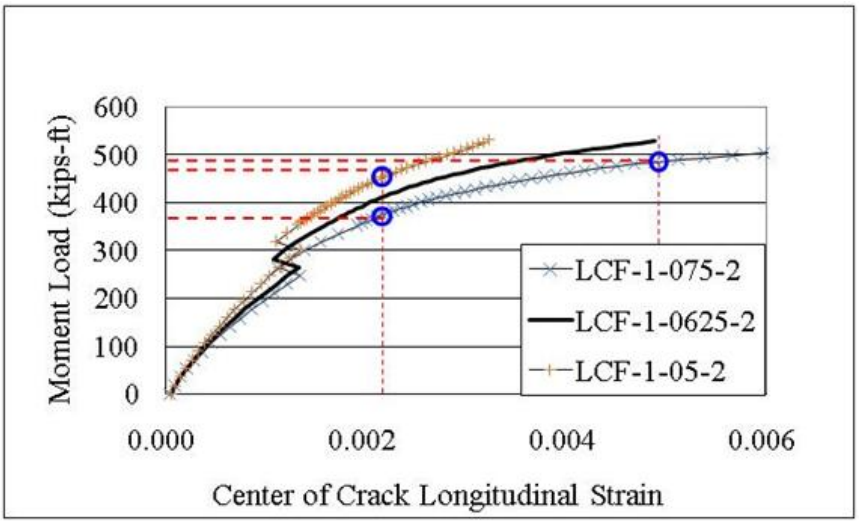

Figure 5.15 End plate thickness group strain result

The bolt distance group shows the distance between bolt and loading position gives effect to the crack strain because the more distance give more out of plate deformation of end plate shown as Figure 5.7.

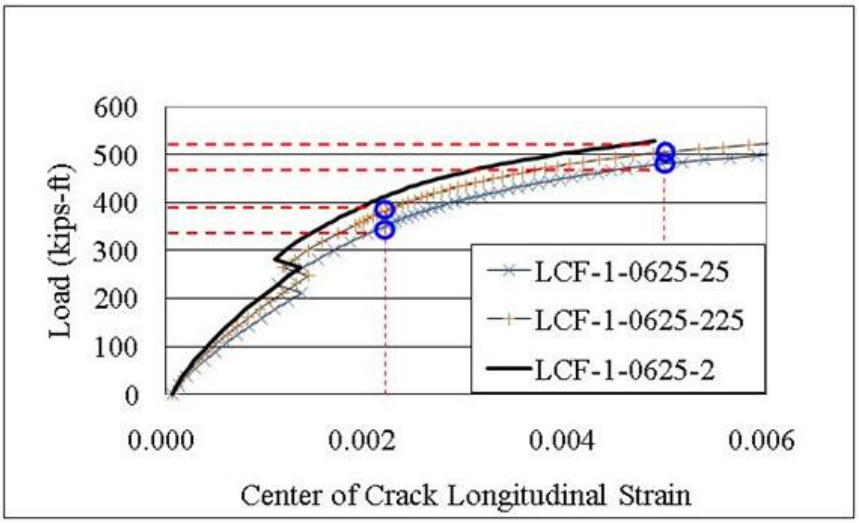

Figure 5.16 Bolt distance group strain result

The LCF model can be plotted by several different load options. In this chapter, the y-

axis S was applied peak displacement. However, in order to generate other geometry LCF model using parametric study, the “S” is changed to the applied moment load. The graph is log-log plot.

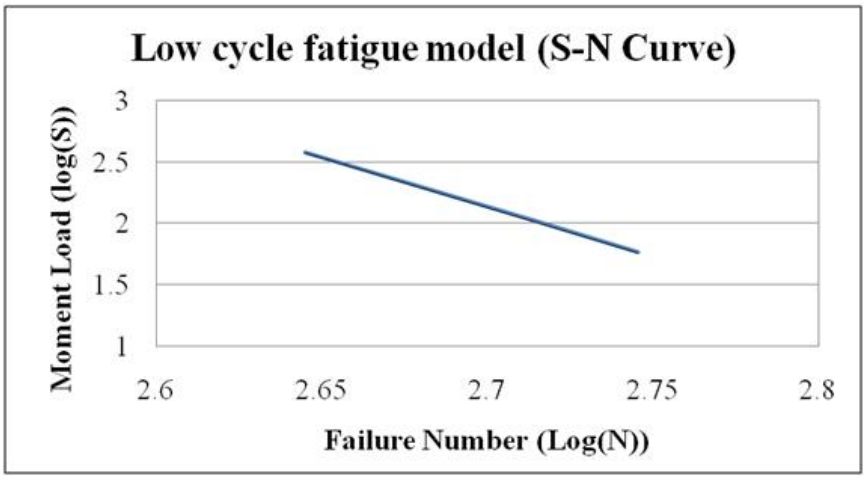

Figure 5.17 LCF model (Moment load base)

Based on the two guideline data point, adjusted LCF models were generated in Figure 5.18. In the LCF model, the solid line is the original LCF model (LCF-1-0625-2) which was derived from experimental tests. The upper line means the longer-life and lower line means the shorter-life of structure.

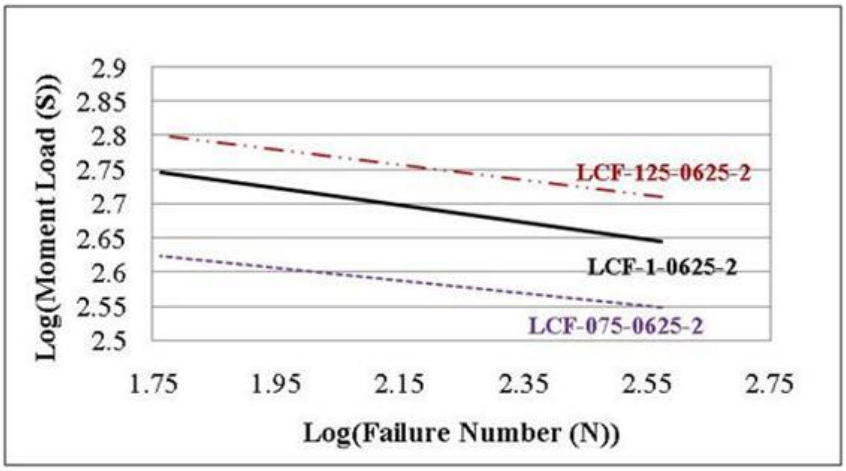

(a) End plate thickness group

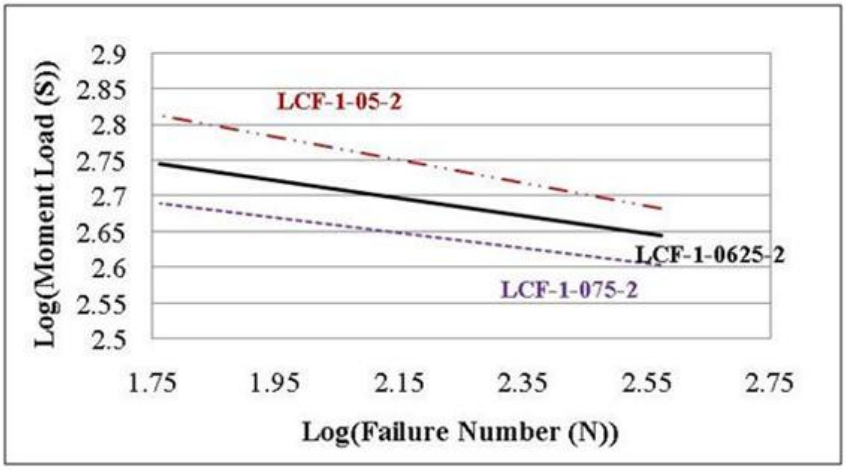

(b) Beam flange thickness group

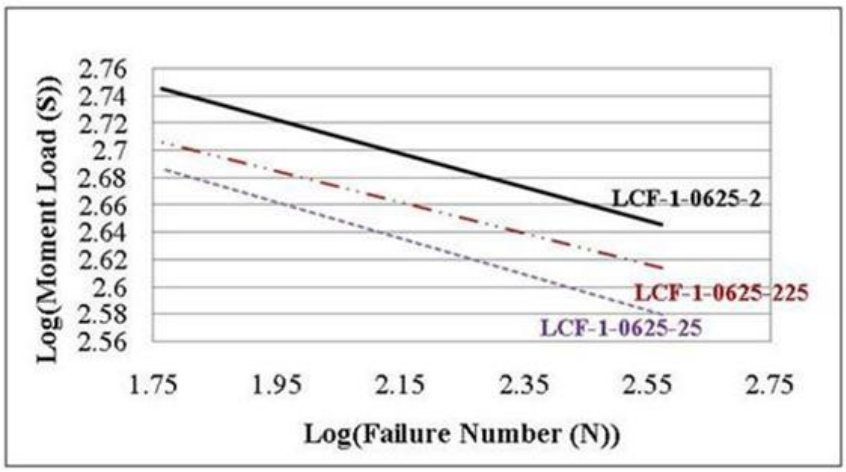

(c) Bolt distance group

Figure 5.18 Adjusted LCF models

5.6 Conclusions

Parametric study on the influence of three parameters was conducted with a prequalified numerical method; end plate thickness, beam flange thickness and bolt pitch. The end plate thickness is directly related with the strength of the end plate and deformation. The beam flange thickness is related with the loading area. The bolt distance gives a geometrical effect to the end plate. The Von-mises stress contour (Figure 5.6) and maximum out of plane deformation (Figure 5.7) were used to evaluate the general behavior of system. All of the models exhibited symmetrical behavior and a significant stress concentration was observed at the crack line. Based on the results of the parametric study, the following conclusions can be summarized.

- Different geometry connection LCF model can be produced using numerical analysis (FEM).
- The most critical parameter in 4E EPMC is end plate thickness. The end plate thickness parameter gave a significant effect to both the strength of system and LCF model.
- Parametric study can be utilized to define the geometric characteristic for LCF behavior.

5.7 Future Work

- Additional parametric study is needed with other geometric parameter in order to characterize the LCF behavior in EPMC.
- Additional experimental tests are needed to verify the modified LCF model.

5.8 References

ASTM (1998) , ASTM E606: Standard Practice for Strain-Controlled Fatigue Testing, Philadelphia, PA, vol. 03.01, pp. 525-539.

Adany, S., Dunai, L., (2004). "Finite Element Simulation of The Cyclic Behavior of End-Plate Joints", Computers & Structures, 82, 2131-2143

Bose, B., Wang, Z. M., Sarkar, S., (1997). "Finite-Element Analysis of Unstiffened Flush End-Plate Bolted Joints", Journal of Structural Engineering, Vol. 123, No. 12

Mays, T. W., (2000). " Application of The Finite Element Method to The Seismic Design and Analysis of Large Moment End-Plate Connections", Ph.D. Dissertation, Virginia Polytechnic Institute and State University, Blacksburg. VA.

Rothert, H., Gebbeken, N., Binder, B., (1992). "Non-Linear Three-Dimensional Finite Element Contact Analysis of Bolted Connections in Steel Frames", International Journal for Numerical Methods in Engineering, Vol. 34, 303-3 18

Sherbourne, A. N., Bahaari, M. R., (1994). "3D Simulation of End-Plate Bolted Connections", Journal of Structural Engineering, Vol. 120, No. 11

Sumner, E. A., (2003). "Unified Design of Extended End-Plate Moment Connections Subject to Cyclic Loading", Ph.D. Dissertation, Virginia Polytechnic Institute and State University, Blacksburg, VA.

Sumner, E. A. and Murray, T. M. (2002). "Behavior of Extended End-Plate Moment Connections Subject to Cyclic Loading", Journal of Structural Engineering, ASCE, vol. 128, no. 4, pp. 501-508.

Wade, P., (2006). "Characterization of High-strength Bolt Behavior in Moment Connections", Master's Dissertation, North Carolina State University, Raleigh, NC.

Chapter 6 Summary and Conclusion

6.1 Summary

The primary objectives of this study were to investigate critical geometric and material parameters for 4E EPMC on the LCF life of the connections and to evaluate the accumulation of LCF damage so that the LCF life can be predicted. To achieve these objectives, extensive literature review, theoretical analysis, numerical analysis, three phases of experimental program, and a parametric study were performed.

Extensive literature review is summarized in chapter 2. The literature review is classified with three topics, low cycle fatigue life, end plate moment connection, other bolted connection LCF. Verified and advanced research approaches were selected through the literature review stage and these approaches were adopted to develop the current limit of knowledge.

The three phases of experimental program were performed with theoretical and numerical analysis method. All of phases were adopted three-dimensional finite element numerical analysis, and theoretical analysis to predict the experimental test behavior. In chapter 3, the first phase of experimental program is presented. This phase of research conducted to evaluate the pre-analysis of LCF test with reduced EPMC specimen. Four tests were conducted with a T-stub specimen which represented a reduced EPMC. The results verified that the theoretical and numerical analysis method could be used as the pre-analysis to anticipate the experimental results. In addition, the results showed that the reduced end plate specimen could be used as the economical test protocol to get the LCF model for EPMC.

The second and third phase of the experimental program are presented in chapter 4.

Three full scale experimental tests were conducted to develop the LCF model using cyclic constant peak displacement load. These results were used to develop the LCF model. To predict the LCF life of the connection, an accumulated damage model was evaluated by one full scale 4E EPMC test using random loading.

In the chapter 5, the details and results of the parametric study are presented. Three critical parameters, (end plate thickness (t_p), beam flange thickness (t_f), and bolt distance (p_{fo})) were evaluated as a part of the study. Numerical analysis was employed to evaluate the parameters, modified LCF models were proposed to account for the change of particular parameters.

6.2 Conclusions

Based on the result of experimental program and analytical study as part of this research primary research programs, the primary conclusion summarized as follows:

- The yield line theory can be use to predict the end plate flexural yield force.
- The numerical model (FEM) can accurately simulate the behavior of end plate.
- The yield line theory and numerical model can be used as the pre-analysis tool for simulate the end plate moment connection experimental test behavior.
- The numerical modeling can accurately simulate the non-linear behavior EPMC with large deflections.
- The location of low cycle fatigue failure can be predicted by the numerical model. The weld root at the face of the end-plate is the most critical location for crack initiation.

- The LCF model can be use to predict the life of EPMCs.
- The displacement load can successfully be used as the LCF model index “S”.
- Different geometry connection LCF model can be produced using numerical analysis (FEM).
- The most critical parameter in 4E EPMC is end plate thickness. The end plate thickness parameter gave a significant effect to both the strength of system and LCF model.
- Parametric study can be utilized to define the geometric characteristic for LCF behavior.

6.3 Future Work

After finished current research program, several topics were interested to define the research results and to develop the design concept.

- Additional T-stub experimental study needed to develop the simplified LCF modeling protocol.
- Additional T-stub experimental tests are needed to define the full scale test LCF model.
- Additional full scale experimental cyclic tests are needed to verify the developed LCF model.
- LCF investigation program needed to determine the LCF behavior on beam flange.

- Additional theoretical analysis needed to apply different LCF modeling method.
- Additional parametric study is needed with other geometric parameter in order to characterize the LCF behavior in EPMC.
- Additional experimental tests are needed to verify the modified LCF model.
- Fracture mechanic analysis approach is needed to do the cross-validation for the LCF model. Additional LCF material property tests are needed to apply in the numerical model for fracture mechanic concept.
- Whole structure seismic damage evaluation is needed to verify the application of LCF life prediction.

REFERENCES

AISC (2006). "Seismic Design Manual", American Institute of Steel Construction, Chicago.

AISC (2005). "Steel Construction Manual", American Institute of Steel Construction, Chicago.

AISC (2003). "Steel Design Guide 4 Extended End-Plate Moment Connections Seismic and Wind Applications", Chicago

AISC (2002), "AISC Design Guide 16: Flush and Extended Multiple-Row Moment End-Plate Connections", American Institute of Steel Construction, Chicago.

ASTM (2001). "Standard Specification for General Requirements for Rolled Structural Steel Bars, Plates, Shapes, and Steel Piling, ASTM A6.

ASTM (1998) , ASTM E606: Standard Practice for Strain-Controlled Fatigue Testing, Philadelphia, PA, vol. 03.01, pp. 525-539.

AWS (2002). "Structural Welding Code - Steel", American Welding Society, AWS D1.1-98, Miami

Adany, S., Dunai, L., (2004). "Finite Element Simulation of The Cyclic Behavior of End-Plate Joints", Computers & Structures, 82, 2131-2143

Adey, B.T., Grondin, G.Y., and Cheng, J.J.R. (1997). "Extended End Plate Moment Connections under Cyclic Loading", Department of Civil Engineering University of Alberta, Structural Engineering Report No. 216

Bahaari, M. R.,Sherbourne, A. N., (2000). "Behavior of eight-bolt large capacity endplate connections", Computers & Structures, 77, 315-325

Ballio, G., Calado, L., Castiglioni, C. A., (1997). "Low cycle Fatigue Behavior of Structural Steel Members and Connections", Fatigue & Fracture of Engineering Materials & Structures, vol. 20, no 8, 1129-1146

Barsom, J. M., Pellegrino, J. V., (2002). "Failure Analysis of Welded Steel Moment-Resisting Frame connections", Journal of materials in civil engineering.

Borgsmiller, J., (1995). "Simplified Method for Design of Moment-End-Plate Connections", M.S. Thesis, Virginia Polytechnic Institute and State University, Blacksburg, VA.

Bose, B., Wang, Z. M., Sarkar, S., (1997). "Finite-Element Analysis of Unstiffened Flush End-Plate Bolted Joints", Journal of Structural Engineering, Vol. 123, No. 12

Bursi, O. S., Jaspart, J. P., (1997). "Calibration of a Finite Element Model for Isolated

Bolted End-Plate Steel Connections", J. Construct. Steel Res. Vol. 44, No. 3, pp. 225-262

Bursi, O. S., Ferrario, F., Fontanari, V., (2002) "Non-linear Analysis of the Low-cycle Fracture Behaviour of Isolated Tee Stub Connections", Computers & Structures, 80, 2333-2360.

Coffin, Jr., C.F. (ed.) (1969). Manual on Low Cycle Fatigue Testing, ASTM, STP 465, American Society for Testing and Materials, Philadelphia

Coffin, L. F., Jr.,(1954). "A study of the Effects of Cyclic Thermal Stresses on a Ductile metal", Trans. ASME, Vol. 76 .p.p . 931-950.

Ewens, S., (1997). "Experimental Verification of A Simplified Method for Design of Structural Tee Hangers", M.S. Dissertation, Virginia Polytechnic Institute and State University, Blacksburg, VA.

FEMA. (2000a), FEMA 350 Recommended Seismic Design Criteria for New Steel Moment-Frame Buildings, FEMA, Washington, DC.

FEMA. (2000b), FEMA 351 Recommended Seismic Evaluation and Upgrade Criteria for Existing Welded Steel Moment-Frame Buildings, FEMA, Washington, DC.

Garlock, M. M., Ricles, J. M., Sause, R., (2003). "Cyclic Load Tests and Analysis of Bolted Top-and-Seat Angle Connections", Journal of Structural Engineering.

Garlock, M. M., Ricles, J. M., Sause, R., (2005). "Experimental Studies of Full-Scale Posttensioned Steel Connections". Journal of Structural Engineering ASCE.

Ghobarah, A., Osman, A., Korol, R.M., (1990). "Behaviour of extended end-plate connections under cyclic loading", J. Struct. Engr. 12 1, pp. 15-27

Hendrick, D., Kukreti, A. R., Murray, T. M., (1984). "Analytical and Experimental Investigation of Stiffened Flush End-Plate Connections with Four Bolts at The Tension Flange", Research Report FSEL/MBMA 84-02, Fears Structural Engineering Laboratory, University of Oklahoma, Norman, OK.

Kaufmann, E. J., Fisher, J. W.; DiJulio, R. M., Jr.; Gross, J. L., (1997). "Failure Analysis of Welded Steel Moment Frames Damaged in the Northridge Earthquake", NISTIR 5944; 175 p.

Kasai, K., Xu, Y., (2003). "Cyclic behavior and low-cycle fatigue of semi-rigid connections (Part II: bolted T-stub connections)", Behaviour of Steel Structures in Seismic Areas, STESSA 2003, Balkema, pp. 321–327

Kennedy, N.A., Vinnakota, S., Sherbourne, A.N., (1981). "The Split-Tee Analogy in Bolted Splices and Beam-Column Connections", Joints in Structural Steelwork, John Wiley & Sons, London-Toronto, pp. 2-138-2.157.

Krawinkler, H., Popov, E.P., (1982). “Seismic Behavior of Moment Connections and Joints”, Journal of Structural Division, ASCE 108 2 , pp. 373-391

Krishnamurthy, N., Graddy, D.E., (1976). “Correlation Between 2- and 30 Dimensional Finite Element Analysis of Steel Bolted End-Plate Connections,” Computers & Structures, Pergamon, 6(4-5/6), 381-389

Kuwamura, H., (1997). "Transition between Fatigue and Ductile Fracture in Steel", Journal of Structural Engineering, Vol. 123, No. 7.

Kuwamura, H., and Suzuki, T. (1992). "Low-Cycle Fatigue Resistance of Welded Joints of High-Strength Steel under Earthquake Loading", Proceedings of the Tenth World Conference on Earthquake Engineering, Madrid, Spain, Vol.5, pp.2851-2856

Landgraf, R.W., Morrow, J., Endo, T., (1969). “Determination of the cyclic stress–strain curve”, Journal of Materials, JMLSA, 4(1), pp.176-188

Mays, T. W., (2000). “ Application of The Finite Element Method to The Seismic Design and Analysis of Large Moment End-Plate Connections”, Ph.D. Dissertation, Virginia Polytechnic Institute and State University, Blacksburg. VA.

Manson, S.S., Freche, J.C., Ensign, C.R., (1967). "Application of a double linear damage rule to cumulative fatigue. Fatigue Crack Propagation", ASTM STP 415, pp. 384-41

Matteis, D., Mandara, A., Mazzolani, F.M. (2000). "T-stub Aluminium Joints: the Influence of Behavioural Parameters", Computers and Structures, Pergamon, ISSN 0045-7949, Oxford (UK),Vol. 78, No. 1-3, 311-327.

Matteis, G. De, (2004). "Experimental Behaviour of Aluminium T-stub Connections", Connections in Steel Structures V- Amsterdam

Mazzolani, F., (1999). “Moment Resistant Connections of Steel Frames in Seismic Areas”, Taylor & Francis

Meng, R. L. (1996), "Design of Moment End-Plate Connections for Seismic Loading", Ph.D. Dissertation, Virginia Polytechnic Institute and State University, Blacksburg, VA.

Miner, M.A., (1945). Trans. ASME, J. Appl. Mech. 67, p. A159.

Morrison, S. J., Astaneh-Asl,, A., Murray, T. M., (1986). “Analytical and Experimental Investigation of the Multiple Row Extended 1/3 Moment End-Plate Connection with Eight Bolts at the Beam Tension Flange,” Report No. FSEL/MBMA 86-01, University of Oklahoma, Norman, Oklahoma.

Morrow, J., (1965). "Cyclic plastic strain energy and fatigue of metals", American Society for Testing and Materials, ASTM STP 378

Murray, T.M., (1988). "Recent Developments for the Design of Moment End-Plate Connections", Construction Steel Research 10 133-162

Neuber, H., (1961). "Theory of Stress Concentration for Shear-Strained Prismatical Bodies with Arbitrary Nonlinear Stress-Strain Laws," Journal of Applied Mechanics, Trans. ASME, Vol. E28, 544.

Palmgren, A., (1924). "Die Lebensadauer von Kugellagern,", Z. Vereines Deutcher Ingenieure, Vol. 68, pp. 339-341

Partridge, J.C., Paterson S.R. and Richard R.M., (2000). "Low Cycle Fatigue Tests and Fracture Analyses of Bolt-Welded Seismic Moment Frame Connections"

Rothert, H., Gebbeken, N., Binder, B., (1992). “Non-Linear Three-Dimensional Finite Element Contact Analysis of Bolted Connections in Steel Frames”, International Journal for Numerical Methods in Engineering, Vol. 34, 303-3 18

RECOS, (2000). “Moment Resistant Connections of Steel Frames in Seismic Areas Design and Reliability”, Taylor and Francis, ISBN: 978-0-415-23577-8.

SAC Joint Venture. (1997). "Protocol for fabrication, inspection, testing and documentation of beam-column connection tests and other experimental specimens", Rep. No. SAC/BD-97/02, Sacramento, Calif.

Schneider, S. P., Teeraparbwong, I. (2000). "Bolted flange plate con-nections", Rep. No. SAC/BD-00/05, Sacramento, Calif.

Sherbourne, A. N., Bahaari, M. R., (1994). “3D Simulation of End-Plate Bolted Connections”, Journal of Structural Engineering, Vol. 120, No. 11

Srouji, R., Kukreti, A., Murray, T. M., (1983). “Yield-Line Analysis of End-PlateConnections with Bolt Force Predictions”, Report No. FESL/MBMA 83-05, University of Oklahoma, Norman, Oklahoma.

Stojadinovic, B., (2003) "Stability and Low-Cycle Fatigue Limits of Moment Connection Rotation Capacity," Engineering Structures, Elsevier Science

Sumner, E. A., (2003). “Unified Design of Extended End-Plate Moment Connections Subject to Cyclic Loading”, Ph.D. Dissertation, Virginia Polytechnic Institute and State University, Blacksburg, VA.

Sumner, E. A. and Murray, T. M. (2002). "Behavior of Extended End-Plate Moment Connections Subject to Cyclic Loading", Journal of Structural Engineering, ASCE, vol. 128, no. 4, pp. 501-508.

Tsai, K.C., Popov, E.P., (1990). "Cyclic behaviour of end-plate moment connections", Journal of Structure Engineering, 116 11, pp. 2917-2930

Wade, P., (2006). “Characterization of High-strength Bolt Behavior in Moment

Connections", Master's Dissertation, North Carolina State University, Raleigh, NC.

APPENDIX

APPENDIX A

Experimental Test Summary Report

TEST SUMMARY REPORT

Test Designation :	Tstub01
Test Number :	1
Test Date:	2007-03-09
Wall Width :	6"
Test Type:	Column Uplift
Column Bolts:	(10) 1/2"Ø A325 Galvanized
Anchor Bolts:	(2) 7/8"Ø A325

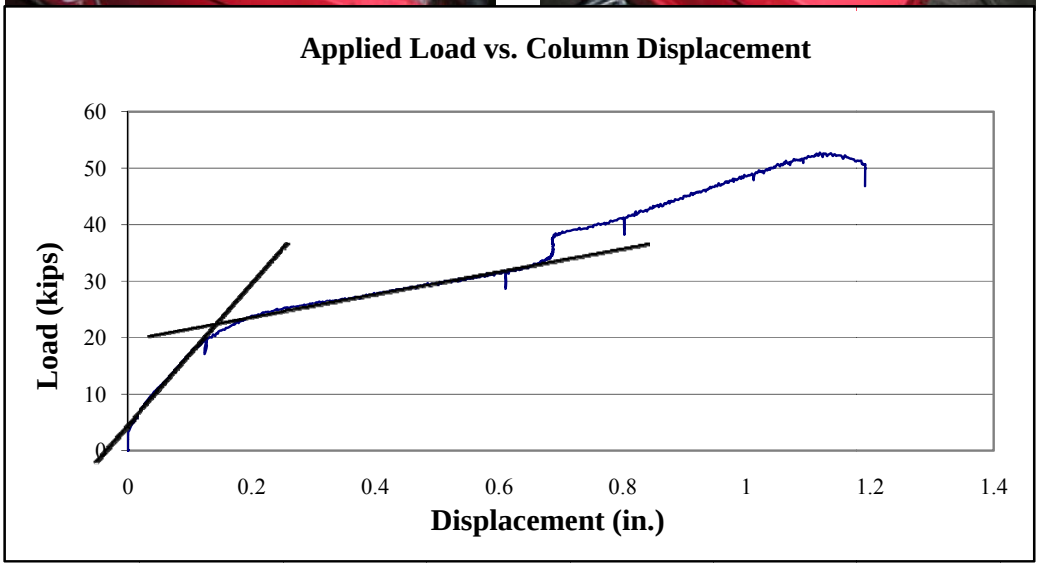

Notes:	Base plate yield first, large deformation was occurred	
Failure:	Short leg bolt rupture.	
Ultimate :	Load (kips)	Column Disp. (in)
	52.7	1.231

TEST SUMMARY REPORT

Test Designation :	Tstub02
Test Number :	2
Test Date:	2007-03-09
Wall Width :	6"
Test Type:	Column Uplift
Column Bolts:	(10) 1/2"Ø A325 Galvanized
Anchor Bolts:	(2) 7/8"Ø A325

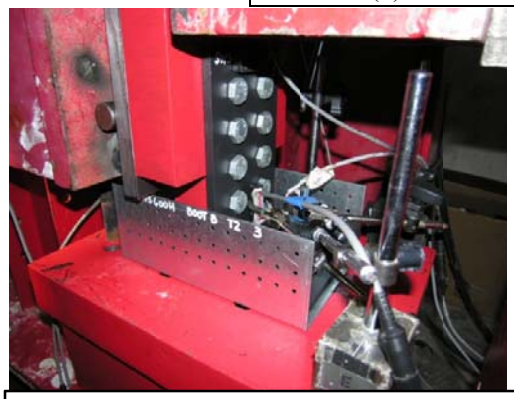

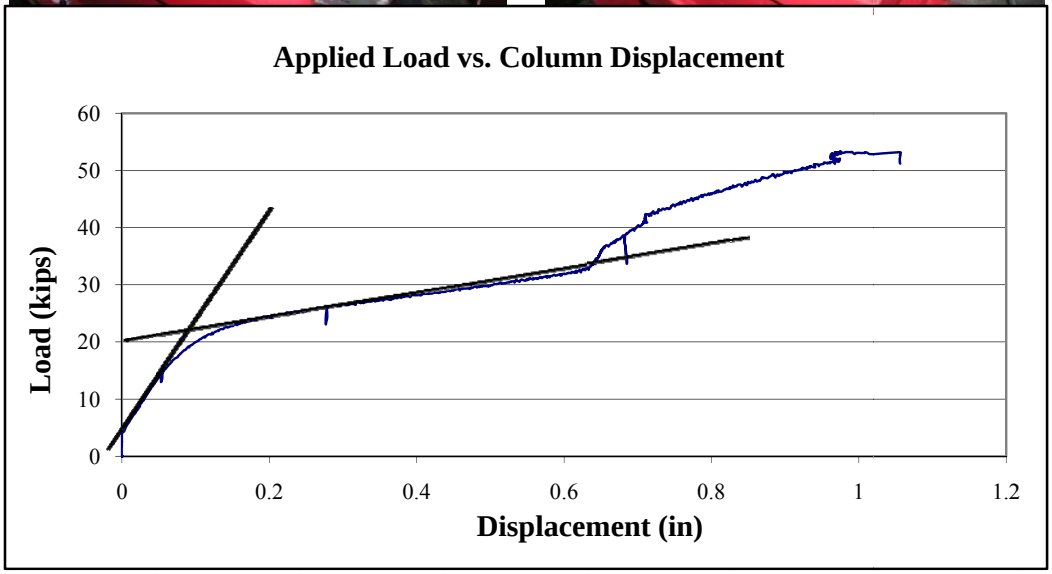

Notes:	Base plate yield first, large deformation was occurred	
Failure:	Short leg bolt rupture.	
Ultimate :	Load (kips)	Column Disp. (in)
	53.4	1.4024

TEST SUMMARY REPORT

Test Designation :	Tstub03
Test Number :	3
Test Date:	2007-07-17
Wall Width :	6"
Test Type:	Column Uplift
Column Bolts:	(10) 1/2"Ø A325 Galvanized
Anchor Bolts:	(2) 7/8"Ø A490

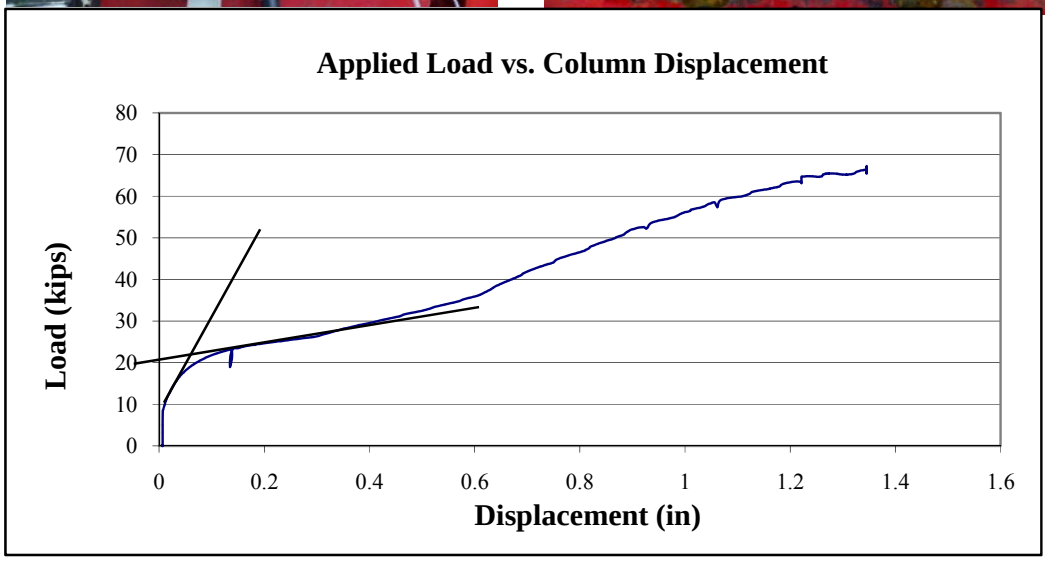

Notes:	Base plate yield first, large deformation was occurred	
Failure:	Bolt hole tears out	
Ultimate :	Load (kips)	Column Disp. (in)
	67.9	1.3452

TEST SUMMARY REPORT

Test Designation :	Tstub04
Test Number :	4
Test Date:	2007-07-18
Wall Width :	6"
Test Type:	Column Uplift
Column Bolts:	(10) 1/2"Ø A325 Galvanized
Anchor Bolts:	(2) 7/8"Ø A490

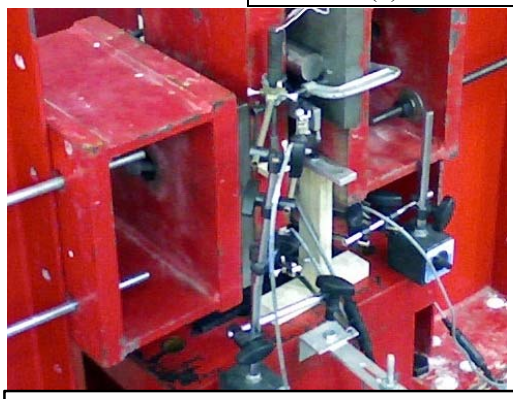

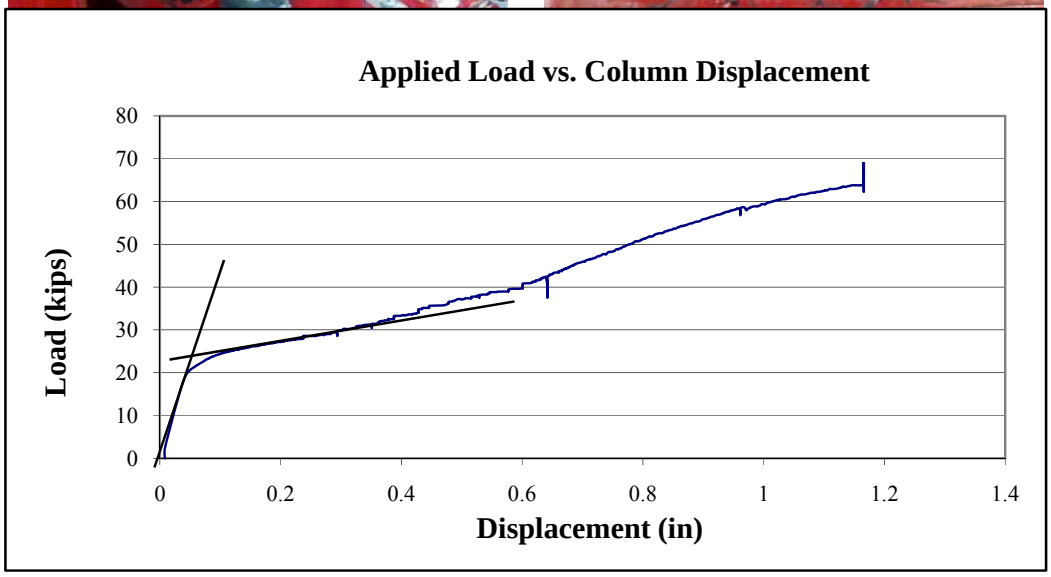

Notes:	Base plate yield first, large deformation was occurred	
Failure:	Bolt hole tear out	
Ultimate :	Load (kips)	Column Disp. (in)
	69	1.1659

TEST SUMMARY REPORT

Test Designation :	LCF01
Test Date:	2008-11-18
Test Type:	4 Bolt Extended End Plate Moment Connection
Column:	W14x74x11’ A992
Beam:	W12x48x12’9" A992
End Plate	0.875x10x25.375 A36
Bolts:	D1.25x3.25 A490

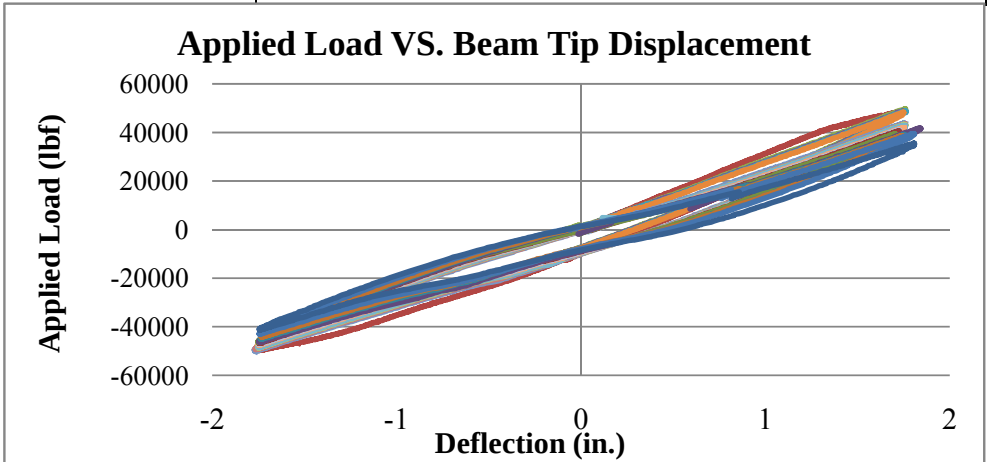

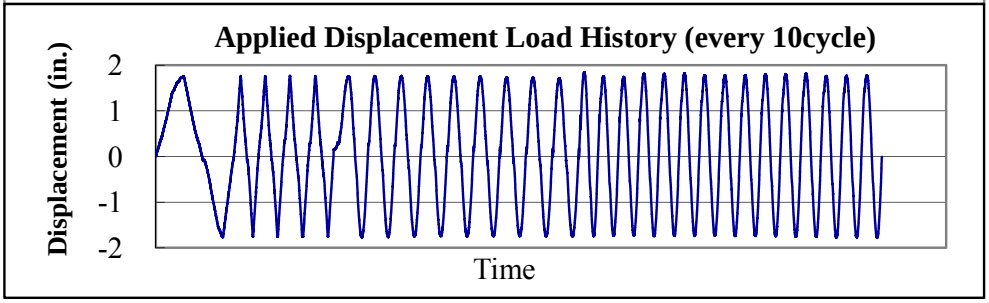

Notes:	End plate LCF failure on the beam top flange side
Failure:	End plate LCF
Ultimate :	
Load (lb)	48071
Net Disp. (in)	1.793
Failure No. (Rev.)	276

TEST SUMMARY REPORT

Test Designation :	LCF02
Test Date:	2008-12-08
Test Type:	4 Bolt Extended End Plate Moment Connection
Column:	W14x74x11’ A992
Beam:	W12x48x12’9" A992
End Plate	0.875x10x25.375 A36
Bolts:	D1.25x3.25 A490

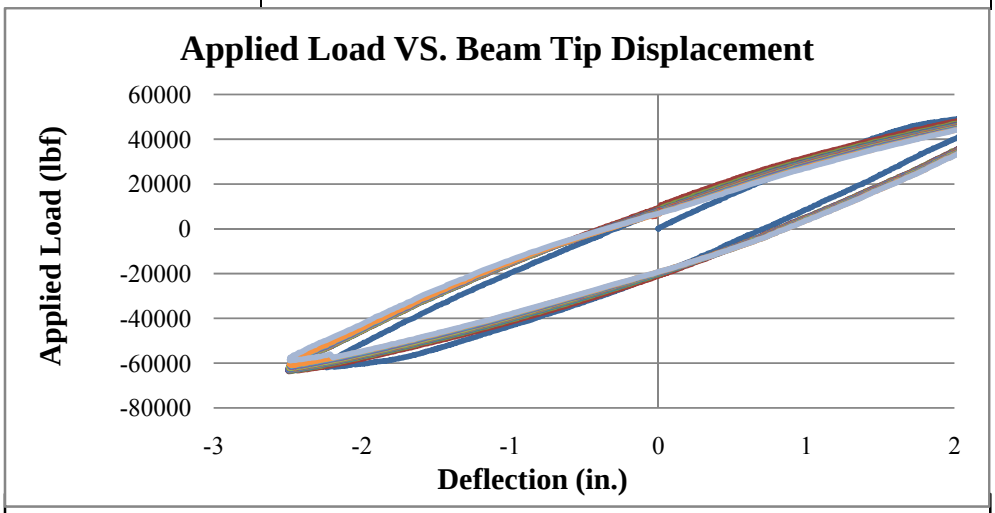

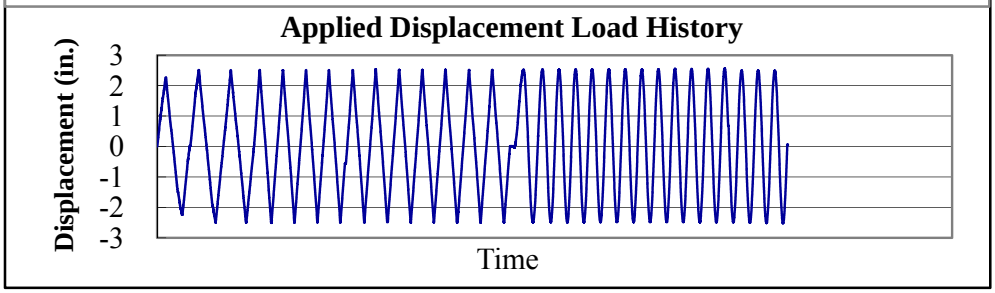

Notes:	End plate LCF failure on the beam top flange side
Failure:	End plate LCF
Ultimate :	
Load (lb)	-63722
Net Disp. (in)	-2.51
Failure No. (Rev.)	50

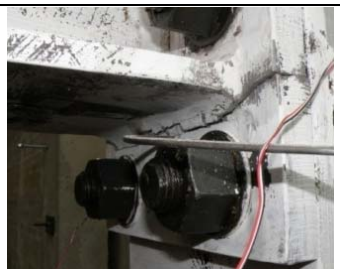

TEST SUMMARY REPORT

Test Designation :	LCF03
Test Date:	2008-03-17
Test Type:	4 Bolt Extended End Plate Moment Connection
Column:	W14x74x11’ A992
Beam:	W12x48x12’9" A992
End Plate	0.875x10x25.375 A36
Bolts:	D1.25x3.25 A490

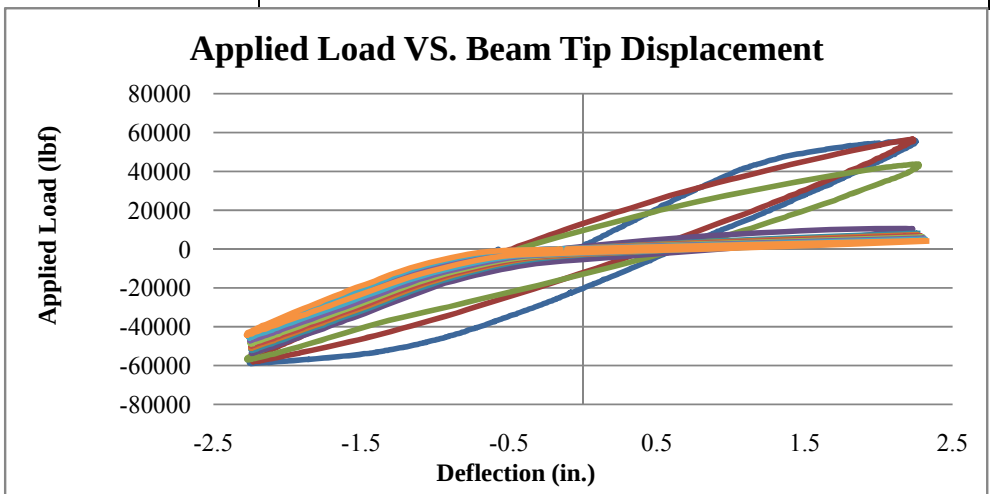

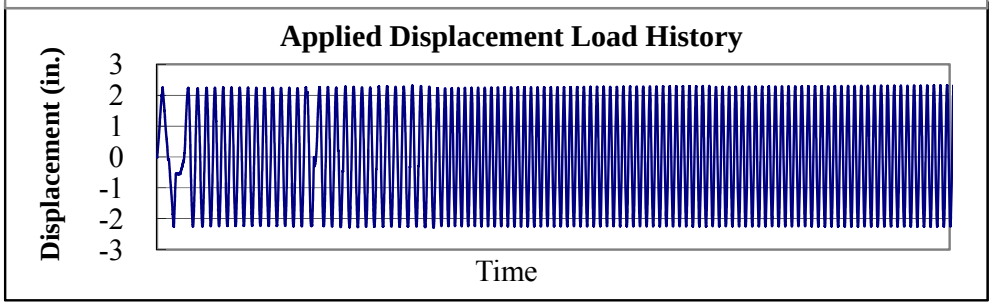

Notes:	End plate LCF failure on the beam top flange side
Failure:	End plate LCF
Ultimate :	
Load (lb)	-58787
Net Disp. (in)	-2.28
Failure No. (Rev.)	158

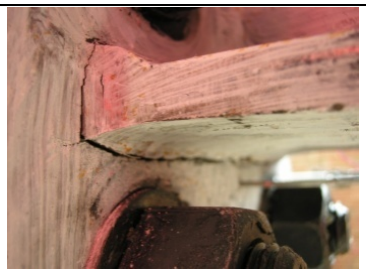

TEST SUMMARY REPORT

Test Designation :	LCF04
Test Date:	2008-03-24
Test Type:	4 Bolt Extended End Plate Moment Connection
Column:	W14x74x11' A992
Beam:	W12x48x12'9" A992
End Plate	0.875x10x25.375 A36
Bolts:	D1.25x3.25 A490

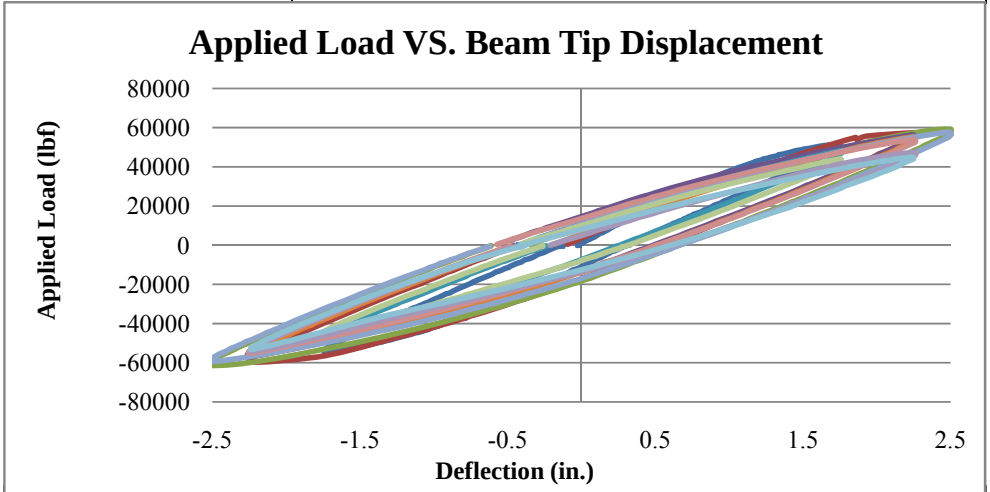

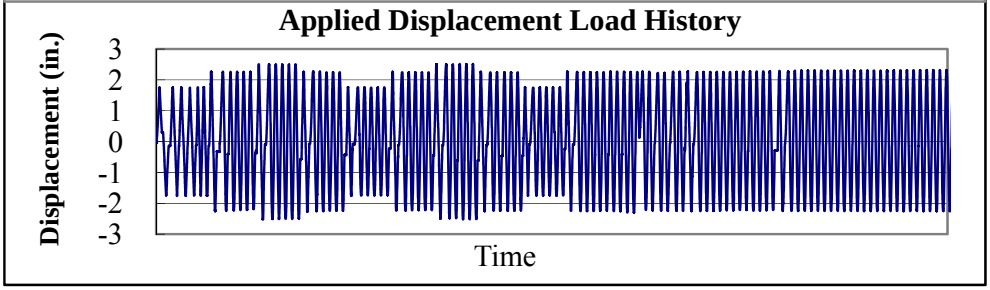

Notes:	End plate LCF failure on the beam top flange side
Failure:	End plate LCF
Ultimate :	
Load (lb)	-60483
Net Disp. (in)	-2.52
Failure No. (Rev.)	110

APPENDIX B

Full Scale Test Result

(Failure Criteria)

LCF 01 Test Result

Total test Cycle: 277 cycles

Failure Cycle: 138th cycles

Failure Mode: End plate LCF failure at beam top flange area

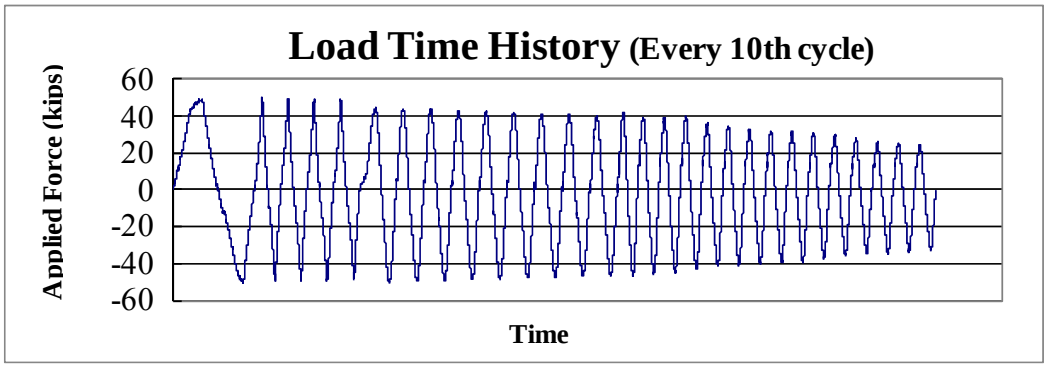

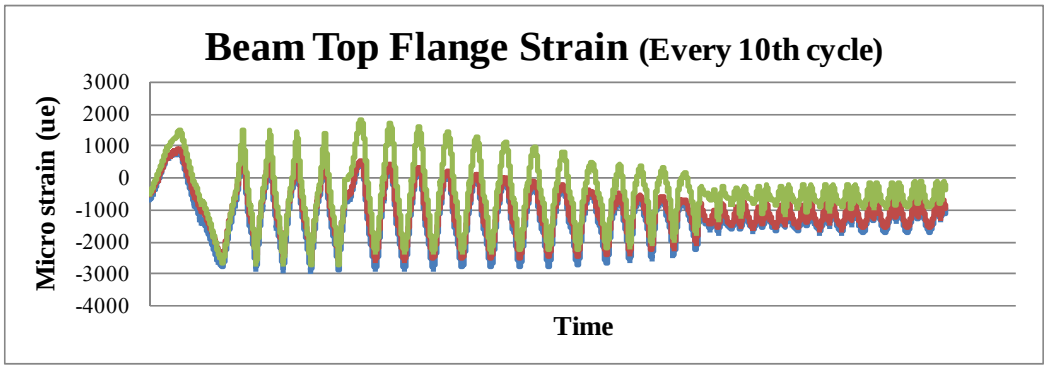

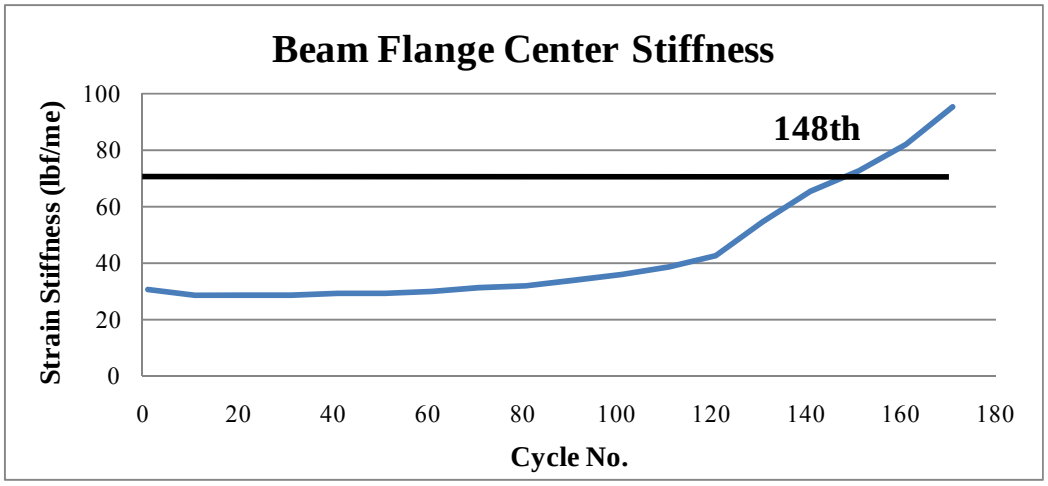

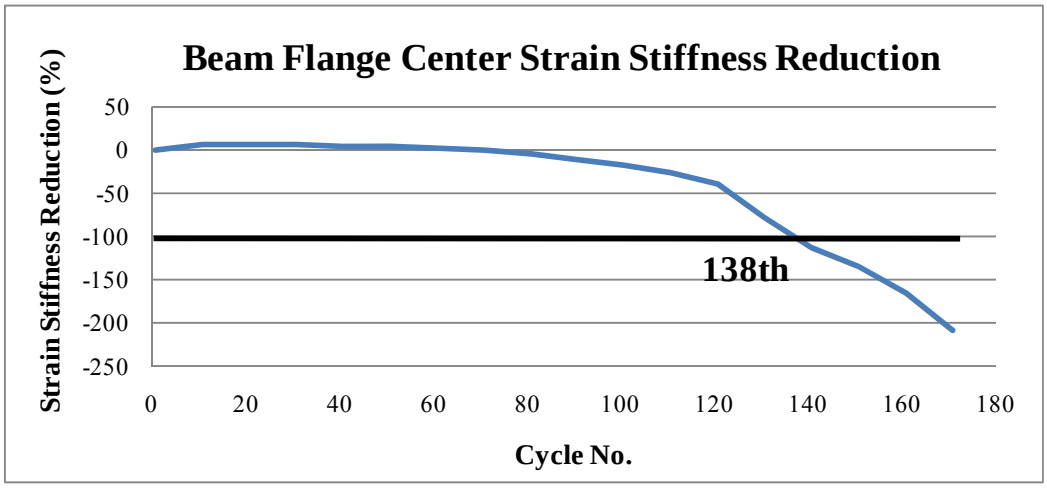
Beam Flange Center Strain Stiffness Reduction
Strain Stiffness Reduction (%)
50
0
-50
-100
-150
-200
-250
138th
0
20
40
60
80
100
120
140
160
180
Cycle No.

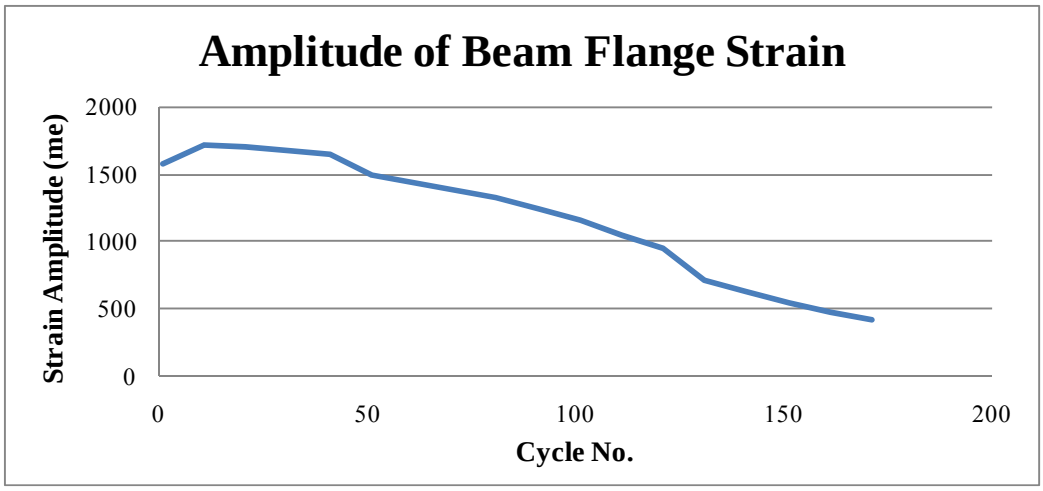
Amplitude of Beam Flange Strain
Strain Amplitude (me)
2000
1500
1000
500
0
0
50
100
150
200
Cycle No.

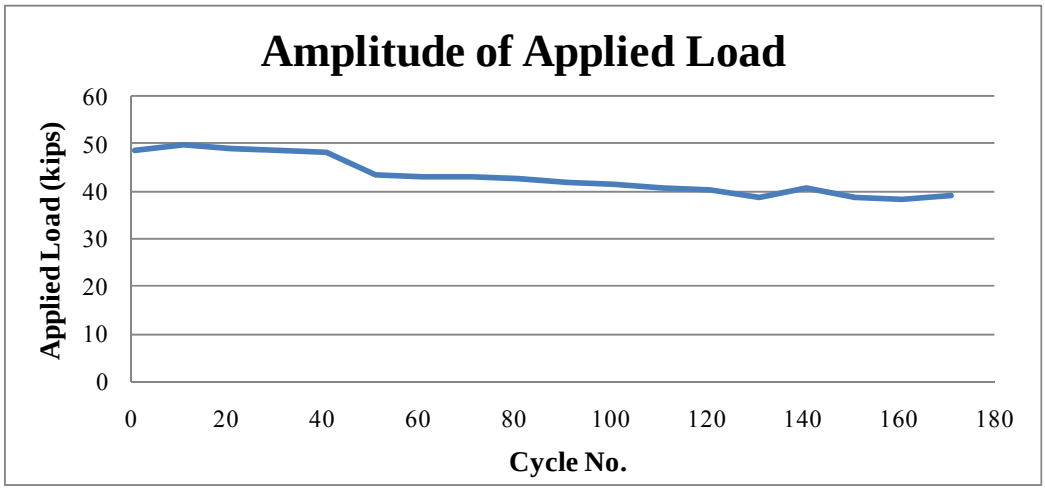
Amplitude of Applied Load
Applied Load (kips)
60
50
40
30
20
10
0
0
20
40
60
80
100
120
140
160
180
Cycle No.

LCF 02 Test Result

Total test Cycle: 30 cycles

Failure Cycle: 25th cycles

Failure Mode: End plate LCF failure at beam bottom flange area

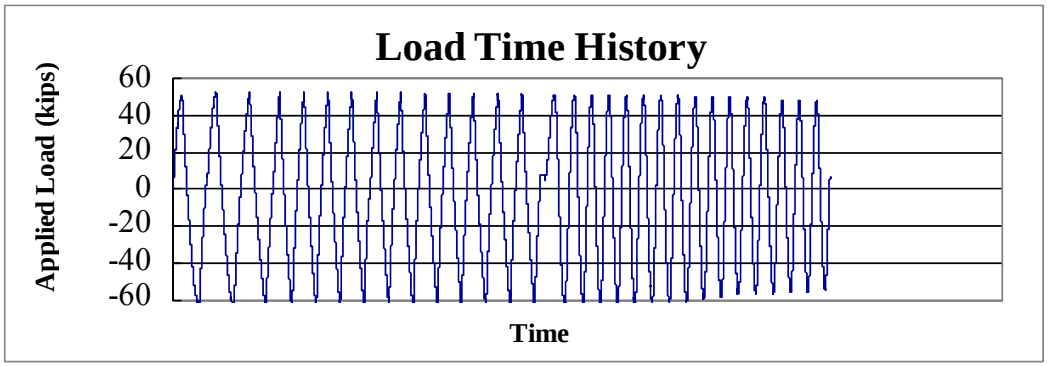

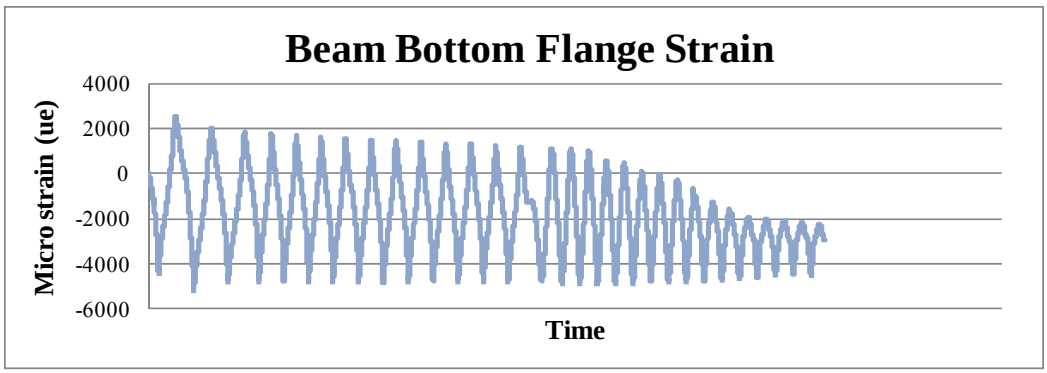

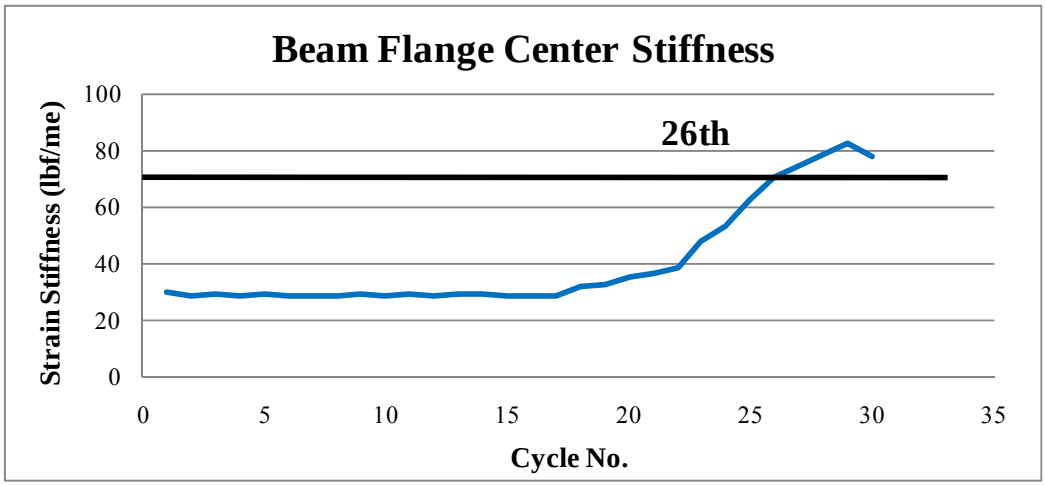

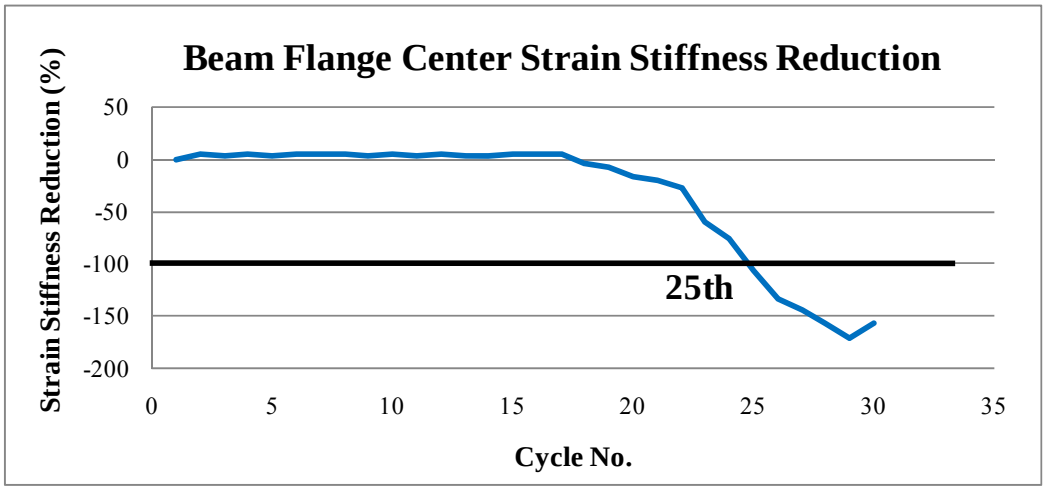
Beam Flange Center Strain Stiffness Reduction
Strain Stiffness Reduction (%)
50
0
-50
-100
-150
-200
25th
0
5
10
15
20
25
30
35
Cycle No.

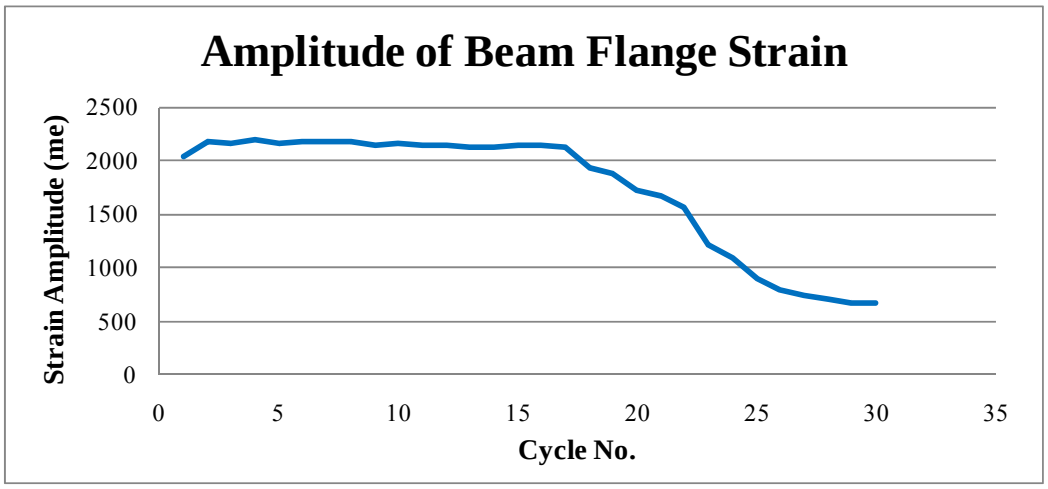
Amplitude of Beam Flange Strain
Strain Amplitude (me)
2500
2000
1500
1000
500
0
0
5
10
15
20
25
30
35
Cycle No.

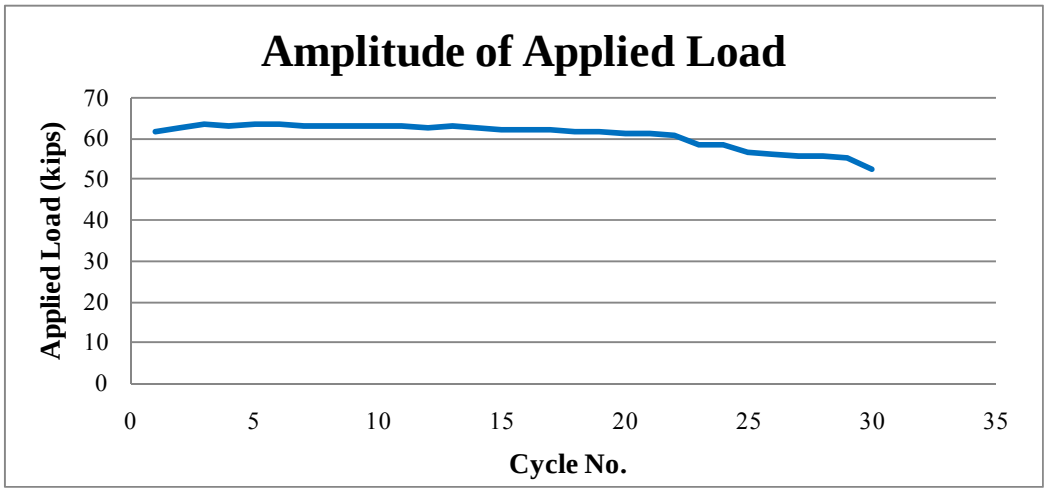
Amplitude of Applied Load
Applied Load (kips)
70
60
50
40
30
20
10
0
0
5
10
15
20
25
30
35
Cycle No.

LCF 03 Test Result

Total test Cycle: 141 cycles

Failure Cycle: 138th cycles

Failure Mode: End plate LCF failure at beam bottom flange area

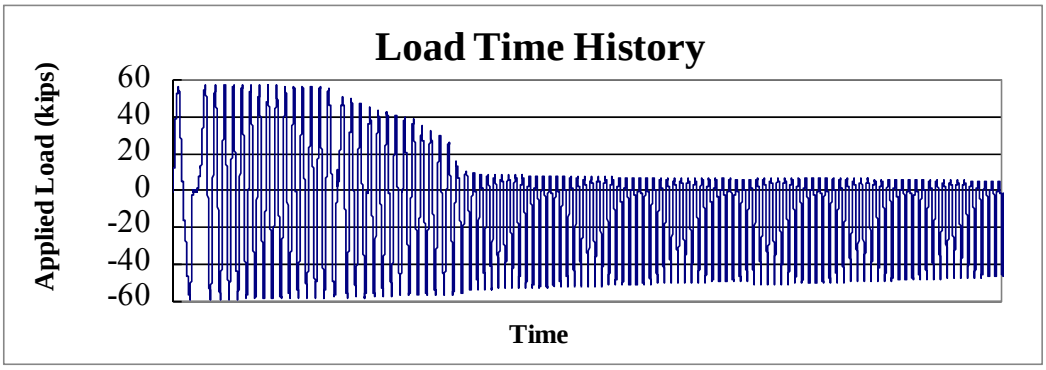

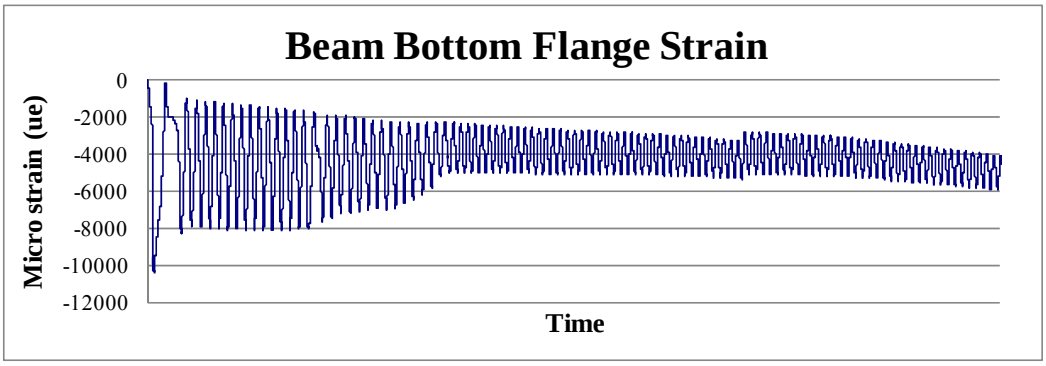

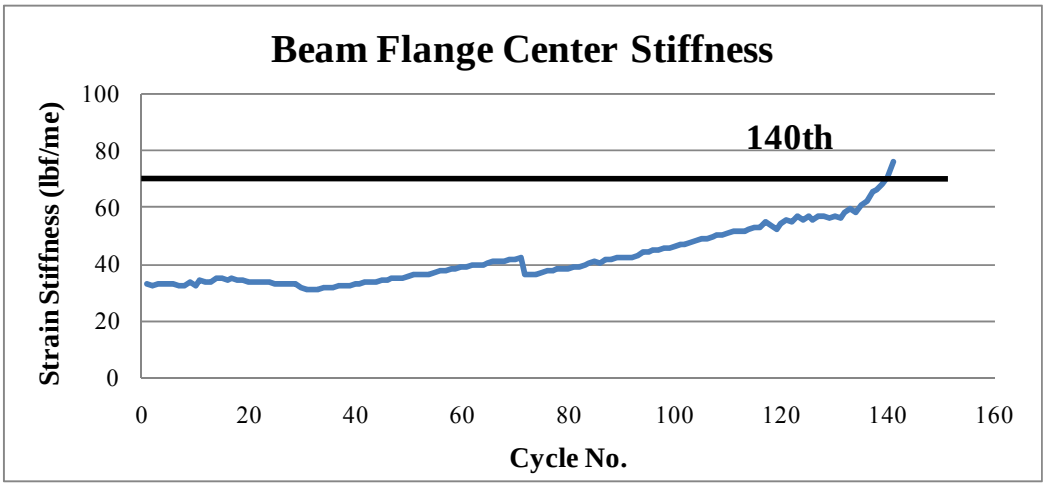

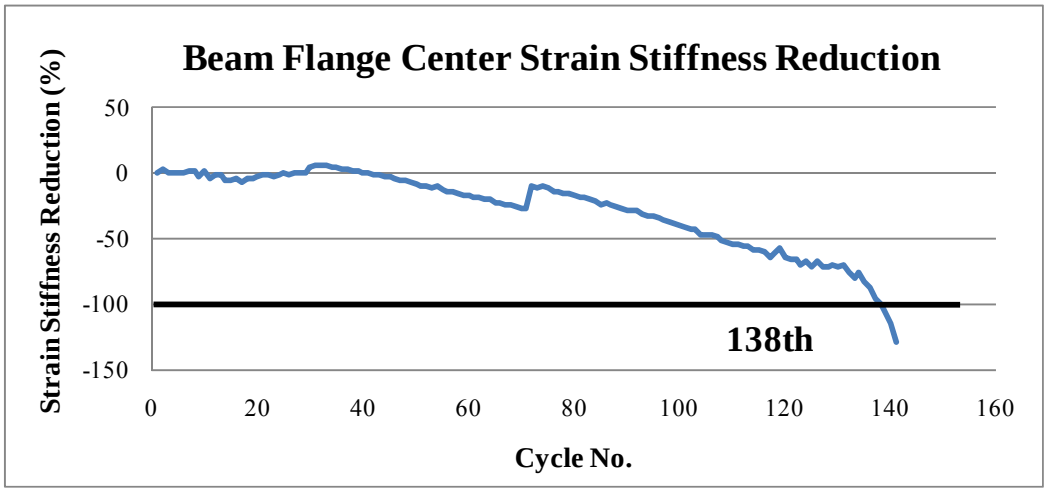
Beam Flange Center Strain Stiffness Reduction
Strain Stiffness Reduction (%)
50
0
-50
-100
-150
138th
0
20
40
60
80
100
120
140
160
Cycle No.

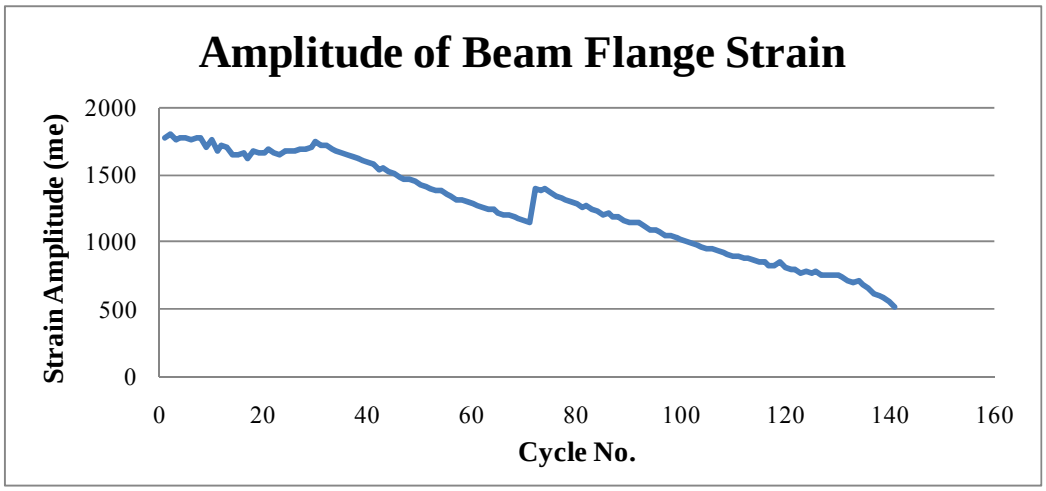
Amplitude of Beam Flange Strain
Strain Amplitude (me)
2000
1500
1000
500
0
0
20
40
60
80
100
120
140
160
Cycle No.

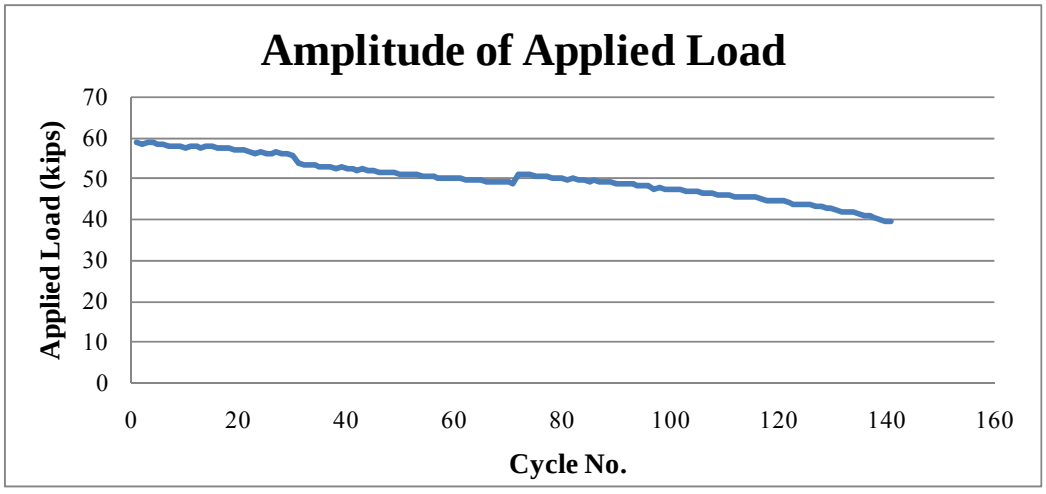
Amplitude of Applied Load
Applied Load (kips)
70
60
50
40
30
20
10
0
0
20
40
60
80
100
120
140
160
Cycle No.

LCF 04 Test Result

Total test Cycle: 100 cycles

Failure Cycle: 84th cycles

Failure Mode: End plate LCF failure at beam bottom flange area

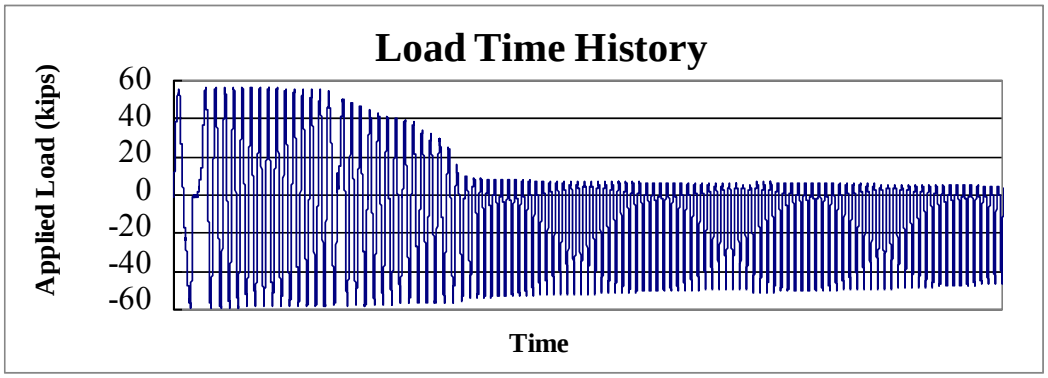

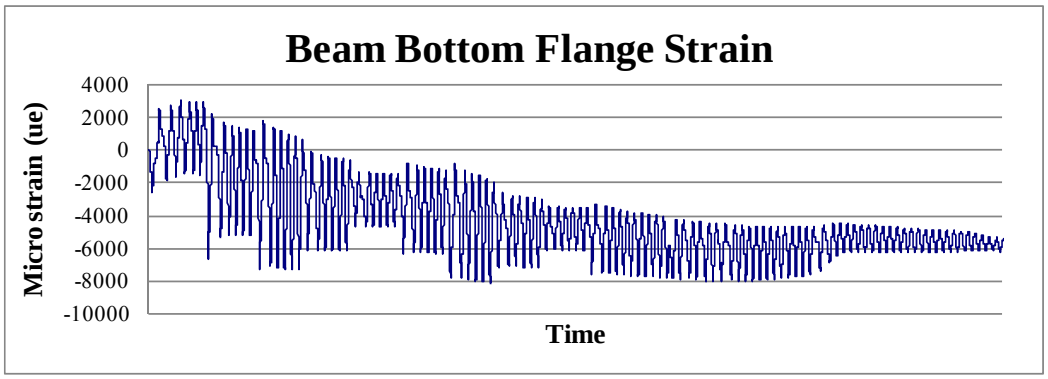

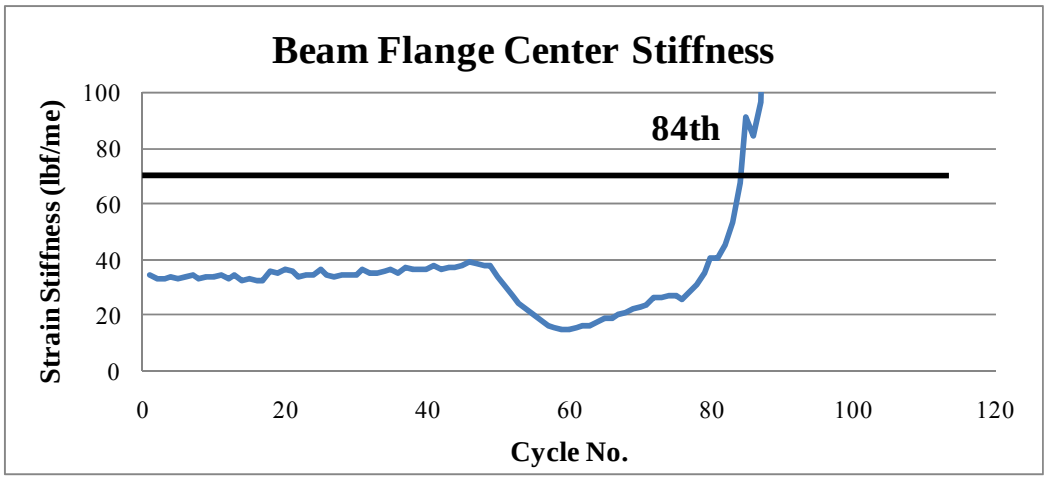

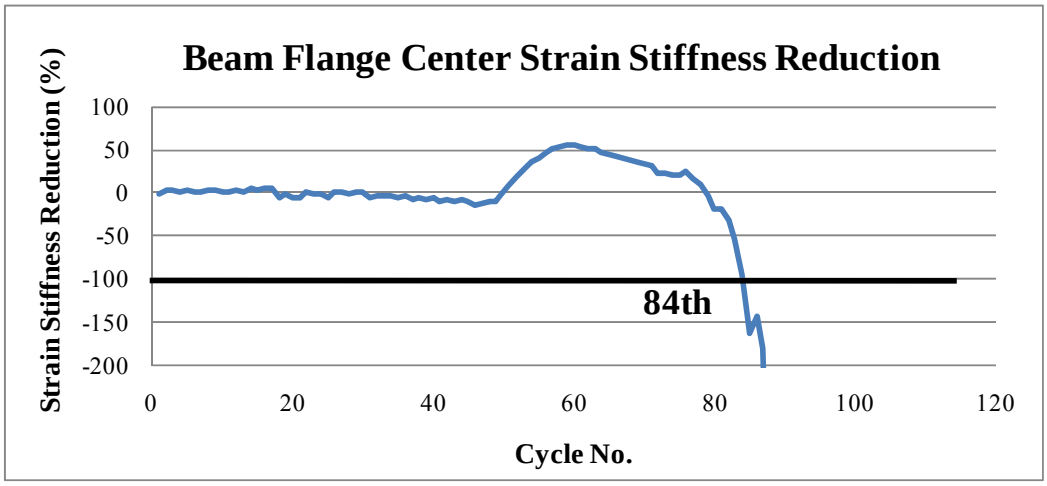
Beam Flange Center Strain Stiffness Reduction
Strain Stiffness Reduction (%)
100
50
0
-50
-100
-150
-200
84th
0
20
40
60
80
100
120
Cycle No.

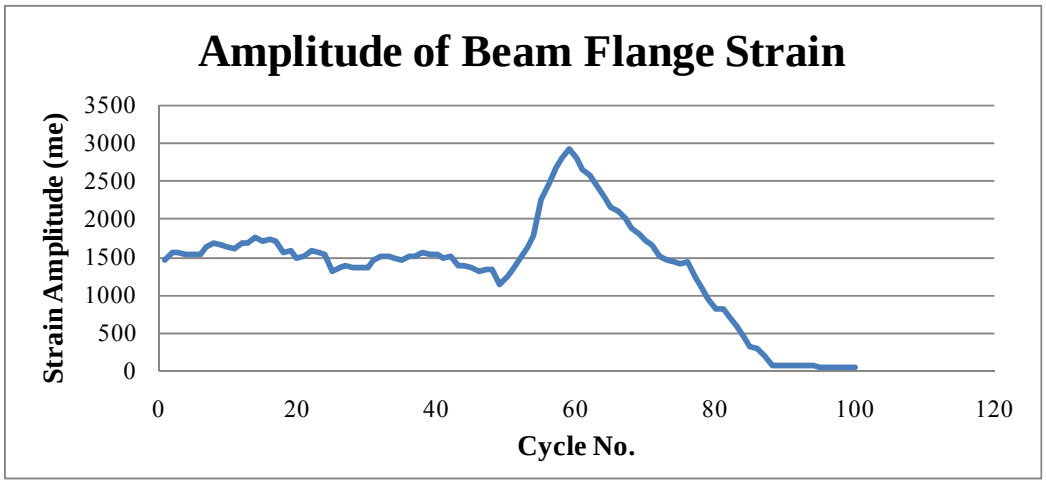
Amplitude of Beam Flange Strain
Strain Amplitude (me)
3500
3000
2500
2000
1500
1000
500
0
0
20
40
60
80
100
120
Cycle No.

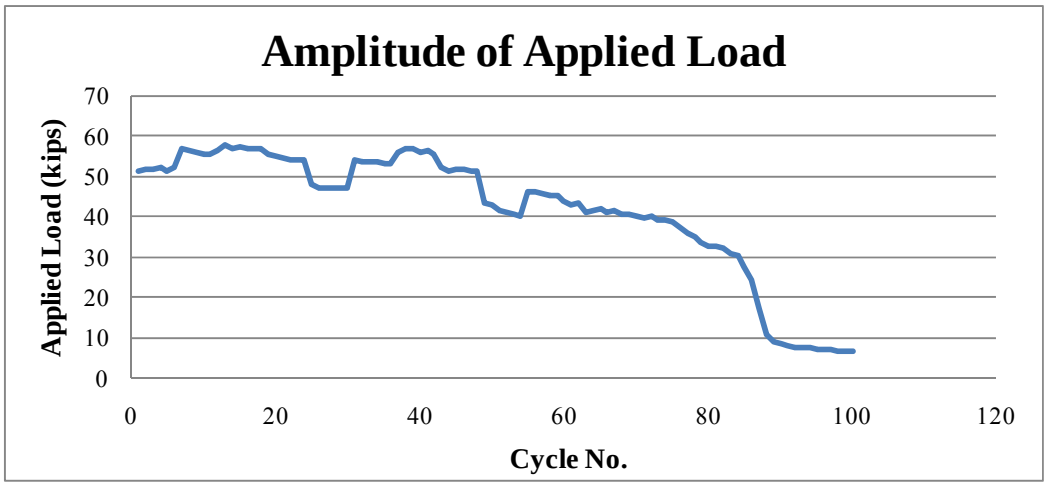
Amplitude of Applied Load
Applied Load (kips)
70
60
50
40
30
20
10
0
0
20
40
60
80
100
120
Cycle No.

APPENDIX C

Test Specimen Design Calculations

Reduced End Plate Moment Connection (T-stub) Calculation

End Plate limit state (Yield Line Theory)

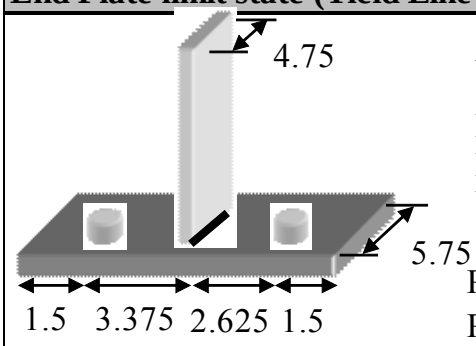

Asymmetric geometry
Stem plate: Grade 50 steel (3/8" THK)
Bottom plate: Same material (3/8" THK)
Bolt: A490 Bolt (7/8" Diameter)
Weld: One side 3/4" fillet weld

Plate yield strength:	Fy=	50 ksi
Plate thickness:	tp=	3/8 inch

Yield Line Theory (virtural work)

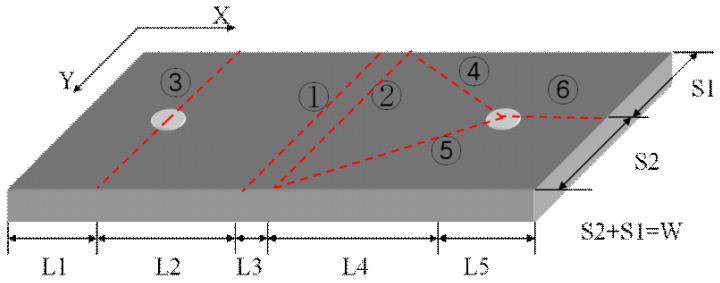

θ	1	2	3	4	5	6	7	8
X	1/L2	1/L4	1/L2	1/L2	1/L4	1/L4	0	0
Y	0	0	1/S1	1/S2	1/S1	1/S2	1/S2+1/S	1/S2+1/S1

L	1	2	3	4	5	6	7	8
	S1+S2	S1+S2	$\sqrt{L2^2+S1^2}$	$\sqrt{L2^2+S2^2}$	$\sqrt{L4^2+S1^2}$	$\sqrt{L4^2+S2^2}$	L	L

After simplification

$$W_i = \sum_{n=1}^{N} (m_{px}\theta_{nx}L_x + m_{py}\theta_{ny}L_y)$$

$$F = \frac{t_p^{\,2}}{4}\sigma_y \times \left(\frac{2W}{L_2} + \frac{2W}{L_4} + \frac{4L_4}{W} + \frac{4L_5}{W}\right)$$

Geometry information

L_1	L_2	L_3	L_4	L_5	S_1	S_2	W
1.5	3	0.75	2.625	1.5	2.875	2.875	5.75

F = 19.5 kips

Therefore, yield line was formed at 19.5kips loading applied.
That means, the limit of the plate (yield limit) is 19.5kips loading.

Bolt limit state (Original Kennedy method)

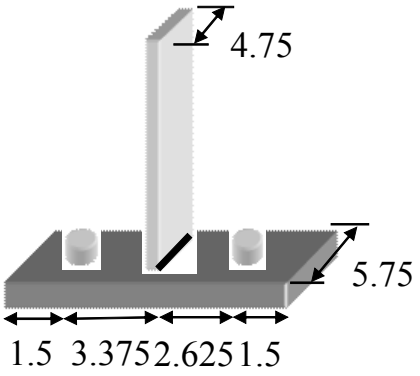

Section Properties

(Fy=)Plate yield strength (grade 50)=	50 ksi
(tp=)Base Plate thickness(3/8)=	0.375 inch
(Fby=)Bolt yield strengh (A490)=	150 ksi
(Db=)Bolt Diameter (7/8)=	0.875 inch
Weld size (3/4)=	0.75 inch
(Ag=)Bolt net area=	0.60132 In^2

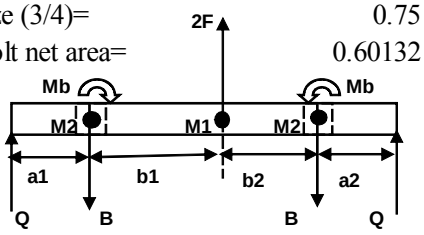

Case II

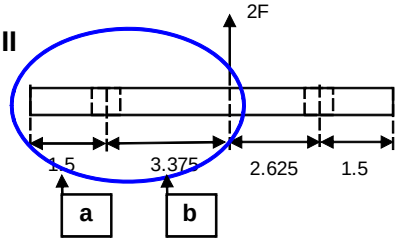

a_1= 1.5 b_1= 3

Case I

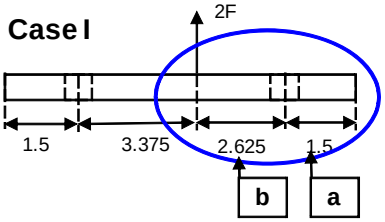

a_2= 1.5 b_2= 2.625

Thick Plate behavior limit Q=0 B=F

The general equation of the kennedy method is

$$Fb - Qa = \frac{wt_p^{\,2}}{4}\sqrt{\sigma_y^{\,2} - 3\left(\frac{F}{wt_p}\right)^2}$$

Q=0 therefore

$$Fb = \frac{wt_p^{\,2}}{4}\sqrt{\sigma_y^{\,2} - 3\left(\frac{F}{wt_p}\right)^2}$$

$$F = \frac{wt_p^{\,2}}{4}\sigma_y \Big/ \sqrt{b^2 + 3\left(\frac{t_p}{4}\right)^2}$$

F= 3.36422	F= 3.8431

Therefore the Thick Plate Limitation is 2* 3.3642 = **6.728432** kips (2F)

Bolt Limitation (Thick plate case Q=0 therefore 2B=2F)

Tensile Strength of Bolts (7/8 inch diameter)

A490: Ft=Ag*Fby= 90.2 kips

Number of Bot= 2

Therefore the Bolt resist the force:

Ft*2= **180.4** kips

Thin plate behavior limit M1=Fb-Qa-Mb; M2=Qa=Mp2

Fb-Mb=Mp1+Mp2 Mb= PI()*Db^3*Fby/32= 7.89233

W'= W-Db= 4.875

$$Fb - M_b = \frac{wt_p^{\,2}}{4}\sqrt{\sigma_y^{\,2} - 3\left(\frac{F}{wt_p}\right)^2} + \frac{w't_p^{\,2}}{4}\sqrt{\sigma_y^{\,2} - 3\left(\frac{F}{w't_p}\right)^2}$$

Iteration solve

F	Left Side	Right Side
8.6	17.9077	18.46527
8.62	17.9677	18.46428
8.63	17.9977	18.46379
8.632	18.0037	18.46369

Therefore the Thin Plate limitation is 2*F= **17.26**

Iteration solve

F	Left Side	Right Side
9	15.732669	18.445
9.5	17.045169	18.4184
9.8	17.832669	18.4017
9.84	17.937669	18.3994

Therefore the Thin Plate limitation is 2*F= **19.7**

Bolt Limitation (Thin plate case Q_max therefore 2B=2F+2Q_max)

Maximum Prying Force Calculation

Qmax= Mp/a

$$Q_{max} = \frac{M_p}{a} = \frac{w't_p^{\,2}}{4a}\sqrt{\sigma_y^{\,2} - 3\left(\frac{F}{w't_p}\right)^2}$$

$$a = 3.682\left(\frac{t_p}{d_b}\right)^3 - 0.085$$

= 0.2048

= 41.2715 kips

B= 90.1981

Q= 41.2715

F= **48.927** kips

= 41.101298 kips

B= 90.19807

Q= 41.101298

F= **49.09677** kips

Therefore the Bolt resist the force:

F*2= **97.853** kipsf

The plate has thin plate behavior .
And the bolt rupture force (=97.85kips) is much larger than plate yield force(=19.5kips)
Therefore, the T-stub limit state is controled by plate yield (yield line theory value)

Full Scale 4 Bolts Extended EPMC design

Premise

The required shear resistance

Vu= 40kips

Properties

			yield	ultimate	Ry	
Beam material	ASTM	A992		65	1.5	Φ=0.75
Column material	ASTM	A992		65	1.5	
Plate material	ASTM	A572	40	60		Coupon test result
Bolt material	ASTM	A490	113	150		

Beam Geometric	w18*55								
d_b=	18.13	t_wb=	0.375	b_fb=	7.5	t_fb=	0.625	k_b=	1.03
W.G_b=	3.5	Z_xb=	112	F_yb=		F_ub=	65		

Column Geometric	W14*82								
d_c=	14.25	t_wc=	0.5	b_fc=	10.13	t_fc=	0.875	k_c=	1.6875
W.G_c=	5.5	Z_xc=	139	F_yc=		F_uc=	65	(h/t_w)=	25.4

Beam Side Design

1. Connection Design Moment

Mpe= 1.1*Ry_b*Fy_b*Z_xb 6776 k-in = 564.7 kip s-ft

Location of plastic hinge

Lp= min(d_b/2,3*b_fb) 9.0625 in

Moment at the face of column (connection design moment)

Muc= Mpe+Vu*Lp 7138.5 k-in = 594.9 kip s-ft

2. Select connection configuration: Four bolt extended unstiffened

Assumed Geometric Desgin Data

bp= b_fb+1= 8.5 in Use bp= 10 in

g= 5.5 in

p_fi= 2 in

p_f0= 2 in

d_e= 1.625 in

Fy_p= 40 ksi

Fu_p= 60 ksi

Using assumed dimensions

h_0= d_b+p_f0-t_fb/2 = 19.81 in

h_1= d_b-t_fb-p_fi-t_fb/2 = 15.19 in

plate height= 25.375

3. Determine the required bolt diameter

d_breq

= sqrt(2*Muc/(pi()*0.75*F_t*(h_0+h_1)) = 1.238 in

4. Select Trial bolt diameter and calculate the no prying bolt moment

Use db= 1.25 in

Bolt Tensile Strength

Pt= F_t*A_b = 138.7 kips

Mnp= 2*Pt(h_0+h_1) 9707 k-in 809 kips-ft

ΦMnp

= 0.75*Mnp = 7280 k-in > 7139 OK

Muc

5. Determine the required end plate thickness (yield line mechanism)

s= 1/2*sqrt(bp*g) 3.708 in > 2 P_fi

Yp= bp/2*(h_1*(1/p_fi+1/s)+h_0*(1/p_f0)-1/2)+2/g*(h_1*(p_fi+s))

= 137.003 in

Required end plate thickness

t_preq

= SQRT(1.11*0.75*Mnp/(0.9*Fy_p*Yp))

= 1.28003 Can be selected 1.25in. THK plate

6. Select end plate thickness

Use

t_p= 1 in

7. Calculate the factored beam flange force

Ffu= Muc/(d_b-t_fb)

= 407.914 kips

8. Check shear yiedling of extended portion of end plate

ΦRn= 0.9*(0.6*Fy_p)*bp*t_p

= 216 kips

Check inequality

Ffu/2= 203.957 < 216 OK

9. Check shear rupture of extended portion of end plate

An= (bp-2*(db+1/8))*t_p
= 7.25 in^2
ΦRn= Φ*(0.6*Fu_p)*An
= 195.75 kips
Check inequality
Ffu/2= 203.957 < 195.8 NG

10.End plate is unstiffened (therefore, this step is not required)

11. Check Compression bolt shear rupture strength

Vu<=ΦRn ΦRn= Φn_b*Fv*A_b= 221 kips OK

12. Check compression bolts Bearing/Tearout

i) End plate n_i=2 n_o=2
Vu<=ΦRn ΦRn= n_i*(ΦRn)_i+n_o*(ΦRn)_o
Bearign strength= 2.4*db*t_p*Fu_p
= 180 kips/bolt
Tearout outer bolt
Lc= (p_fi+t_fb+p_f0)-(db+1/16) = 3.31 in
Rn,inner= 1.2*Lc*t_p*Fu_p = 238.5 kips > 180
By inspection, bearing controls for the inner bolts
ΦRn= 4*(Φ*243.75) = 540 > Vu OK
ii) Column flange
ΦRn= E98*(t_fc/t_p)*(Fy_p/Fy_c) = 378 > Vu OK

13. Design welds

i) Beam Flanges to End-plate weld
use CJP welds and the procedure
ii) Beam web to End-plate weld
Minimum weld size for 1 1/4in end plate is 5/16 in .
The required seld to develop the bending stress in the beam web near the tension bolt suing E70 electrodes is
D= 0.6*Fy_b*t_wb/(2*(1.392)) = 4.04 sixteenths
Use 5/16 in Fillet welds
Effective length of weld
d_b/2-t_fb= 8.4375 in
D= 40/(2*(1.392)*C112) = 1.7 sixteenths
Use 5/16 in Fillet welds

Column Side Design

14. check the column flange for flexural yielding

s_c= 1/2*sqrt(b_fc*g) 3.731 in

c= p_f0+t_fb+p_fi= 4.625 in

Yc= b_fc/2*(h_1*(1/s_c)+h_0*(1/s_c))+2/g*(h_1*(s_c+3*c_c/4)+h_0*(s_c+c_c/4)+(c_c^2)/2)+g/2

= 129.102

Required Unstiffended column flange thickness

t_fcreq

= SQRT(1.11*Φ*Mnp/(0.9*Fy_c*Yc))

= 1.1794 in > t_fc(=0.8125in) Add flange stiffeners

Assume 0.5 in stiffener plates

ts= 0.5 in

p_so= p_si= 2.0625 in

For stiffened column flange

Yc= b_fc/2*(h_1*(1/s_c+1/p_si)+h_0*(1/s_c+1/p_so))+2/g*(h_1*(s_c+p_si)+h_0*(s_c+p_so))

= 207.135 in

t_fcreq

= SQRT(1.11*Φ*Mnp/(0.9*Fy_c*Yc))= 0.93 in > t_fc OK

15. Calculate strength of unstiffened column flange to determine stiffener design force

ΦMcf= 0.9*Fy_c*Yc*t_fc^2= 4448 k-in

ΦRn= ΦMcf/(d-t_fb)= 254.17 kips < 407.9 OK

16. Calculate local web yielding strength

Ct= 1 (Assume not a top of column)

N= t_fb+0= 0.625

Note: If fillet welds are used N=t+fb+0.707t_w (where t_w is fillet weld leg size)

ΦRn= Φ*Ct*(6*kc+N+2*t_p)*Fy_c*t_wc

= 318.75 kips < 407.91 OK

Therefore, Column stiffener required.

17. Calculate web buckling strength

h= (h/tw)c*t_wc= 12.7 in

ΦRn= Φ*24*(t_wc^3)*sqrt(E*Fy_c)/h= 256 kips

Ffu= 407.914 kips > 256 (=ΦRn)

Therefore, Column stiffener required.

18. Calculate web crippling strength

ΦRn= Φ*0.80*(t_wc^2)*(1+3*(N/d_c)*(t_wc/t_fc)^1.5)*sqrt(E*Fy_c*t_fc/t_wc)

= 252.524 kips < 407.91 OK

Therefore, Column stiffener required.

19.Determine stiffener design force

Fcu= Ffu-minΦRn

= 155.391 kips

20.Stiffener design and panel zone check

AISC Desgin guide 13

Summary

Beam	w18*55
Colum n	W14*82
End plate	1 * 10
Bolt Diameter	1.25
Column Stiffeners	Add flange stiffeners

APPENDIX D

Specimen Drawing

SWS600H

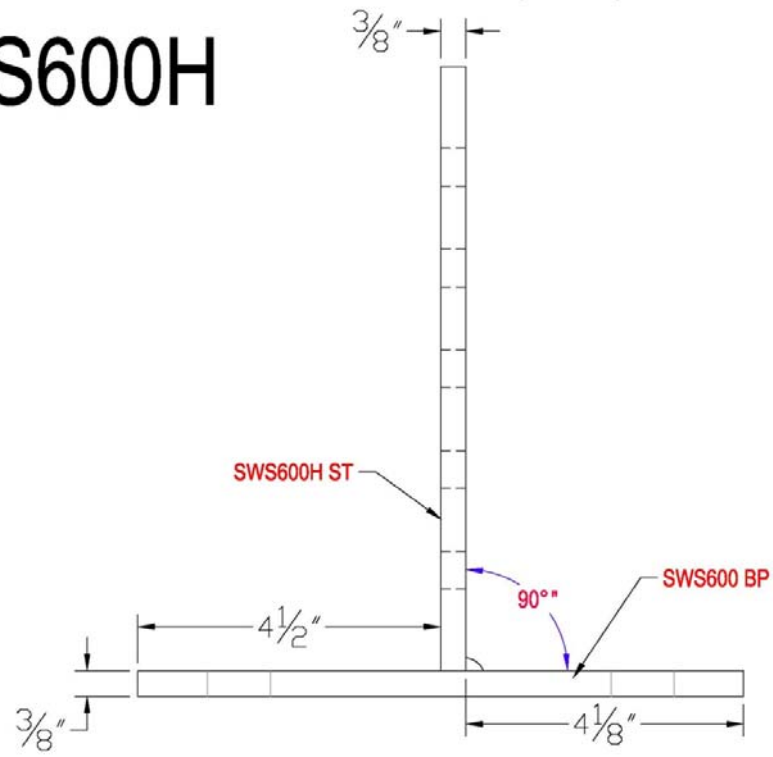

SWS600H

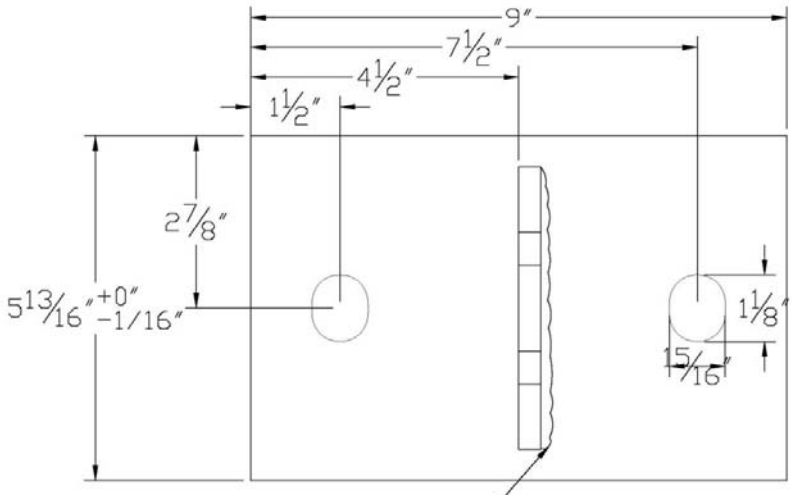

1/4" Fillet Weld, With E70XX Metal Arc or Similar.
All welds must be performed by an AWS certified welder or inspector and proof of certification is required.

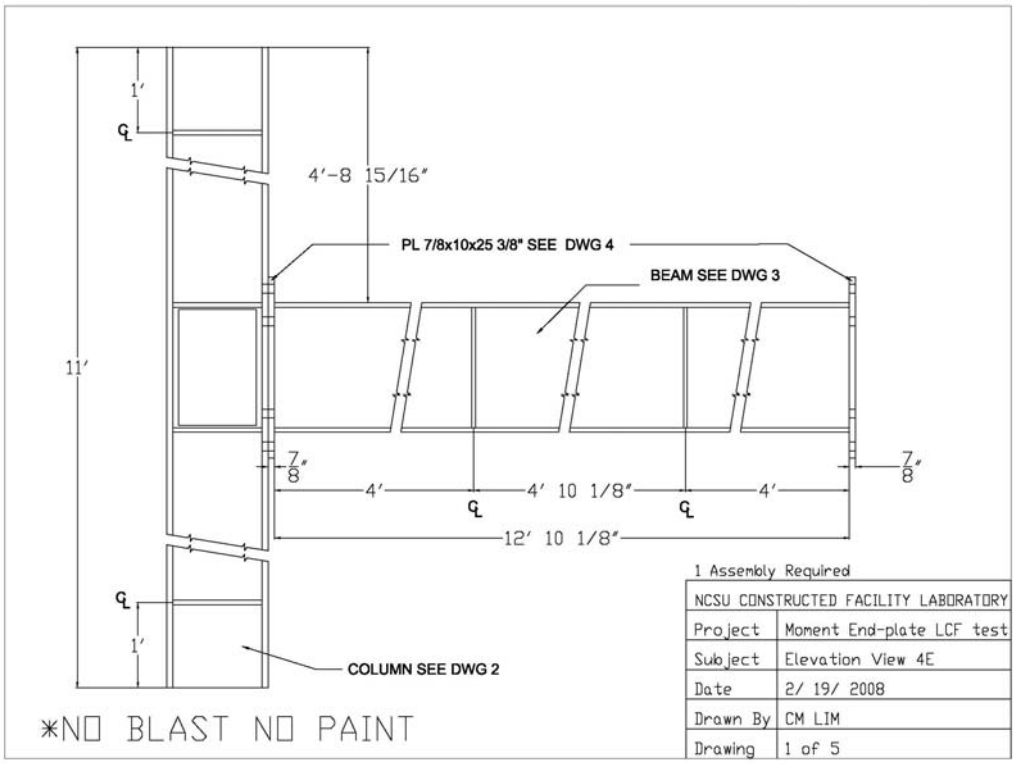

*NO BLAST NO PAINT

1 Assembly Required

NCSU CONSTRUCTED FACILITY LABORATORY	
Project	Moment End-plate LCF test
Subject	Elevation View 4E
Date	2/ 19/ 2008
Drawn By	CM LIM
Drawing	1 of 5

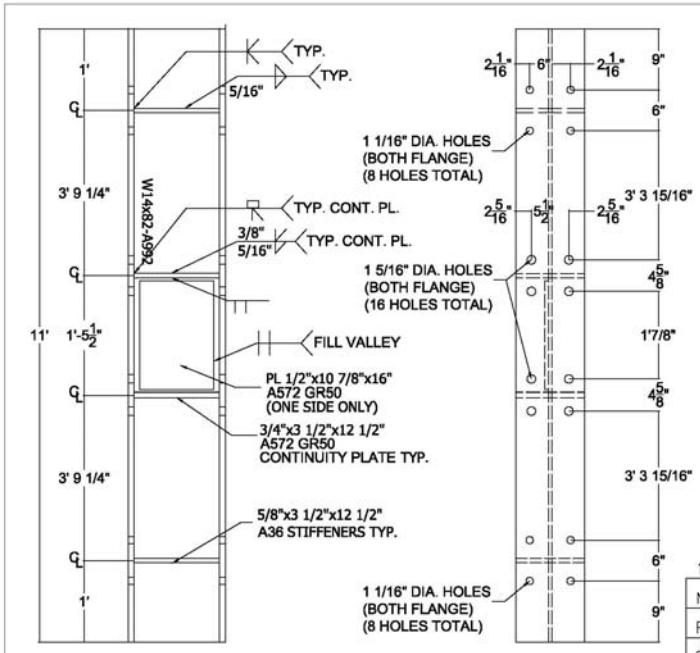

*NO BLAST NO PAINT

1 Column Required

NCSU CONSTRUCTED FACILITY LABORATORY	
Project	Moment End-plate LCF test
Subject	Column Detail 4E
Date	2/ 19/ 2008
Drawn By	CM LIM
Drawing	2 of 5

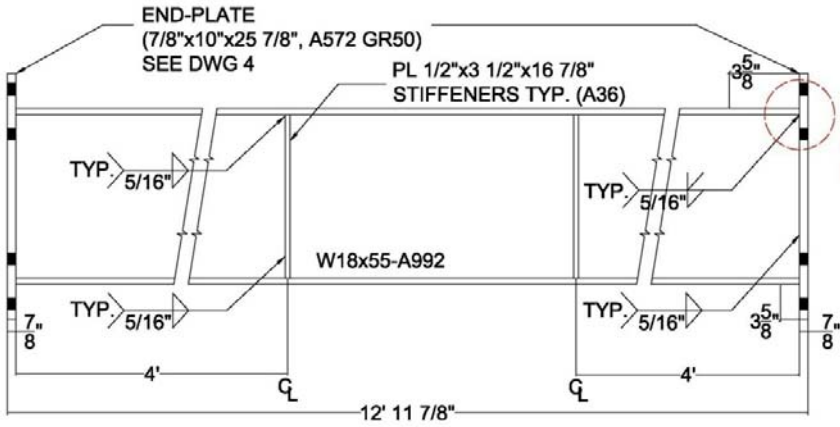

1 Beam Required

NCSU CONSTRUCTED FACILITY LABORATORY	
Project	Moment End-plate LCF test
Subject	Beam Detail 4E
Date	2/ 19/ 2008
Drawn By	CM LIM
Drawing	3 of 5

*NO BLAST NO PAINT

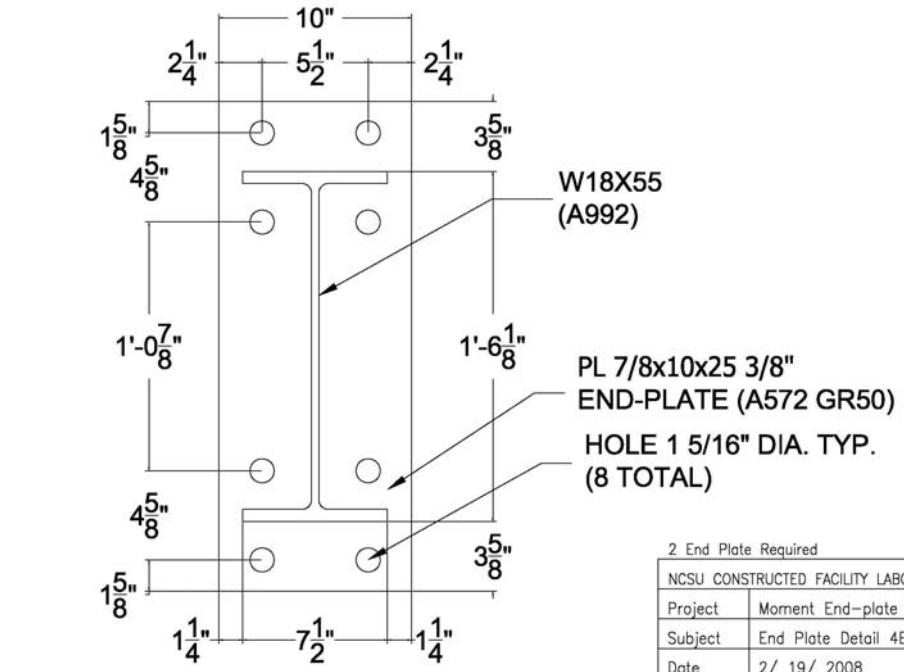

2 End Plate Required

NCSU CONSTRUCTED FACILITY LABORATORY	
Project	Moment End-plate LCF test
Subject	End Plate Detail 4E
Date	2/ 19/ 2008
Drawn By	CM LIM
Drawing	4of 5

*NO BLAST NO PAINT

WELD PROCEDURE

- Prepare the flanges of the beam with a 45 degree, full depth bevel.
- Fit up the end-plate and beam with a minimum root opening.
- Preheat the specimens as required by AWS specifications.
- Prepare the surfaces for welding as required AWS specifications.
- Install the web welds (1).
- Install the 5/16 in. backing fillet welds on the beam web side of the beam flanges (2).
- Backgouge the root of the bevel to remove any contaminants from the 5/16 in. backer fillet welds (3).
- Install the flange groove welds (AWS TC-U4b-GF).
- All welding is to be done in the down hand or flat position.

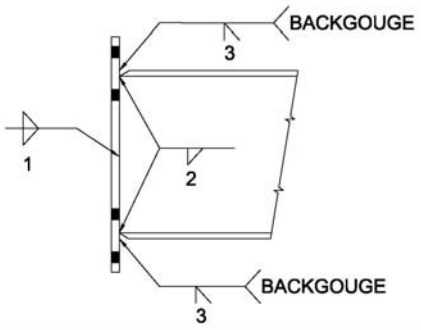

*NO BLAST NO PAINT

NCSU CONSTRUCTED FACILITY LABORATORY	
Project	Moment End-plate LCF test
Subject	Weld Procedure Detail 4E
Date	2/ 19/ 2008
Drawn By	CM LIM
Drawing	5 of 5

APPENDIX E

End Plate Material Test

End Plate Steel Plate Material Test

Test Specimen Dimension

A 370 – 08b

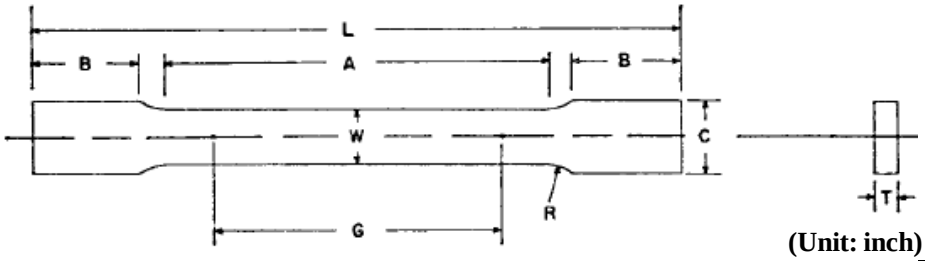

(Unit: inch)

	L	B1	B2	A	G	W	C	T
EP01	9.938	3.375	3.500	2.250	2.000	1.505	1.992	0.994
						1.502	1.980	0.996
						1.503	1.992	0.994
EP02	9.938	3.313	3.375	2.250	2.000	1.512	2.012	0.994
						1.511	2.001	0.994
						1.513	2.012	0.993
EP03	9.938	3.375	3.438	2.250	2.000	1.501	1.971	0.995
						1.499	1.982	0.994
						1.499	1.989	0.994
EP00	9.875	3.500	3.375	2.250	2.000	1.511	1.976	0.994
						1.509	2.020	0.995
						1.509	1.975	0.994

Test Result

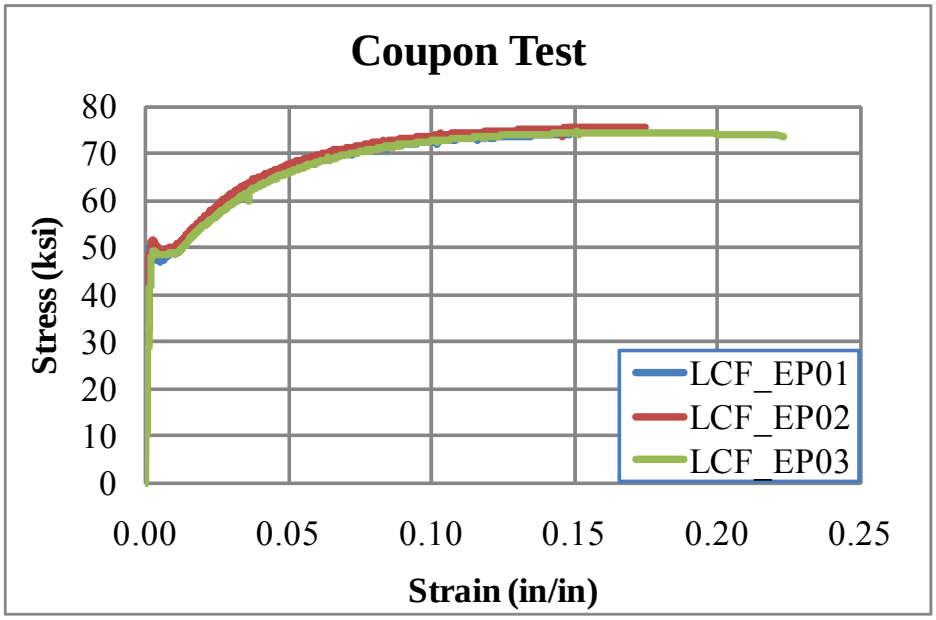

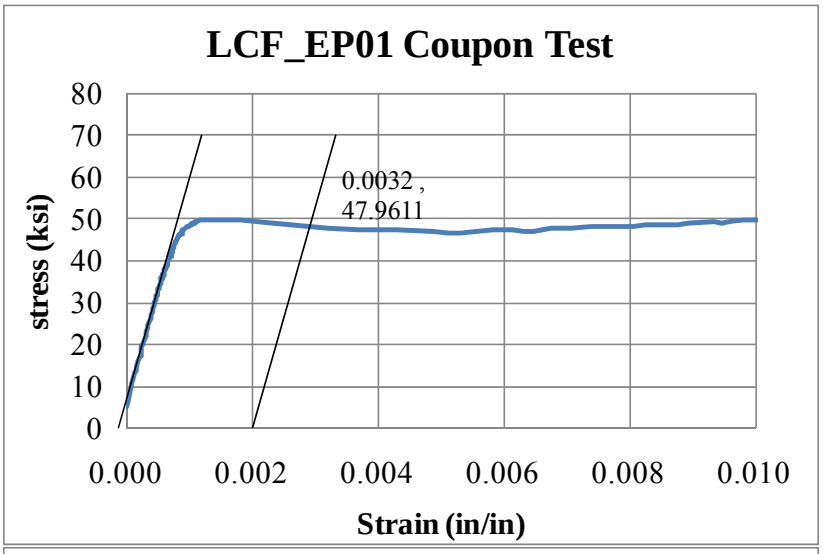
LCF_EP01 Coupon Test
stress (ksi)
80
70
60
50
40
30
20
10
0
0.0032 ,
47.9611
0.000
0.002
0.004
0.006
0.008
0.010
Strain (in/in)

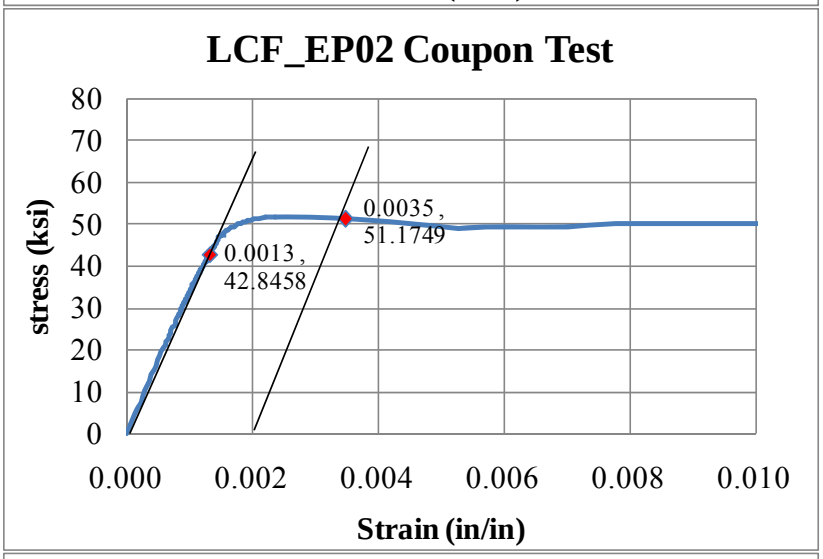
LCF_EP02 Coupon Test
stress (ksi)
80
70
60
50
40
30
20
10
0
0.0035 ,
51.1749
0.0013 ,
42.8458
0.000
0.002
0.004
0.006
0.008
0.010
Strain (in/in)

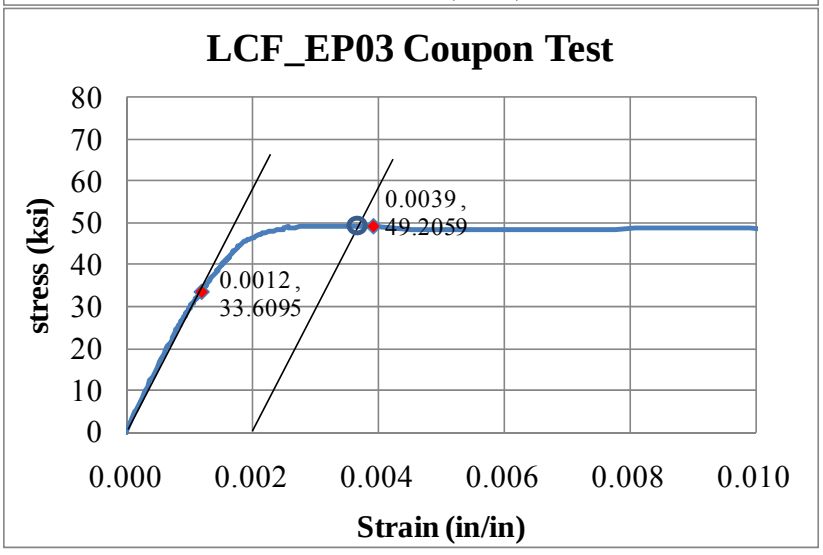
LCF_EP03 Coupon Test
stress (ksi)
80
70
60
50
40
30
20
10
0
0.0039 ,
49.2059
0.0012 ,
33.6095
0.000
0.002
0.004
0.006
0.008
0.010
Strain (in/in)

APPENDIX F

4E EPMC 3D Solid Finite Element Model

(ANSYS 11ver.)

```
finish
/clear
/title,Project Title :4E EPMC 3D analysis -Half section
! Model ID:    LCF2_1_0625_2out
! include new pretension model correctly~!!!!    (100k)

! reduced hole size - no gap between hole and stud
! Fillet weld include


! assign 2 bolt stud contact condition, new multi linear material
! apply contact friction value 0.3(max)

/com, ================================================================
/com, owner : clim
/com, written by chemin Lim,                                2009-05-27
/com, Units : klbf(force), in(length), ksi(pressure)
/com, ================================================================



/com, define parameter for Analysis ==========================================
/prep7



/com, define element type ====================================================

ET,1,SOLID45,0,,,,,3       ! PLATE 8 nodes solid element
  MP,EX,1,                   28968.71
  MP,EY,1,                   28968.71
  MP,EZ,1,                   28968.71
  MP,NUXY,1,.3
TB,MELAS,1,1,3                 ! 3 data point A50 TB,BKIN,1
TBPT,,                     0.001726,                        50! Data points !strain-stress
TBPT,,                     0.023228,                        50
TBPT,,                     0.283674,                        65


ET,2,SOLID45,0,,,,,3                  ! BOLT head
  MP,EX,2,                     28260
  MP,EY,2,                     28260
  MP,EZ,2,                     28260
  MP,NUXY,2,.3
TB,MELAS,2,1,3                 ! 3 data point A490 bolt          (yield )
TBPT,,                     0.003185,                         90
TBPT,,                     0.011039,                         90! Data points !TBDATA,1,50
TBPT,,                     0.131028,                        105
```

```
!------------bolt stud propertis (reduced stiffness-rectangular area)

ET,3,SOLID45,0,,,,,3                    ! Stud
  MP,EX,3,                  22777
  MP,EY,3,                  22777
  MP,EZ,3,                  22777
  MP,NUXY,3,.3
TB,MELAS,3,1,3                ! 3 data point A490 bolt
TBPT,,                    0.003951,                       90
TBPT,,                    0.011039,                       90! Data points !TBDATA,1,50
TBPT,,                    0.131028,                      105
ET,7,SOLID45,0,,,,,3                    ! End plate
  MP,EX,7,                  28467.73
  MP,EY,7,                  28467.73
  MP,EZ,7,                  28467.73
  MP,NUXY,7,.3
TB,MELAS,7,1,3
TBPT,,                    0.001181,                     33.609
TBPT,,                     0.00258,                    49.14453! Data points !TBDATA,1,50
TBPT,,                    0.065156,                    69.14708

ET,8,SOLID92,                                                   ! Weld 20 node solid
  MP,EX,8,                  28260
  MP,EY,8,                  28260
  MP,EZ,8,                  28260
  MP,NUXY,8,.3
TB,MELAS,8,1,3                ! 3 data point A50 TB,BKIN,1
TBPT,,                    0.003185,                       90! Data points !strain-stress
TBPT,,                    0.011039,                       90
TBPT,,                    0.131028,                      105
/com, define parameters ================================================
mesh_topplate=                          0.25
mesh_bottomplate=                       0.25
mesh_bolthead=                          0.185
mesh_boltstud=                          0.185
mesh_beamA=                             0.3125
mesh_beamL=                               0.5


 FKN_C=                                 0.01
 TLN_C=                                 0.15
 FRIC=                                   0.3
 ICON_C=                              0.00001
/com, Modeling    ========================================
!Top plate
BLC4,              0,             11.6875,              1.625,                1,                1
BLC4,          1.625,             11.6875,               1.25,                1,                1
BLC4,          2.875,             11.6875,              2.125,                1,                1
BLC4,              0,             10.4375,              1.625,             1.25,                1
```

```
BLC4,     2.875,    10.4375,     2.125,     1.25,     1
BLC4,         0,     7.0625,     1.625,     3.375,    1
BLC4,     1.625,     7.0625,      1.25,     3.375,    1
BLC4,     2.875,     7.0625,     2.125,     3.375,    1
BLC4,         0,     5.8125,     1.625,     1.25,     1
BLC4,     2.875,     5.8125,     2.125,     1.25,     1
BLC4,         0,          0,     1.625,     5.8125,   1
BLC4,     1.625,          0,      1.25,     5.8125,   1
BLC4,     2.875,          0,     2.125,     5.8125,   1

!Bottom plate
BLC4,         0,    11.6875,     1.625,          1,   -1
BLC4,     1.625,    11.6875,      1.25,          1,   -1
BLC4,     2.875,    11.6875,     2.125,          1,   -1
BLC4,         0,    10.4375,     1.625,     1.25,     -1
BLC4,     2.875,    10.4375,     2.125,     1.25,     -1
BLC4,         0,     7.0625,     1.625,     3.375,    -1
BLC4,     1.625,     7.0625,      1.25,     3.375,    -1
BLC4,     2.875,     7.0625,     2.125,     3.375,    -1
BLC4,         0,     5.8125,     1.625,     1.25,     -1
BLC4,     2.875,     5.8125,     2.125,     1.25,     -1
BLC4,         0,          0,     1.625,     5.8125,   -1
BLC4,     1.625,          0,      1.25,     5.8125,   -1
BLC4,     2.875,          0,     2.125,     5.8125,   -1

WPOFFS    ,         2,          11.0625,          1


!Bolt1
!head
BLC4,    -0.875,     0.625,      0.25,     0.25,     0.75
BLC4,    -0.625,     0.625,      1.25,     0.25,     0.75
BLC4,     0.625,     0.625,      0.25,     0.25,     0.75
BLC4,    -0.875,    -0.625,      0.25,     1.25,     0.75
BLC4,    -0.625,    -0.625,      1.25,     1.25,     0.75
BLC4,     0.625,    -0.625,      0.25,     1.25,     0.75
BLC4,    -0.875,    -0.875,      0.25,     0.25,     0.75
BLC4,    -0.625,    -0.875,      1.25,     0.25,     0.75
BLC4,     0.625,    -0.875,      0.25,     0.25,     0.75
!stud
BLC4,    -0.625,    -0.625,      1.25,     1.25,     -2

WPOFFS    ,         0,          -4.625,           0

!Bolt2
BLC4,    -0.875,     0.625,      0.25,     0.25,     0.75
BLC4,    -0.625,     0.625,      1.25,     0.25,     0.75
BLC4,     0.625,     0.625,      0.25,     0.25,     0.75
BLC4,    -0.875,    -0.625,      0.25,     1.25,     0.75
BLC4,    -0.625,    -0.625,      1.25,     1.25,     0.75
BLC4,     0.625,    -0.625,      0.25,     1.25,     0.75
```

```
BLC4,      -0.875,      -0.875,       0.25,       0.25,       0.75
BLC4,      -0.625,      -0.875,       1.25,       0.25,       0.75
BLC4,       0.625,      -0.875,       0.25,       0.25,       0.75
!stud
BLC4,      -0.625,      -0.625,       1.25,       1.25,         -2
WPOFFS   ,      -2,    -6.4375,         -1

WPOFFS   ,       0,           0,          1
!------------------------- beam modeling
!beam
BLC4,       1.25,      8.4375,     3.5625,      0.625,          8
BLC4,     4.8125,      8.4375,     0.1875,      0.625,          8
BLC4,     4.8125,           0,     0.1875,     8.4375,          8
WPOFFS   ,       0,           0,         -1

! Bottom design
!Top plate
BLC4,          0,    -11.6875,       1.625,         -1,          1
BLC4,      1.625,    -11.6875,        1.25,         -1,          1
BLC4,      2.875,    -11.6875,       2.125,         -1,          1
BLC4,          0,    -10.4375,       1.625,      -1.25,          1
BLC4,      2.875,    -10.4375,       2.125,      -1.25,          1
BLC4,          0,     -7.0625,       1.625,     -3.375,          1
BLC4,      1.625,     -7.0625,        1.25,     -3.375,          1
BLC4,      2.875,     -7.0625,       2.125,     -3.375,          1
BLC4,          0,     -5.8125,       1.625,      -1.25,          1
BLC4,      2.875,     -5.8125,       2.125,      -1.25,          1
BLC4,          0,           0,       1.625,     -5.813,          1
BLC4,      1.625,           0,        1.25,     -5.813,          1
BLC4,      2.875,           0,       2.125,     -5.813,          1

!Bottom plate
BLC4,          0,    -11.6875,       1.625,         -1,         -1
BLC4,      1.625,    -11.6875,        1.25,         -1,         -1
BLC4,      2.875,    -11.6875,       2.125,         -1,         -1
BLC4,          0,    -10.4375,       1.625,      -1.25,         -1
BLC4,      2.875,    -10.4375,       2.125,      -1.25,         -1
BLC4,          0,     -7.0625,       1.625,     -3.375,         -1
BLC4,      1.625,     -7.0625,        1.25,     -3.375,         -1
BLC4,      2.875,     -7.0625,       2.125,     -3.375,         -1
BLC4,          0,     -5.8125,       1.625,      -1.25,         -1
BLC4,      2.875,     -5.8125,       2.125,      -1.25,         -1
BLC4,          0,           0,       1.625,     -5.813,         -1
BLC4,      1.625,           0,        1.25,     -5.813,         -1
BLC4,      2.875,           0,       2.125,     -5.813,         -1

WPOFFS   ,       2,    -11.0625,          1


!Bolt1
!head
```

```
BLC4,    -0.875,   -0.625,    0.25,   -0.25,   0.75
BLC4,    -0.625,   -0.625,    1.25,   -0.25,   0.75
BLC4,     0.625,   -0.625,    0.25,   -0.25,   0.75
BLC4,    -0.875,    0.625,    0.25,   -1.25,   0.75
BLC4,    -0.625,    0.625,    1.25,   -1.25,   0.75
BLC4,     0.625,    0.625,    0.25,   -1.25,   0.75
BLC4,    -0.875,    0.875,    0.25,   -0.25,   0.75
BLC4,    -0.625,    0.875,    1.25,   -0.25,   0.75
BLC4,     0.625,    0.875,    0.25,   -0.25,   0.75
!stud
BLC4,    -0.625,    0.625,    1.25,   -1.25,   -2

WPOFFS   ,   0,   4.625,   0

!Bolt2
BLC4,    -0.875,   -0.625,    0.25,   -0.25,   0.75
BLC4,    -0.625,   -0.625,    1.25,   -0.25,   0.75
BLC4,     0.625,   -0.625,    0.25,   -0.25,   0.75
BLC4,    -0.875,    0.625,    0.25,   -1.25,   0.75
BLC4,    -0.625,    0.625,    1.25,   -1.25,   0.75
BLC4,     0.625,    0.625,    0.25,   -1.25,   0.75
BLC4,    -0.875,    0.875,    0.25,   -0.25,   0.75
BLC4,    -0.625,    0.875,    1.25,   -0.25,   0.75
BLC4,     0.625,    0.875,    0.25,   -0.25,   0.75
!stud
BLC4,    -0.625,    0.625,    1.25,   -1.25,   -2
WPOFFS   ,   -2,   6.4375,   -1

WPOFFS   ,   0,   0,   1
!------------------------- beam modeling
!beam
BLC4,     1.25,    -8.4375,   3.5625,   -0.625,   8
BLC4,     4.8125,  -8.4375,   0.1875,   -0.625,   8
BLC4,     4.8125,   0,        0.1875,   -8.438,   8
WPOFFS   ,   0,   0,   -1
!------------------------- beam stiffner modeling
WPOFFS   ,   1,   8.4375,   8
BLC4,     0,   0,   3.5625,   -16.88,   0.5
WPOFFS   ,   -1,   -8.4375,   -8

vsel,   s,   loc,   z,   0   ,   1
vsel,u,volu,,   36
vsel,u,volu,,   46
vsel,u,volu,,   85
vsel,u,volu,,   95
vglue,   all
vsel,   s,   loc,   z,   0   ,   -1
vsel,u,volu,,   36
vsel,u,volu,,   46
vsel,u,volu,,   85
vsel,u,volu,,   95
```

```
vglue,                                  all
vsel,                                   s,          volu,           ,           27,             36
vglue,                                  all
vsel,                                   s,          volu,           ,           37,             46
vglue,                                  all
vsel,                                   s,          volu,           ,           76,             85
vglue,                                  all
vsel,                                   s,          volu,           ,           86,             95
vglue,                                  all
allsel
vglue,                                  47,         48,             49,         96,             97,             98


!---------------------------------------define
vsel,                                   s,          loc,            z,                  0       ,               1
vsel,u,volu,,                                                       19
vsel,u,volu,,                                                       29
vsel,u,volu,,                                                       39
vsel,u,volu,,                                                       65
cm,                                     topplate_volu,volu
vsel,                                   s,          loc,            z,                  -1      ,               0
vsel,u,volu,,                                                       19
vsel,u,volu,,                                                       29
vsel,u,volu,,                                                       39
vsel,u,volu,,                                                       65
cm,                                     bottomplate_volu,volu
vsel,s,loc,z,                               1       ,               1.75        ,,1
vsel,a,volu,,                                                       19
vsel,a,volu,,                                                       29
vsel,a,volu,,                                                       39
vsel,a,volu,,                                                       65
cm,bolt_volu,volu
vsel,s,loc,z,                               1       ,               1.75        ,,1
cm,bolthead_volu,volu
vsel,s,loc,z,                               1       ,               1.75        ,,1
vsel,u,volu,,                                                       20
vsel,u,volu,,                                                       30
vsel,u,volu,,                                                       40
vsel,u,volu,,                                                       66
cm,boltheadex_volu,volu
vsel,s,volu,,                                                       19
vsel,a,volu,,                                                       29
vsel,a,volu,,                                                       39
vsel,a,volu,,                                                       65
cm,boltstud_volu,volu
vsel,s,volu,,topplate_volu
vsel,a,volu,,bottomplate_volu
cm,plate_volu,volu

vsel,                                   s,          loc,            z,                  1.75    ,               8
vsel,u,volu,,                                       bolthead_volu
```

```
vsel,                    r,    loc,    y,    8.4375   ,    9.06
cm,beamtopflange_volu,volu
vsel,                    s,    loc,    z,    1.75     ,    8
vsel,u,volu,,                  bolthead_volu
vsel,                    r,    loc,    y,    -8.438   ,    -9.06
cm,beambottomflange_volu,volu
vsel,                    s,    loc,    z,    1.75     ,    8
vsel,u,volu,,                  bolthead_volu
vsel,                    r,    loc,    y,    -8.438   ,    8.44
cm,beamweb_volu,volu
vsel,s,volu,,beamtopflange_volu
vsel,a,volu,,beambottomflange_volu
vsel,a,volu,,beamweb_volu
cm,beam_volu,volu
vsel,s,loc,z,            8   ,          8.5   ,,1
cm,beamstiff_volu,volu
! Weld modeling with key point
k,                       1001,       1.25   ,    9.0625   ,    1
k,                       1002,       1.25   ,    9.5625   ,    1
k,                       1004,          5   ,    9.0625   ,    1
k,                       1005,          5   ,    9.5625   ,    1
k,                       1003,       1.25   ,    9.0625   ,    1.5
k,                       1006,          5   ,    9.0625   ,    1.5
v,                       1001,  1002,   1003,  1004,   1005,  1006,
cm,weld_volu,volu


!------------------------------------------------ mesh   (mesh   size:   standard)
vsel,s,volu,,topplate_volu,,,1
lsel,r,line,,all
lesize,all,mesh_topplate
Mat,7
type,7
vmesh,all

allsel
vsel,s,volu,,bottomplate_volu,,,1
lsel,r,line,,all
lesize,all,mesh_bottomplate
Mat,1
type,1
vmesh,all
allsel

vsel,s,volu,,bolthead_volu,,,1
lsel,r,line,,all
lesize,all,mesh_bolthead
Mat,2
type,2
vmesh,all
allsel
```

```
vsel,s,volu,,boltstud_volu,,,1
lsel,r,line,,all
lesize,all,mesh_boltstud
Mat,3
type,3
vmesh,all

vsel,s,volu,,beam_volu,,,1
lsel,r,loc,z,                    1
lesize,all,mesh_beamA
vsel,s,volu,,beam_volu,,,1
lsel,r,loc,z,                    9
lesize,all,mesh_beamA
vsel,s,volu,,beam_volu,,,1
lsel,r,loc,z,                    1   ,              9
lsel,u,loc,z,                    1
lsel,u,loc,z,                    9
lesize,all,mesh_beamL
vsel,s,volu,,beam_volu,,,1
Mat,1
type,1
vmesh,all

vsel,s,volu,,beamstiff_volu,,,1
lesize,all,mesh_beamA
Mat,1
type,1
vmesh,all

vsel,s,volu,,weld_volu,,,1                    ! Weld material use bolt head material
lesize,all,mesh_beamA
Mat,8
type,8
vmesh,all

!=======================! Bolt head contact to top plate
!--------------------------------contact pair 1
!Bolt head
vsel,s,volu,,boltheadex_volu,,,1          ! select head
nsel,r,loc,z                                        ,              1
nsel,r,loc,y,                          5.5625   ,          7.313
cm,contact1_1,node              ! call this group of nodes '
vsel,s,volu,,boltheadex_volu,,,1          ! select head
nsel,r,loc,z                                        ,              1
nsel,r,loc,y,                          10.188   ,          11.94
cm,contact1_2,node              ! call this group of nodes '
vsel,s,volu,,boltheadex_volu,,,1          ! select head
nsel,r,loc,z                                        ,              1
nsel,r,loc,y,                          -5.563   ,          -7.313
cm,contact1_3,node              ! call this group of nodes '
```

```
vsel,s,volu,,boltheadex_volu,,,1                ! select head
nsel,r,loc,z                                    ,                1
nsel,r,loc,y,                                -10.19   ,          -11.94
cm,contact1_4,node              ! call this group of nodes '
nsel,s,node,,contact1_1
nsel,a,node,,contact1_2
nsel,a,node,,contact1_3
nsel,a,node,,contact1_4
cm,contact1,node                ! call this selection 'source'
! Plate (target)
vsel,s,volu,,topplate_volu,,,1                  ! select top volume
nsel,r,loc,x,                                 1.375   ,          3.125
nsel,r,loc,y,                                5.5625   ,          7.313
nsel,r,loc,z,                                        1
cm,target1_1,node                                    ! select bottom layer of nodes in this area
vsel,s,volu,,topplate_volu,,,1                  ! select top volume
nsel,r,loc,x,                                 1.375   ,          3.125
nsel,r,loc,y,                                10.188   ,          11.94
nsel,r,loc,z,                                        1
cm,target1_2,node                                    ! select bottom layer of nodes in this area
vsel,s,volu,,topplate_volu,,,1                  ! select top volume
nsel,r,loc,x,                                 1.375   ,          3.125
nsel,r,loc,y,                                -5.563   ,          -7.313
nsel,r,loc,z,                                        1
cm,target1_3,node                                    ! select bottom layer of nodes in this area
vsel,s,volu,,topplate_volu,,,1                  ! select top volume
nsel,r,loc,x,                                 1.375   ,          3.125
nsel,r,loc,y,                                -10.19   ,          -11.94
nsel,r,loc,z,                                        1
cm,target1_4,node                                    ! select bottom layer of nodes in this area
nsel,s,node,,target1_1
nsel,a,node,,target1_2
nsel,a,node,,target1_3
nsel,a,node,,target1_4
cm,target1,node                 ! call this selection 'source'


ET,4,174,0,1,0,,0
KEYOPT,4,7,0
KEYOPT,4,9,1
KEYOPT,4,10,0
Real,4
R,4,,,FKN_C,TLN_C,ICON_C
MP,MU,4,0.3


ET,5,170
REAL,4
R,4
MAT,4
allsel
```

```
nsel,s,node,,target1
nsel,a,node,,contact1
CPINTF, all,                                    0.15


!====================! bottom plate contact to top plate
!---------------------------------contact pair 2
!Top plate (contact)
! first select the contact nodes
vsel,s,volu,,topplate_volu,,,1              ! select top
nsel,r,loc,z,0                  ! select bottom layer of nodes in this area
cm,contact2,node                    ! call this group of nodes 'source'

! Bottom plate (target)
allsel                              ! relect everything
vsel,s,volu,,bottomplate_volu,,,1                   ! select bottom volume
nsel,r,loc,z,0                  ! select bottom layer of nodes in this area
cm,target2,node                     ! call this selection 'target'

nsel,s,node,,target2
CM,_TARGET,NODE
TYPE,5
ESLN,S,0
ESURF

nsel,s,node,,contact2
CM,_CONTACT,NODE
TYPE,4
ESLN,S,0
ESURF

! ============================bolt stud contact
!---------------------------------    contact pair 3
!plate
vsel,s,volu,,plate_volu,,,1
nsel,r,loc,x,                                       1.625   ,           2.875
nsel,r,loc,y,                                      5.8125   ,          7.0625
cm,target3_1,node                           ! Bottom bolt portion
vsel,s,volu,,plate_volu,,,1
nsel,r,loc,x,                                       1.625   ,           2.875
nsel,r,loc,y,                                     10.4375   ,          11.688
cm,target3_2,node                           ! Top bolt portion
vsel,s,volu,,plate_volu,,,1
nsel,r,loc,x,                                       1.625   ,           2.875
nsel,r,loc,y,                                     -5.8125   ,          -7.063
cm,target3_3,node
vsel,s,volu,,plate_volu,,,1
nsel,r,loc,x,                                       1.625   ,           2.875
nsel,r,loc,y,                                     -10.438   ,          -11.69
cm,target3_4,node
```

```
nsel,s,node,,target3_1
nsel,a,node,,target3_2
nsel,a,node,,target3_3
nsel,a,node,,target3_4
cm,target3,node
!stud
vsel,s,volu,,boltstud_volu,,,1
nsel,r,loc,x,                    1.625          !left surface of stud
cm,contact3_1,node
vsel,s,volu,,boltstud_volu,,,1
nsel,r,loc,x,                    2.875          !right surface of stud
cm,contact3_2,node
vsel,s,volu,,boltstud_volu,,,1
nsel,r,loc,y,                    7.0625  ,      10.438
cm,contact3_3,node
vsel,s,volu,,boltstud_volu,,,1
nsel,r,loc,y,                    5.8125
cm,contact3_4,node               !outside bottom(y-dir) surface of stud
vsel,s,volu,,boltstud_volu,,,1
nsel,r,loc,y,                    11.6875
cm,contact3_5,node               !outside top(y-dir) surface of stud
vsel,s,volu,,boltstud_volu,,,1
nsel,r,loc,y,                    -7.0625  ,     -10.44
cm,contact3_6,node
vsel,s,volu,,boltstud_volu,,,1
nsel,r,loc,y,                    -5.8125
cm,contact3_7,node               !outside bottom(y-dir) surface of stud
vsel,s,volu,,boltstud_volu,,,1
nsel,r,loc,y,                    -11.688
cm,contact3_8,node               !outside top(y-dir) surface of stud

nsel,s,node,,contact3_1
nsel,a,node,,contact3_2
nsel,a,node,,contact3_3
nsel,a,node,,contact3_4
nsel,a,node,,contact3_5
nsel,a,node,,contact3_6
nsel,a,node,,contact3_7
nsel,a,node,,contact3_8
cm,contact3,node

nsel,s,node,,target3
CM,_TARGET,NODE
TYPE,5
ESLN,S,0
ESURF

nsel,s,node,,contact3
CM,_CONTACT,NODE
TYPE,4
ESLN,S,0
```

```
ESURF

!coupling node------------beam and end plate
vsel,s,volu,,topplate_volu,,,1
nsel,r,loc,x,                1.25   ,              5
nsel,r,loc,y,              8.4375   ,          9.063
nsel,r,loc,z,                   1
cm,single01,node
vsel,s,volu,,topplate_volu,,,1
nsel,r,loc,x,                1.25   ,              5
nsel,r,loc,y,              -8.438   ,         -9.063
nsel,r,loc,z,                   1
cm,single02,node
vsel,s,volu,,topplate_volu,,,1
nsel,r,loc,x,              4.7625   ,              5
nsel,r,loc,y,              -8.538   ,          8.538
nsel,r,loc,z,                   1
cm,single03,node
nsel,s,node,,single01
nsel,a,node,,single02
nsel,a,node,,single03
cm,single,node

vsel,s,volu,,beam_volu,,,1
nsel,r,loc,z,                   1
cm,couple,node
nsel,s,node,,single
nsel,a,node,,couple
CPINTF, all,                 0.15

!coupling node------------beam and beam stiffner
vsel,s,volu,,beam_volu,,,1
nsel,r,loc,z,                   8   ,            8.5
cm,single1,node
vsel,s,volu,,beamstiff_volu,,,1
nsel,r,loc,z,                   8   ,            8.5
cm,couple1,node
nsel,s,node,,single1
nsel,a,node,,couple1
CPINTF, all,                 0.15

!Constraint

!coupling node------------weld and beam
vsel,s,volu,,weld_volu,,,1
nsel,r,loc,y,              9.0625
nsel,r,loc,z,                 1.1   ,            1.5
cm,single_weld1,node
vsel,s,volu,,beam_volu,,,1
nsel,r,loc,y,              9.0625
nsel,r,loc,z,                 1.1   ,            1.5
```

```
cm,couple_weld1,node
nsel,s,node,,single_weld1
nsel,a,node,,couple_weld1
CPINTF, all,                                    0.15
!coupling node----------weld and end plate
vsel,s,volu,,weld_volu,,,1
nsel,r,loc,z,                                      1
nsel,r,loc,y,                                 9.1625   ,              9.563
cm,single_weld2,node
vsel,s,volu,,topplate_volu,,,1
nsel,r,loc,z,                                      1
nsel,r,loc,y,                                 9.1625   ,              9.563
cm,couple_weld2,node
nsel,s,node,,single_weld2
nsel,a,node,,couple_weld2
CPINTF, all,                                    0.15
!--------------------symetric B.C
nsel,s,loc,x,                                      5
d,all,ux,0
!bolt stud is fixed to the floor for B.C.
vsel,s,volu,,boltstud_volu,,,1
nsel,r,loc,z,                                                  -1
d,all,all,0
! Column flange is fixed column web position
allsel
vsel,s,volu,,bottomplate_volu,,,1
nsel,r,loc,z,                                                  -1
d,all,all,0
!================================CM name assign and color
vsel,s,volu,,bottomplate_volu,,,1
cm, bottomplate_ele,element
vsel,s,volu,,topplate_volu,,,1
cm,topplate_ele,element
vsel,s,volu,,bolt_volu,,,1
cm, bolt_ele,element
vsel,s,volu,,beam_volu,,,1
cm, beam_ele,element
vsel,s,volu,,beamstiff_volu,,,1
cm, beamstiff_ele,element
vsel,s,volu,,bottomplate_volu,,,1
/color,cm,13, bottomplate_ele
vsel,s,volu,,topplate_volu,,,1
/color,cm,2,topplate_ele
vsel,s,volu,,bolt_volu,,,1
/color,cm,8,bolt_ele
vsel,s,volu,,beam_volu,,,1
/color,cm,11, beam_ele
vsel,s,volu,,beamstiff_volu,,,1
/color,cm,7, beamstiff_ele
!================================pretensioning
allsel
```

```
psmesh,11,example1,,volu,                                    19   ,0,z,0,,,,
psmesh,12,example2,,volu,                                    29   ,0,z,0,,,,
psmesh,13,example3,,volu,                                    39   ,0,z,0,,,,
psmesh,14,example4,,volu,                                    65   ,0,z,0,,,,
allsel

finish
/com, solution ============================
/solution
!-------------------------------------pretensioning                  100   k
eqslve,pcg,1e-8


sload,11,pl01,tiny,force,                  100   ,1,2
sload,12,pl01,tiny,force,                  100   ,1,2
sload,13,pl01,tiny,force,                  100   ,1,2
sload,14,pl01,tiny,force,                  100   ,1,2

time,1

solve
!Loading point
vsel,s,volu,,beam_volu,,,1


nsel,r,loc,z,                  9
cm,loading,node                                                  ! 190

vsel,s,volu,,beam_volu,,,1
asel,r,loc,z,                  9
cm,loading_area,area

!First loading----------                        40   k

SFGRAD,PRES,0,Y,0,                -3.8276
nsel,s,node,,loading
!asel,s,area,,loading_area
!SFA,ALL,PRES,0
SF,all,pres,0

nsel,s,node,,loading
F, all, fy,               -0.10526316
allsel
antype,0    !analysis type is static

solcontrol,off
nropt,full
lnsrch,on
neqit,100
kbc,0
```

```
!convergence tolerance settings
CNVTOL,u,,0.05,,0.01                    ! CNVTOL, Lab, VALUE, TOLER, NORM, MINREF

! Result output options
outpr,all,all
outres,all,all

!Auto time-steipping options
NLGEOM,ON !--------non-linear solution
Autots,off
Nsubst,                 20
time,2
solve

!Second loading-----------------------------------------------
-                                                       60    k
SFGRAD,PRES,0,Y,0,              -5.7414
nsel,s,node,,loading
!asel,s,area,,loading_area
!SFA,ALL,PRES,0
SF,all,pres,0

nsel,s,node,,loading
F, all, fy,             -0.15789474



allsel
antype,0        !analysis type is static

solcontrol,off
nropt,full
lnsrch,on
neqit,100
kbc,0

!convergence tolerance settings
CNVTOL,u,,0.05,,0.01                    ! CNVTOL, Lab, VALUE, TOLER, NORM, MINREF

! Result output options
outpr,all,all
outres,all,all

!Auto time-steipping options
NLGEOM,ON !--------non-linear solution
Autots,off
Nsubst,                 40
time,3

solve
/com, post processing ================================
```

```
/post26
NUMVAR, 40
esel,s,elem,,                21309
esol,11,      21309   ,      29033   ,s,z,sz       21309
esol,14,      21309   ,      29033   ,s,eqv,seq    21309
esel,s,elem,,                21314
esol,12,      21314   ,      29123   ,s,z,sz       21314
esol,15,      21314   ,      29123   ,s,eqv,seq    21314
esel,s,elem,,                21638
esol,13,      21638   ,      29419   ,s,z,sz       21638
esol,16,      21638   ,      29419   ,s,eqv,seq    21638
esel,s,elem,,                 958
esol,17,       958    ,       1159   ,s,y,sz        958
esol,20,       958    ,       1159   ,s,eqv,seq     958
esel,s,elem,,                1630
esol,18,      1630    ,       1947   ,s,y,sz       1630
esol,21,      1630    ,       1947   ,s,eqv,seq    1630
esel,s,elem,,                1637
esol,19,      1637    ,       1913   ,s,y,sz       1637
esol,22,      1637    ,       1913   ,s,eqv,seq    1637
nsel,s,node,,          29419
nsol,23,      29419   ,u,z,uz 29419
nsel,s,node,,          1913
nsol,24,      1913    ,u,z,uz  1913
```